Technische Universität München

Fakultät für Chemie

# Exploration of Photochemical Mechanisms in Hydrated DNA Bases and in DNA Base Pairs

## DISSERTATION

Zur Erlangung des akademischen Grades
Doktor der Naturwissenschaften
vorgelegt von

**Xiuxiu Wu**

Garching bei München, 2018

TECHNISCHE UNIVERSITÄT MÜNCHEN

Theoretische Chemie

# Exploration of Photochemical Mechanisms in Hydrated DNA Bases and in DNA Base Pairs

Xiuxiu Wu

Vollständiger Abdruck der von der Fakultät für Chemie der Technischen Universität München zur Erlangung des akademischen Grades eines

Doktors der Naturwissenschaften

genehmigten Dissertation.

Vorsitzender: Prof. Dr. Michael Groll

Prüfer der Dissertation:

1. Prof. Dr. Wolfgang Domcke
2. Prof. Dr. Ville Kaila

Die Dissertation wurde am 25. 09. 2018 bei der Technische Universität München eingereicht und durch die Fakultät für Chemie am 18. 10. 2018 angenommen.

# Abstract

This thesis presents the results of quantum-chemical investigations into the photophysics and photochemistry of the DNA base adenine in water clusters and of several DNA base pairs *in vacuo*. Using state-of-the-art ab initio electronic-structure methods, photophysical and photochemical properties of adenine-water clusters and the anionic 8-oxo-guanine-adenine and 8-oxo-guanine-cytosine base pairs have been computed. The ab initio methods comprise Møller-Plesset perturbation theory of second order (MP2), the second-order algebraic-diagrammatic-construction method (ADC(2)) and complete-active-space second-order perturbation theory (CASPT2). The photochemical reactivity of these systems was characterized by calculating the potential-energy profiles of relevant photochemical reaction paths. The conical intersections associated with the studied reaction paths were identified and analyzed. The studied systems include hydrogen-bonded clusters of the nucleobase 9H-adenine with water molecules, two representatives of anionic 8-oxo-guanine-adenine base pairs and the anionic 8-oxo-guanine-cytosine base pair. The latter are the most common products of oxidative damage of DNA structures. The purpose of these investigations was the identification of novel photoreactivity mechanisms which are responsible for the ultrafast radiationless excited-state deactivation of electronically excited states of DNA bases in water and in base pairs. The results clarify the intrinsic reactivity of water molecules in the radiationless decay dynamics of adenine in water clusters and provide an explanation of the pronounced shortening of the excited-state lifetime of adenine in aqueous solution. These findings suggest that adenine may have been a photostabilizer as well as a photocatalyst for water splitting at the beginning of life. For the anionic 8-oxo-guanine-adenine and 8-oxo-guanine-cytosine base pairs, the results provide computational evidence that anionic 8-oxo-guanine may play a role in repairing cyclobutane pyrimidine dimer lesions in DNA. The potential-energy profiles presented in this thesis provide references for further investigations of the photoreactivity of DNA bases and base pairs by nonadiabatic nuclear-dynamics simulations.

# Zusammenfassung

Diese Dissertationsschrift präsentiert die Ergebnisse quantenchemischer Untersuchungen der Photophysik und Photochemie der DNA-Base Adenin in Wasserclustern sowie von einigen DNA-Basenpaaren im Vakuum. Die photophysikalischen und photochemischen Eigenschaften von Adenin-Wasser-Clustern sowie von anionischen 8-oxo-Guanin-Adenin und 8-oxo-Guanuin-Cytosin Basenpaaren wurden mit quantenchemischen ab initio Methoden berechnet. Als ab initio Methoden wurden Møller-Plesset-Störungstheorie zweiter Ordnung (MP2), die algebraisch-diagrammatische Konstruktion zweiter Ordnung (ACD(2)) sowie die complete-active-space-Störungstheorie zweiter Ordnung (CASPT2) benutzt. Die photochemische Reaktivität der untersuchten Systeme wurde durch Berechnung der Energieprofile der relevanten Reaktionswege charakterisiert. Die konischen Durchschneidungen auf diesen Reaktionswegen wurden identifiziert und analysiert. Die untersuchten Systeme sind Wasserstoffbrücken-gebundene Cluster der Nucleobase Adenin mit Wasser-Molekülen, zwei Repräsentanten von anionischen 8-oxo-Guanin-Adenin Basenpaaren sowie ein anionisches 8-oxo-Guanin-Cytosin Basenpaar. Die letztgenannten stellen die häufigsten Produkte oxidativer Schädigung von DNA dar. Der Zweck der Untersuchungen war die Identifizierung neuartiger photochemischer Reaktionsmechanismen, welche für die ultraschnelle strahlungslose Deaktivierung angeregter Zustände von DNA-Basen in Wasser und von DNA-Basenpaaren verantwortlich sind. Die Resultate zeigen die intrinsische Reaktivität von Wasser-Molekülen in der strahlungslosen Deaktivierung von Adenin in Wasser-Clustern und liefern eine Erklärung für die ausgeprägte Reduktion der Lebensdauer angeregter elektronischer Zustände von Adenin in wässriger Lösung. Diese Ergebnisse legen nahe, dass Adenin ein Photostabilisator und ein Photokatalysator für Wasser-Spaltung am Ursprung des Lebens gewesen sein könnte. Für die anionischen 8-oxo-Guanin-Adenin und 8-oxo-Guanin-Cytosin Basenpaare liefern die Ergebnisse Hinweise, dass 8-oxo-Guanin eine Rolle in der Reparatur von

Cyclobutan-Dimer-Strahlenschäden in DNA spielen könnte. Die in dieser Arbeit berechneten Energieprofile stellen Referenz-Ergebnisse für zukünftige Untersuchungen der Photoreaktivität von DNA-Basen und Basenpaaren mit nichtadiabatischen Dynamik-Simulationen dar.

This doctoral thesis is a publication-based thesis. The work presented in this thesis has been published in international scientific journals or has been submitted for publication in an international scientific journal by the time of submission of this thesis. This thesis provides computational insight into the photophysics and photochemistry of the DNA base adenine in water clusters and of several DNA base pairs *in vacuo*. A broad overview on the employed theoretical concepts and ab initio methodologies is given. A short summary of one publication manuscript and two published articles as well as a description of my individual contribution to each piece of work is given. Discussion and Conclusions integrate my work into the existing literature on each studied system and provides an outlook for future studies. One publication manuscript and two published articles are attached to this thesis.

Xiuxiu Wu, Garching bei München, September 2018

The presented work was performed from November 2014 to September 2018 in the Department of Chemistry of Technische Universität München under the supervision of Prof. Dr. Wolfgang Domcke.

# Contents

**1 Introduction** **1**

**2 Theoretical Concepts and Computational Methods** **11**

2.1 Theoretical Concepts………………………………………… 11

2.1.1 Born-Oppenheimer Approximation…………………………… 11

2.1.2 Potential Energy Surfaces……………………….…………. 12

2.1.3 Conical Intersections……..…………………………………… 13

2.1.4 Photochemical Reaction Paths……………………………….... 14

2.2 Ab Initio Electronic-Structure Methods …………………… 15

2.2.1 MP2…………………………………….………………… 15

2.2.2 ADC(2) ……………………………………..…………….. 16

2.2.3 CASPT2…………………………………….…..………… 17

2.2.4 Technical Aspects………………………………………………. 18

**3 Summaries of Publications** **21**

3.1 Mechanisms of the Photoreactivity of Adenine in Water………………. 21

3.2 Excited-State Deactivation of Adenine by Electron-Driven Proton-Transfer Reactions in Adenine–Water Clusters: A Computational Study………. 23

3.3 Role of Electron-Driven Proton-Transfer Processes in the Ultrafast Deactivation of Photoexcited Anionic 8-oxoGuanine-Adenine and 8-oxoGuanine-Cytosine Base Pairs……………………………………………………. 24

**4 Discussion and Conclusions** **28**

Bibliography 35

Acknowledgements 47

List of Publications 49

Appendices: Publication Manuscript and Published Articles 51

# Chapter 1

# Introduction

Nucleobase molecules absorb photons in the ultraviolet (UV) wavelength region of the electromagnetic spectrum. After elevated to an electronically excited state, they can decay back to the electronic ground state in two ways: either by photophysical processes or by photochemical processes. Photophysical processes are deactivation processes which do not involve any chemical change. They include radiative deactivation by the emission of a photon and radiationless transitions such as internal conversion and intersystem crossings. The radiative deactivation of singlet excited states is known as fluorescence. The efficiency of the fluorescence process is measured by the fluorescence quantum yield $\Phi$, which is defined as the ratio of the number of photons emitted to the number of photons absorbed [1]. Alternatively, the chromophore can first undergo a transition from the singlet excited state to a triplet excited state, which is known as intersystem crossing, followed by radiative deactivation of the triplet excited state to the ground state. The latter process is called phosphorescence. The triplet excited state can also relax to the ground state by a radiationless transition, which is called intersystem degradation. These transitions are usually summarized in the so-called Jablonski diagram [2], named after the Polish physicist Aleksander Jabłoński.

In phtochemical process, on the other hand, a chemical reaction take place after a photon absorption and new chemical species (photoproducts) maybe form during the photoinduced deactivation. The first law of photochemistry, known as the Grotthuss-Draper law, states that light must be absorbed by a chemical substance (the photoreactant) for a photochemical reaction to take place. According to the second law of photochemistry, known as the Stark-Einstein law, for each photon of light absorbed by a chemical system, no more than one molecule is activated for a photochemical reaction. After excitation to a singlet excited state or the subsequent radiationless transition to a triplet excited state, the photoreactant exhibits half empty molecules orbitals and is consequently more oxidizing than in the ground state. Consequently, the photoexcited reactant is susceptible to be active in chemical reactions, especially for processes which are driven by electron transfer.

The electron-driven proton transfer (EDPT) process is widely acknowledged to be a widespread photochemical reaction and is also known as proton-coupled electron transfer (PCET) in the literature [3]. The EDPT concept was proposed by Domcke and Sobolewski and proved to be an efficient mechanism of nonradiative decay via conical intersections in hydrogen-bonded systems [4]. It has been extensively investigated in the photochemistry of hydrogen-bonded molecular systems like indole and pyridine with solvents in the past two decades [4]. More recently, it was discussed in the photochemistry of nucleobases (adenine, cytosine, guanine and thymine) in water/ammonia environments and in the photochemistry of DNA bases pairs [5-13]. After photon absorption, an electron from the highest occupied molecular orbital (HOMO) of the H-atom donor is elevated to the vacant lowest unoccupied molecular orbital (LUMO) of the H-atom acceptor, resulting in a charge separation. Due to the Coulomb attraction, this electron transfer in turn triggers an ultrafast proton transfer from the donor to the acceptor, thus accomplishing a complete H-atom transfer. When the H-atom donor and acceptor are two groups from the same molecule, it is called intramolecular EDPT. This can happen in some organic molecules [14-16] like oxybenzone, where a hydroxyl group acts as the H-atom donor and a carbonyl group acts as the acceptor. The photoinduced intramolecular EDPT mechanism has been proposed to account, for example, for the ultrafast excited-state deactivation of oxybenzone [16].

More commonly, EDPT processes are widely invoked to explain the ultrafast deactivation of hydrogen-bonded systems via internal conversion, such as the DNA base pairs A=T [6,7] and G≡C [8-13] and in chromophore-water/ammonia clusters, which are called intermolecular EDPT reactions. For instance, in the case of adenine-water clusters, adenine forms hydrogen bonds with water molecules through its acidic (NH) and basic (N) sites. In the latter case, adenine acts as the H-atom acceptor, while, the water molecule acts as the donor. By photoexcitation to the lowest bright $^1\pi\pi^*$ excited state, an electron from the lone pair p-orbital on the oxygen atom of the water molecule is transferred to a $\pi^*$ orbital localized on adenine, forming an intermolecular charge separation. Subsequently, the proton from the water molecule is attracted by the nitrogen atom of adenine and a (adenine+H)•-OH• biradical is formed. Many intermolecular EDPT processes have been identified to be efficient barrierless or nearly barrierless deactivation pathways of biological systems via low-lying conical intersections in aqueous solutions.

In addition, EDPT processes have been invoked in searching for photocatalyzers for the photoinduced homolytic dissociation of water. Similar to the mechanism described for the hydrogen-bonded adenine-water clusters, the photocatalyzers (chromophores) can undergo intermolecular EDPT reactions to abstract a H-atom from water, yielding a (chromophore+H)• radical and an OH• radical. With the absorption of another photon, the surplus H from the intermediate (chromophore-H)• radical can be detached and the chromophore is regenerated. Overall, the water molecule has been split into H• and OH• radicals by the absorption of two photons. Several organic molecules have been identified to qualify as photocatalyzers for photocatalytic water splitting by first-principle computations [17-25], which is relevant for the future generation of clean and renewable chemical energy carriers.

In the present context, intermolecular EDPT processes are explored to understand the photoinduced ultrafast decay mechanisms of the DNA base 9H-adenine (as representative of purine bases) in water environments. Adenine is one of the main building blocks of DNA/RNA structures in biological systems. Along with the other nucleobases thymine, guanine and cytosine, it is the most essential molecule for the storage of the genetic information of life. The fluorescence quantum yield of adenine is very low [26,27]. Adenine exhibits a remarkable photostability in the UV spectral range. The photostability of adenine is explained by ultrafast deactivation from the photo-excited states to the electronic ground state via internal conversion [28].

Several ultrafast deactivation mechanisms for adenine in the gas phase have been proposed and confirmed by experimental and computational methods. It is consensus that the excited-state decay of adenine occurs mainly via conical intersections which are better accessible by out-of-plane puckering of the six-memberd aromatic ring. However, by hydrogen-bonding to surrounding solvent molecules, the photochemistry of adenine can be significantly altered in aqueous solution. For example, the excited-state lifetime in aqueous solution is observed to be much shorter than that in the gas phase (1.2 ps vs 200 fs). On one hand, solvation effects may modify the electronic exitation energies, which can change the energy barriers on reaction paths to conical intersections. On the other hand, hydrogen-bonding interactions with surrounding water molecules may lead to explicit participation of water molecules in the excited-state relaxation dynamics, resulting in new photorelaxation channels not available in the isolated adenine molecule.

The EDPT process was proposed to be a possible pathway for photoinduced deactivation of adenine in aqueous solution. Excited-state dynamics simulations have been performed to investigate the decay behevior of an adenine-water complex by Došlić et al with the ADC(2) method [29]. They identified a photoinduced EDPT process from the water molecule to the N atom of adenine which could be responsible for the observed shortened excited-state lifetime of adenine in aqueous environments. To compliment and extend the exploration of the proposed EDPT mechanism, calculations of the energy profiles of excited-state minium-energy reaction energy paths are presented. In the first part of the present thesis content, for five clusters of adenine with a single water molecule (see Fig. 1), the reaction paths for H-atom transfer involving the three basic sites (N1, N3 and N7) and the two acidic sites (N9H and N10H) have been investigated with the ADC(2) method. This comprehensive “bottom up” investigation of the photoreactivity provides insight into the role of EDPT reactions in microsolvated adenine, and provides instruction for further investigations of the aqueous photochemistry of adenine with ab initio nonadiabatic nuclear-dynamics simulations.

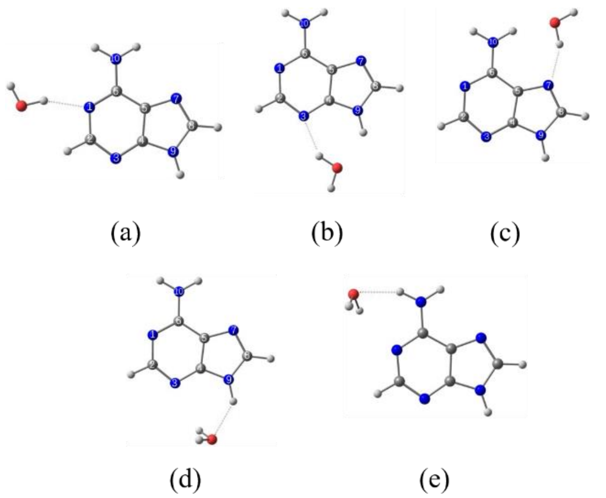

Figure 1: Structures of the five adenine–$H_2O$ clusters that have been studied in this thesis.

In a more realistic environment, *e.g.* in aqueous solution, adenine is microhydrated by finite number of water molecules. Hydrogen bonding with more than one water molecule results in nontrivial modifications of the photoproperties of adenine chromophore. Experimental investigations on the photoinduced dynamics of microhydrated adenine have made some progress. Ritze et al. applied femtosecond time-resolved photoionization spectroscopy to study the photophysics of adenine-water clusters [30]. They confirmed the substantially shortened excited-state lifetime (≈ 100 fs) of adenine-water clusters compared to isolated adenine. The ultrafast excited-state relaxation was explained by a lowering of the energy of the photoreactive $^1\pi\sigma^*$ state in microhydrated adenine [30]. Canuel et al. investigated the excited-state dynamics of microhydrated 9-methyladenine with femtosecond time-resolved photoelectron and photo-ion spectroscopy [31]. They reported a strongly accelerated excited-state decay (lifetime of ≈ 200 fs), which they explained as a lowering of the energy and direct population of the short-lived $L_a$ state in the clusters. Park and co-workers applied multiphoton ionization spectroscopy to adenine-water clusters and observed a significant amount of protonated adenine after cluster fragmentation, which is an indication of proton transfer processes operating in excited or ionized clusters [32]. From theoretical studies aspect, exploration of the reaction mechanisms and the nonadiabatic dynamics has been done but far from enough. Mitrić et al. explained the shortening of the ${}^1\pi\pi^*$ lifetime in microhydrated 9H-adenine within the framework of conventional mechanisms [33]. Ritze et al. emphasized the redshift of reactive ${}^1\pi\sigma^*$ states in the hydrates [30]. Barbatti found evidence for an electron-transfer pathway from water to adenine in the 7H-adenine–$(H_2O)_5$ cluster by using excited-state dynamics simulations with the ADC(2) method [34]. This is the first indication that not only the acidic sites of adenine (NH, NH2), but also the basic sites (N) might be relevant for the excited-state relaxation dynamics of adenine in water. We proposed a different charge-transfer mechanism via EDPT reaction process in all three basic sites (N) of adenine in 9H-adenine–$(H_2O)_5$ cluster (see Fig. 2). We investigated in detail the excited-state EDPT reaction mechanism in the 9H-adenine–$(H_2O)_5$ cluster with the ADC(2) method, focused on the characterization of vertical excitation energies, minimum-energy excited-state reaction paths and the identification of relevant conical intersections, which is summarized in section 3.2 of this thesis.

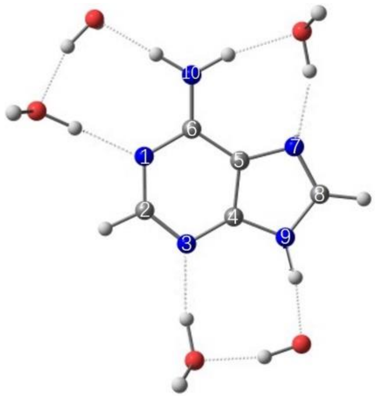

Figure 2: Structure of the studied adenine–$(H_2O)_5$ cluster.

Guanine is the second purine nucleobase of DNA and RNA. The oxidation of guanine generates 8-oxo-guanine (8-oxo-G), one of the most common lesions found in oxidatively damaged DNA [35]. Compared with guanine, 8-oxo-G has significant lower reduction potential, which makes it a viable candidate for protecting DNA by scavenging highly oxidizing species such as OH radicals. Besides, 8-oxo-G has been shown to be capable of repair of cyclobutane pyrimidine dimers [36-38], which are the most abundant form of lesions found in photodamaged DNA. The deprotonated anionic form 8-oxo-G$^-$ has been found to have a significantly longer excited-state lifetime than the neutral form 8-oxo-G. The anionic form is therefore more favorable for DNA protection and repair of UV damage and the study of the excited-state properties of anionic 8-oxo-G$^-$ are thus of biological relevance. A recent study by fluorescence spectroscopy and calculations revealed that neutral 8-oxo-G exhibits an ultrafast radiationless decay via two conical intersections which are accessible by certain out-of-plane deformations of guanine, whilst the longer lifetime of anionic 8-oxo-G$^-$ was attributed to the existence of sizable barriers along the reaction paths connecting the Franck-Condon region to the $S_1/S_0$ conical intersections [39].

In double-stranded DNA, nucleobases are organized in horizontally oriented hydrogen-bonded base pairs and vertically oriented stacks stabilized by $\pi$-$\pi$ interactions. Both architectural motifs may modify the dynamics of the intrinsic decay paths of the individual nucleobases by providing additional decay channels by which the excited-state populations can evolve. Such modifications have been studied, for example, by Crespo-Hernandez and co-workers who have shown that base stacking of A-T DNA oligomers leads to the formation of intra-strand excimer states with lifetimes of 50–150 ps [40] with additional decay features that are somewhat longer lived [41,42]. Kohler and co-workers recently studied the excited-state dynamics of a $\pi$-stacked dinucleotide containing the 8-oxo-G$^-$ anion at the 5′-end and neutral adenine at the 3′-end, using time-resolved transient UV-pump IR-probe spectroscopy. They found that UV excitation of the dinucleotide leads to prompt electron transfer from 8-oxo-G$^-$ to the $\pi$-stacked adenine, generating a neutral 8-oxo-G radical and an adenine radical anion [43,44]. For stacked base pairs, the inter-base hydrogen bonds provide additional paths along which coupled electron/proton transfer reactions can occur [45,46].

8-oxo-G$^-$ can form Hoogsteen (HG) base pairs with adenine in two low-energy conformations 8-oxo-G$^-$-A, indicated as 8-oxo-G$^-$-A HG1 and 8-oxo-G$^-$-A HG2, as is shown in Fig. 3 (a) & (b). The bases are connected by two types of hydrogen bonds: a

O···H–N bond and a N···H–N bond. Meanwhile, 8-oxo-G$^-$ can form a base pair 8-oxo-G$^-$-C with cytosine connected by two N···H–N hydrogen bonds, as the structure shown in Fig. 3 (c). The photochemistry of 8-oxo-G$^-$ is significantly changed by bonding to another chromophore; on the other hand, inter-base hydrogen-bonds provide new possible excited-state decay channels involving hydrogen transfer between bases. In 2013, with TD-DFT calculations, Kumara and Sevilla explored the role of inter-base proton-coupled electron transfer (PCET) processes in the deactivation of excited neutral 8-oxo-G-A and 8-oxo-G-C base pairs [47]. They found the presence of a low-lying conical intersection between the lowest charge-transfer ${}^1\pi\pi^*$ excited state and the ground state for 8-oxo-G-C base pair which could be responsible for the ultrafast decay via a PCET process. However, for 8-oxo-G-A base pair, the charge-transfer ${}^1\pi\pi^*$ excited state lies at higher energy and its crossing with ground state is inhibited because of a high energy gap between charge-transfer ${}^1\pi\pi^*$ excited state and ground state. Since 8-oxo-G$^-$ is more relevant to DNA repair because of longer excited-state lifetime, a study of the pairing of 8-oxo-G$^-$ with adenine and cytosine is undoubtedly essential. In section 3.3, we present the potential-energy surfaces of 8-oxo-G$^-$-A HG1 and 8-oxo-G$^-$-A HG2, as well as of 8-oxo-G$^-$-C for comparison. With ab initio wavefunction-based electronic structure method, the barrierless EDPT reaction paths are proved to be efficient excited-state channels via conical intersections.

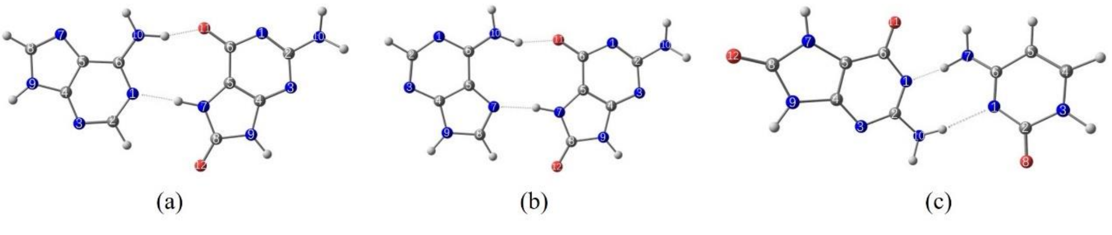
(a) (b) (c)

Figure 3: Structures of the anionic 8-oxo-G$^-$-A HG1 base pair (a), HG2 base pair (b) and the anionic 8-oxo-G$^-$-C base pair (c) studied in this thesis.

The investigations of the present work have been done with quantum-chemical calculations using state-of-the-art ab initio electronic structure methods. These include several wavefunction-based post-Hartree-Fock methods: MP2, CASSCF, CASPT2 and ADC(2), which will be briefly introduced in the next chapter. The initial light-absorption processes are characterized by the computation of the vertical excitation energies and their corresponding oscillator strengths of singlet excited states, together with the characterization of relevant molecular orbitals. The reactivity of the hydrogen-bonded molecular clusters in the excited states has been clarified by calculations of minimum-energy profiles along selected reactive paths, the identification of relevant conical intersections and the determination of locations of local minima and saddle points on their potential-energy surfaces. These results provide direct evidence for the possible channels of photochemical reactivity.

# Chapter 2

# Theoretical Concepts and Computational Methods

In the first section of this chapter, the relevant theoretical concepts underlying the work of this thesis are described. These include the Born-Oppenheimer approximation, potential energy surfaces, conical intersections and photochemical reaction paths. In the second section, the computational methodologies that have been used for the investigation of the energy profiles of molecular systems considered in this thesis are briefly introduced. Some calculational techniques used to describe photochemical reaction paths are also presented.

## 2.1 Theoretical Concepts

### 2.1.1 Born–Oppenheimer Approximation

The Born-Oppenheimer (BO) approximation is based on the assumption that the motion of atomic nuclei and electrons in a molecule can be separated. The reasonability of the assumption lies in the fact that atomic nuclei is much heavier and hence moves much more slowly than electrons. In mathematical terms, it allows the wavefunction of a molecule to be broken into its electronic and nuclear (vibrational, rotational) components:

$$\Psi_{\text{total}}\,(r, R) = \Psi_{\text{nuclei}}\,(R)\,\Psi_{\text{electrons}}\,(r; R)$$

where r and R refers to coordinates of electrons and nuclei, respectively. The BO approximation was proposed in 1927 by German physicist Max Born and American physicist Julius Robert Oppenheimer [48]. It is quite basic in quantum chemistry and provides a prescription for the calculations potential energy surfaces using computational quantum chemistry.

For a given nuclear configuration, with the BO approximation, the electronic time-independent Schrödinger equation (TISE) is solved, yielding the wavefunction $\Psi_{electrons}$ and energies ($E_{electrons}$) depending on electrons only. In the second step, this function serves as a potential energy in the TISE for nuclear wavefunction. The BO approximation simplifies the computation of energy and wavefunction of an average-size molecule. It is widely used in computations of molecular wavefunctions for large molecules. Without it only the lightest molecule, $H_2$, can be handled. Even in the cases where the BO approximation breaks down, it is used as a point of departure for the computations. The BO approximation introduced little error for the ground electronic states of diatomic molecules. Corrections for excited electronic states are larger than for the ground states, but are still usually small as compared with the errors introduced by the approximations used to solve the electronic TISE of a many-electron molecule [49]. BO approximation becomes invalid in the situation where the electronic energy level spacings are close to the vibrational level spacings. This is because at these regions of nuclear coordinate space the electronic states are strongly coupled by vibrational degree of freedom of molecules.

### 2.1.2 Potential Energy Surfaces

A potential energy surface (PES) describes the electronic energy of a molecular system as a function of its internal nuclear degrees of freedom such as bond lengths that specify the position of the nuclei. Since a PES only depend on the relative positions (internal coordinates) other than the absolute positions of the atoms, in 3-dimensional space, the dimensionality of a PES becomes $3N-6$, where $N$ is the number of atoms. The internal coordinates may be represented by simple stretch, bend, torsion coordinates, or symmetry-adapted linear combinations, or redundant coordinates, or normal modes coordinates, etc. PES can be used to theoretically explore properties of molecular structures, for example, finding the minimum energy geometry of a molecule or computing the rates of a chemical reaction. The most interesting points on PESs are the stationary points, where the gradients with respect to all internal coordinates are zero. Stationary points have physical meaning: energy minima correspond to physically stable or quasi-stable chemical species; saddle points correspond to transition states, the highest energy point on the reaction coordinate (which is the lowest energy pathway connecting a chemical reactant to a chemical product). A minimum on the PES is defined by curvatures that are all positives. A saddle point is characterized by a negative curvature in one direction and positive curvatures in all other directions. In our investigations, one-dimensional PES (potential energy curve) as a function of one coordinate of a bond distance and two-dimensional PES as a function of two bond distances were calculated for locating the conical intersections, characterizing the energy minima and saddle points of specific reaction paths.

### 2.1.3 Conical Intersections

A conical intersection (CI) between two or more PESs where the PESs occurs if the non-adiabatic couplings between these states are non-vanishing. A CI is not a single point in *N* dimensionality but rather a beam of points in *N-2* dimensionality. In the vicinity of CI, the BO approximation breaks down and the coupling between electronic and nuclear motion becomes important, allowing non-adiabatic processes to take place. Teller first predicted this property of PESs in 1937 [50], one decade after the BO approximation was proposed [48]. Until late 20th century, the important role of CIs in photochemical processes was discovered [51,52], followed by extensive theoretical and computational supporting [53-60]. From experimental aspect, progress in ultrafast femtosecond techniques has enabled detection of sub-picosecond lifetimes for nonadiabatic events. For example, time-resolved spectroscopic experiments provide means of measuring ultrafast relaxation rates by directly detecting nonadiabatic dynamics around CIs [61]. Nowadays it is widely accepted that CIs have become an established paradigm for understanding reaction mechanisms in a vast number of photochemical processes. For instance, photochemistry of DNA/RNA building blocks upon UV irradiation is mediated through CIs paving a way for their crucial role in the mechanism. This is due to the central role the CIs play in nonradiative relaxation from excited electronic states to the ground electronic state of molecules. The molecular wave packet promoted to an electronic excited state by the UV photon is governed by the forcefield of PES and reaches the CI. At this point, the very large vibronic coupling induces a nonradiative transition which leads the molecule back to its electronic ground state. Conical intersections mediate the internal conversion between states of like multiplicity.

The location and characterization of CIs are essential to the understanding of a lot of important phenomena governed by non-adiabatic events. Therefore, for closed-shell molecules, the determination of the energetic location and the optimization of the geometry at $S_1/S_0$ CIs is a critical step in characterizing photochemical processes [50,58,62,63]. Most well-established optimization algorithms for minimum-energy CI optimization require access to the energy gradient difference and derivative coupling vectors. Based on these algorithms, some schemes for optimization of minimum-energy CIs have been developed and become widely used [64-67]. In the past decade, a new scheme of minimum-energy CI optimization was developed, where neither energy gradient nor derivative coupling vectors are required [68]. This technique may be applied to any electronic structure method that associates unique energies with a particular molecular geometry. For its convenience, this new method has got extensively used.

### 2.1.4 Photochemical Reaction Paths

Photochemical reaction paths show the change of energy profiles from the initially populated reactant in excited state (in the Franck-Condon region) to the relevant configurations such as CIs, transition states and the product. If a photochemical reaction path is barrierless, it means the associated photochemical reaction is kinetically favorable and the path on the relevant excited state to the configurations such as CI is theoretically possible. On the other hand, if a photochemical reaction path is found with a sizable energy barrier, it means associated photochemical reaction has kinetically not favorable on the associated excited state, and the specific CI may not involve in the true reaction path. In fact, the molecular wavepacket often encounters a lot of CIs which are usually associated with high energy or high barrier from the Franck-Condon region. Photochemical reaction paths can be determined in a completely unbiased way by computing minimum energy paths [69] connecting the reactant to the relevant CIs or the product on the $3N-6$ dimensional PES of the system. In this thesis, we explored the photochemical reaction paths by constructing minimum energy paths to the relevant conical intersections on the 2- dimensional PES. On minimum energy paths, every point is at an energy minimum in all directions perpendicular to the path. A minimum energy path is the lowest energy path from reactant to product. It is therefore the most likely (but not the only possible) reaction path that occurs.

## 2.2 Ab Initio Electronic-Structure Methods

In the work of this thesis, all the ground-state equilibrium geometries were optimized with the Møller-Plesset perturbation theory of second order (MP2) [70]. Vertical excitation energies, oscillator strengths, molecular properties and photochemical reaction paths were calculated using the algebraic diagrammatic construction to the second order (ADC(2)) [71] method. In some cases, for benchmarking purpose, vertical excitation energies were also computed using the complete-active-space second-order perturbation theory (CASPT2) method [72]. These three methods are briefly described in the following sections, mainly on the general idea for each method, its strengths and limitations, as well as the reason why the method was chosen for our molecules.

### 2.2.1 MP2

MP2 is a post-Hartree-Fock ab initio method which accounts for electron correlation by treating it as a perturbation to the Hartree-Fock wave function by means of Rayleigh-Schrödinger perturbation theory (RS-PT) to second order [70]. It belongs to the Møller-Plesset perturbation theory proposed by Møller and Plesset in 1934, which is one method of many-body perturbation theory dealing with systems of many interacting particles. Until 1975, the Møller-Plesset perturbation theory was applied in actual molecules in the work of Bartlett [73]. MP2 is the most common level in Møller-Plesset perturbation treatment (MPn) due to its appropriate accuracy and computational efficiency. Besides, MP2 calculations is shown to be size consistent. On the other hand, MP2 calculations are not variational and can give an energy lower than the true energy. However, mostly the size consistency is regarded as more important than being variational. For quantum-chemistry calculations of ground-state and close-shell molecules, MP2 is one of the two most popular methods including electron correlation effects. For species of open shell ground states, the MP2 calculations can be based on the unrestricted SCF wave function, which is called UMP2 method. Alternatively, the MP2 calculations can also be based on the restricted open-shell Hartree-Fock wave function, which is called ROHF MP2 method.

In addition, there are two important limitations of MP2 calculations. One is that it only works well near the equilibrium geometry and fails for geometries far from equilibrium. Another limitation is MP2 calculations are not generally applicable to excited states, which makes its use limited to electronic ground states. In this thesis, all the ground-state equilibrium geometries were optimized at the MP2 level of theory with cc-pVDZ/aug-cc-pVDZ basis set.

### 2.2.2 ADC(2)

The algebraic diagrammatic construction method (ADC) is a polarization-propagator scheme for calculation of excited states based on perturbation theory. One can derive ADC-schemes of different order. In particularly, the second-order ADC(2) [71] scheme, with a second-order perturbation expansion applied to a Hermitian secular matrix, which contains singly and doubly excited determinants of the Hartree-Fock reference wavefunction [71,74], has been extensively used in the computation of excitation energies, oscillator strengths, and molecular properties. It describes physically correct charge-transfer states, doubly excited states, and Rydberg states in principle. Also, its advantages include size extensive character, reliable accuracy and reasonable computational resources. Another vital reason why ADC(2) method is employed is that it performs well in calculations in the vicinity of CIs, as the excitation energies are obtained as the eigenvalues of a Hermitian secular matrix.

The ADC(2) method has disadvantages due to the single-reference character of the underlying Møller-Plesset electronic ground state. Therefore, for a successful ADC(2) calculation, a reasonable description of the ground state by MP2 theory is a necessary prerequisite [75]. However, for organic molecules like DNA nucleobases that were studied in this thesis, the ADC(2) method is applicable, covering a broad range of photochemical processes.

### 2.2.3 CASPT2

The complete-active-space second-order perturbation theory (CASPT2) method [72] is a second-order perturbation theory based on the multiconfiguration self-consistent field theory (CASSCF). In the ansatz of CASPT the zeroth-order wavefunction is a CASSCF wavefunction. For the calculations in this thesis, the CASPT2 method was used with respect to the state-averaged complete-active-space self-consistent field (SA4-CASSCF) [76] reference wavefunction to avoid near-degeneracy correlation effects. The average of the energy of several selected electronic states is minimized [77,78] For calculations with CASSCF method, the choice of the active space is made at first. The orbitals space of the system is partitioned into three subsets: the inactive occupied orbitals, the active orbitals (which contain occupied and unoccupied orbitals of the Hartree–Fock reference wavefunction), and the inactive unoccupied orbitals. Within the active space of molecular orbitals, a full-CI (full configuration interaction) calculation is performed. In contrast to the CI method, not only are the CI coefficients being optimized in the CASSCF procedure, but also the molecular orbitals. However, the choice of the active space is quite flexible and there are no hard rules about it. It totally depends on the chemical problem that one deals with [79,80]. The CASSCF method has many advantages: it is well defined on the whole PES of a chemical reaction if an appropriate active space is chosen; it provides size-consistent results, etc. The combination of CASSCF method geometries optimization with CASPT2 method energies calculation is quite commonly used in the field of computational photochemistry. For example, CASPT2 method is used for single-point energy calculations like vertical excitation energies after geometries optimized at the CASSCF level.

However, there is always a limitation when using CASPT2/CASSCF method because of appearance of intruder states. These could happen when the perturbational energy correction leads to a substantial lowering of the energy of an electronic state that has not been captured by the CASSCF reference wavefunction. As a solution to aid convergence and avoid the effects of intruder states, an imaginary level shift was commonly used by adding a constant to the zeroth-order Hamiltonian [72,81].

When the calculations come to molecules with significant multi-reference character, CASPT2/CASSCF is the right choice other than ADC(2) method above. In the first paper of the thesis, CASPT2 method was used to compute the vertical excitation energies for benchmarking purposes.

### 2.2.4 Technical Aspects

In this thesis, three main techniques are used when performing the exploration of the photoreaction path from the relevant excited-states in the Franck-Condon region to the relevant CIs. The first technique is the rigid PES scan, which consists of single point energy evaluations over a rectangular grid involving selected internal coordinates along the selected reaction path. The starting geometry is usually chosen to be the ground-state equilibrium geometry or the optimized geometry of a conical intersection. As rigid PES scan is not a minimum-energy PES scan, the energy barrier of a photochemical reaction path calculated by rigid PES scan always represents an upper limit level. Sometimes it is quite useful to predict the energy barrier of a true minimum-energy path. Rigid PES scan is commonly used in evaluating photochemical reactions of complex molecules or clusters. The second technique is the relaxed PES scan. It samples points on the PES and performs a molecular geometry optimization with one internal coordinate fixed of the remaining non-scanned coordinates at the relevant electronic excited state at each point. The fixed internal coordinate is usually chosen to approximate the desired reaction coordinate. In the work of this thesis, we performed relaxed PES scans for all the studies systems, including adenine–($H_2O$) complexes, adenine–($H_2O$)$_5$ cluster, 8-oxo-G$^-$-A and 8-oxo-G$^-$-C base pairs. The third technique is the linear interpolation in internal coordinates. It is a rough approximation to the reaction path [82]. In the method, the internal coordinates of two molecular structures are used to interpolate intermediate molecular structures between the two original structures. It is usually used when the geometries of reactant and product are known. In photochemical reaction processes, it is commonly to be used between the ground-state equilibrium geometry and the optimized geometry of a specific CI. In the work of this thesis, the two starting structures are the ground-state equilibrium geometry and an optimized geometry at the selected charge-transfer excited state. The interpolation can be done in cartesian coordinates, internal coordinates or distance matrix coordinates. The approximate reaction path is then obtained via single-point energy calculations along the interpolated path. In this thesis, the linear interpolation was performed with adenine–($H_2O$)$_5$ cluster and 8-oxo-G$^-$-A and 8-oxo-G$^-$-C base pairs.

# Chapter 3

# Summaries of Publications

This chapter summaries the content of two published papers and one submitted manuscript, which represent the main work of the doctorate period. Sections 3.1 and 3.2 are brief summaries of the research obtained on the photodeactivation mechanisms of adenine in water. Section 3.3 gives a brief summary of the work on the ultrafast decay mechanisms of photoexcited base pairs of anionic 8-oxo-guanine with adenine and cytosine. The individual contributions of the candidate to each piece of work are described. The two published papers and the submitted manuscript are in the Appendix.

## 3.1 Mechanisms of the Photoreactivity of Adenine in Water

Summary of "Mechanisms of the Photoreactivity of Adenine in Water" by Xiuxiu Wu, Johannes Ehrmaier, Andreij. L. Sobolewski, Tolga. N. V. Karsili and Wolfgang Domcke, submitted.

In this work, the mechanisms of ultrafast excited-state decay of adenine in clusters with a single water molecule are systematically explored, considering all possible sites of adenine for hydrogen bonding with water. To this end, we built five low-energy conformers of adenine–$H_2O$ clusters as the systems to be investigated (see Fig. 1). The five conformers are divided into two groups: in conformers (a)-(c), adenine acts as an intermolecular hydrogen-bond acceptor; in conformers (d) and (e), adenine is the hydrogen-bond donor. Potential-energy profiles were computed as relaxed scans with the ADC(2) method. We identified two mechanisms in five deactivation pathways of photoexcited adenine in water: H-atom abstraction from water by photoexcited adenine and H-atom photodetachment from adenine to water. The former mechanism exists in the adenine–$H_2O$ conformers (a)-(c), where an electron from one of p orbitals of the water molecule fills in the hole in the $\pi$ orbital of the $\pi\pi^*$ excited state of adenine, forming a charge-separated electronic state. This charge-separation is neutralized by the following proton transfer from the water molecule to adenine, resulting in the (adenine+H)•···OH• biradical in the ground state. In the latter mechanism which exists in the conformers (d) and (e), the $\pi\sigma^*$ states at the acidic sites of adenine provide the mechanisms for the transfer of an electron from adenine to water, which is followed by the rapid transfer of a proton to the hydrogen-bonded water molecule. As a result, an (adenine-H)···$H_3O$ biradical is generated. By detecting the ejected hydrated electron, this mechanism has been confirmed by an experimental study [83]. These two mechanisms are responsible for the six photorelaxation pathways of adenine by EDPT reactions via conical intersections involving direct participation of hydrogen-bonded water molecules, which compete with the well-established intrinsic excited-state deactivation mechanism of adenine by ring-puckering conical intersections. This work exhaustively reveals the reactivity of adenine with water with every potential basic and acidic site of adenine with state-of-the-art electronic structure methods. Especially, in this work we provide for the first time two-dimensional potential-energy surfaces of the H-atom transfer reactions which reveal the specific energy barriers. We also located the conical intersections for the first time. By providing additional decay pathways, the electron/proton transfer reactions with water can account for the substantially shortened excited-state lifetime of adenine in aqueous solution.

*Individual candidate contribution:*

The candidate designed the adenine–$H_2O$ conformers and performed all the calculations, including geometry optimizations, the computation of vertical excitation energies, oscillator strengths and dipole moments. The candidate constructed the relaxed scans of the excited-state minimum-energy reaction paths and computed the two-dimensional potential-energy surfaces. Then with the help of the coauthors, the candidate analyzed and interpreted the data, and created the tables, graphs and figures. The candidate wrote the manuscript and the supporting information. The corresponding author submitted the manuscript.

## 3.2 Excited-State Deactivation of Adenine by Electron-Driven Proton-Transfer Reactions in Adenine-Water Clusters: A Computational Study

Summary of “Excited-State Deactivation of Adenine by Electron-Driven Proton-Transfer Reactions in Adenine-Water Clusters: A Computational Study” by Xiuxiu Wu，Tolga. N. V. Karsili and Wolfgang Domcke. *ChemPhysChem.* 2016, 17, 1298-1304.

In this work the mechanisms of photorelaxation of electronically excited states of 9H-adenine clustered with five water molecules via EDPT reaction processes was explored with the help of ab initio calculations. The cluster is shown in Fig. 2. The adenine–$(H_2O)_5$ cluster is the smallest cluster in which all potential sites for hydrogen bonding are saturated with water molecules. This cluster thus represents the first solvation shell of adenine in liquid water. Three potential photochemical decay pathways of adenine via EDPT reactions with water were predicted. The vertical excitation energies were calculated with the ADC(2) method and the relevant molecular orbitals were characterized. The energy profiles were computed as relaxed scans along reaction paths for electron/proton transfer from water to adenine. By analyzing the topography of the potential-energy surfaces and by identification of the relevant conical intersections, the EDPT reaction mechanism was characterized. Specifically, for two of the three hydrogen-bonded sites, a barrierless or almost barrierless decay path from the bright locally excited $^1\pi\pi^*$ state through a charge transfer state via a low-lying (≈ 4.0 eV) $S_1/S_0$ conical intersection has been established. It involves an electron transfer from the p orbital of water to the $\pi^*$ orbital of adenine, followed by a proton transfer from water to the nitrogen atom of adenine to stabilize the electronic charge transfer. As a result, a hydrogen atom is transferred from water to adenine, forming (adenine+H)• and •$OH(H_2O)_4$ radicals. These reaction channels involve the direct participation of water molecules, complementing the intrinsic ultrafast deactivation pathways of 9H-adenine in the gas phase via well-known ring-puckering conical intersections of the six-membered ring. In particular, this EDPT reaction mechanism can account for the significantly shortened lifetime of the excited states of adenine in aqueous solution. In addition, the generated (adenine+H)• radical may undergo hydrogen atom detachment by absorption of another photon . This finding indicates that adenine might have served as a photocatalyst for energy harvesting by water splitting in the prehistoric period of the evolution of life.

*Individual candidate contribution:*

The candidate performed the computations of vertical excitation energies and reaction paths with the MP2 and ADC(2) methods using the Turbomole program package. The candidate explored the appropriate configurations of the adenine–$(H_2O)_n$ cluster, identified the charge transfer states and interpreted the potential-energy curves. The candidate created the table, the abstract graph and all the figures except figure 2 &4 in the paper. She wrote the manuscript and the supporting information together with the coauthors. The corresponding author submitted the manuscript.

## 3.3 Role of Electron-Driven Proton-Transfer Processes in the Ultrafast Deactivation of Photoexcited Anionic 8-oxoGuanine-Adenine and 8-oxoGuanine-Cytosine Base Pairs

Summary of “Role of Electron-Driven Proton-Transfer Processes in the Ultrafast Deactivation of Photoexcited Anionic 8-oxoGuanine-Adenine and 8-oxoGuanine-Cytosine Base Pairs” by Xiuxiu Wu, Tolga. N. V. Karsili and Wolfgang Domcke. *Molecules*. 2017, 22, 135.

In this project, the role of EDPT processes in the ultrafast deactivation of photoexcited bases pairs: anionic 8-oxo-guanine-adenine (8-oxo-G$^-$-A) and 8-oxo-guanine-cytosine (8-oxo-G$^-$-C) was investigated. This investigation was motivated by the fact 8-oxo-G can repair cyclobutane pyrimidine dimer lesions, which has led to the speculation that 8-oxo-G may have been a primordial precursor of modern flavins in DNA/RNA repair. Since the repair involving an electron transfer reaction occurs in the photoexcited state, a reasonably long excited-state lifetime of 8-oxo-G is essential. The neutral 8-oxo-G was found to have a very short (sub-picosecond) excited-state lifetime, which is not favorable for the repair. On the other hand, anionic 8-oxo-G$^-$ exhibits a significant longer (43 ps) excited-state lifetime and is therefore a more likely cofactor for DNA/RNA repair. Therefore, it has been of interest to investigate the photoproperties of anionic 8-oxo-G$^-$ other than neutral 8-oxo-G. We explored the excited-state quenching mechanisms of anionic 8-oxo-G$^-$ in pairing with adenine and cytosine by inter-base hydrogen bonds in the Hoogsteen and Watson–Crick motifs, respectively, using ab initio wavefunction-based electronic-structure calculations. The potential-energy profiles were calculated along the inter-base hydrogen-atom transfer reaction paths. It is concluded that for the anionic 8-oxo-G$^-$-A (HG1) and 8-oxo-G$^-$-C base pairs (see Fig.3(a) and (c)), there exists a barrierless photodeactivation channel by an inter-base EDPT reaction via a low-lying $S_1/S_0$ conical intersection. For the 8-oxo-G$^-$-A (HG2) base pair (see Fig.3 (b)), a low barrier may exist on the $S_1$ PE surface which may kinetically hinder the access of this conformer to the $S_1/S_0$ conical intersection. More importantly, these EDPT reactions have a specific directionality: the hydrogen atoms transfer occurs only from 8-oxo-G$^-$ to adenine or cytosine, but not in the opposite direction. The reason is that the electron transfer always occurs from 8-oxo-G$^-$ to adenine or cytosine. Due to Coulomb attraction, the proton follows the direction of electron transfer. These findings provide new pathways for excited-state deactivation of nucleobases when pairing with each other in DNA double strands in addition to their widely-known intrinsic ring-puckering deformations. While the isolated anionic 8-oxo-G$^-$ nucleoside may have been a primordial repair cofactor, 8-oxo-G$^-$ paired with adenine or cytosine is unlikely to be able to play the same role in DNA/RNA repair because of the much shorted excited-state lifetimes.

*Individual candidate contribution:*

The advisor designed the three low-energy conformers of base pairs. The candidate performed all the calculations, including geometry optimizations, the vertical excitation energies and oscillator strengths, relaxed scan of minimum-energy reaction paths and linear interpolation reaction paths. With the help of the coauthors, the candidate analyzed and interpreted the data, and created the tables, graphs and figures. All authors contributed equally to writing the manuscript. The corresponding author submitted the manuscript.

# Chapter 4

# Discussion and Conclusions

In this thesis, I investigated photochemical reaction mechanisms of DNA bases in a water environment and in base pairs. By ab initio wave-function electronic-structure calculations for clusters of the representative base 9H-adenine with water molecules, we have systematically explored the role of EDPT reactions in the photochemistry of adenine in a water environment and when pairing with other bases. Five adenine–$H_2O$ complexes, one adenine–$(H_2O)_5$ cluster, two 8-oxo-guanine-adenine base pairs and one 8-oxo-guanine-cytosine base pair were constructed and the energy profiles of specific photochemical reaction routes were calculated. Several novel ultrafast excited-state deactivation pathways via different photochemical reaction mechanisms have been found which are not available in gas-phase adenine.

For clusters of adenine with a single water molecule, we have investigated the potential photochemical reactions occurring at the three basic sites (N1, N3, N7) and the two acidic sites (N9H, $N10H_2$) of adenine, where water molecules are connected by intermolecular hydrogen bonds. At the three basic sites, the potential-energy profiles along EDPT reaction paths from water to N-atoms of adenine were calculated, while at acidic sites, they were calculated along EDPT reaction paths from NH or $NH_2$ groups of adenine to hydrogen-bonded water molecules. By examining the molecular properties of adenine-water clusters, significant effects of an aqueous environment on the photoproperties of adenine were found out. Compared with gas -phase adenine, the vertical excitation energy to the lowest $^1n\pi^*$ state is blueshifted in the adenine-water cluster while the $^1\pi\pi^*(L_a)$ and $^1\pi\pi^*(L_b)$ excitation energies are redshifted. As a result, the vertical excitation energies of the lowest three excited states exibit a change in ordering. In water, $S_1(^1\pi\pi^*(L_a)) < S_2(^1\pi\pi^*(L_b)) < S_3(^1n\pi^*)$, while in the gas phase, $S_1(^1n\pi^*)<S_2(^1\pi\pi^*(L_a))<S_3(^1\pi\pi^*(L_b))$. More importantly, the intrinsic properties of water molecules allow them to participate directly in photochemical reaction processes. By calculating minimum-energy excited-state reaction paths of adenine–$H_2O$ complexes at the ADC(2)/aug-cc-pVDZ level, two different excited-state electron/proton transfer reaction mechanisms have been characterized: H-atom abstraction from water by photoexcited adenine as well as H-atom transfer from photoexcited adenine or the (adenine+H)• radical to water. In the water-to-adenine H-atom transfer reaction, an electron from one of the p orbitals of the water molecule fills the hole in the n ($\pi$) orbital of the $n\pi^*$ ($\pi\pi^*$) excited state of adenine, resulting in a charge-separated electronic state. The electronic charge separation is neutralized by the transfer of a proton from the water molecule to adenine, resulting in the (adenine+H)•···OH• biradical in the electronic ground state. In the adenine-to-water H-atom transfer reaction, on the other hand, $\pi\sigma^*$ states localized at the acidic sites (N9H, $N10H_2$) of adenine provide the mechanism for the photoejection of an electron from adenine, which is followed by proton transfer to the hydrogen-bonded water molecule, resulting in the (adenine-H)•···$H_3O$• biradical.

The former mechanism was also examined at the same basic sites of adenine by the calculation of photoreaction energy profiles of the adenine–$(H_2O)_5$ cluster as relaxed scans at the ADC(2)/cc-pVDZ level. By identifying the position and energies of conical intersections, it can be concluded that the relevant $S_1/S_0$ conical intersections are better accessible in clusters of adenine with several water molecules. The reason is that the (adenine+H)•···OH• biradical in the electronic ground state is stablized by hydrogen bonding with more water molecules. On the other hand, water molecules bonded at the reactive sites can form a small hydrogen-bond network, which may significantly reduce the flexibility of water molecules for geometric relaxation. As a result, the nuclear rearrangement is inhibited, the charge-transfer state is less stabilized and the relevant $S_1/S_0$ conical intersection may disappear. Besides conical intersections, we clarified the role of the energy barrier for the mechanism of H-atom abstraction from water by photoexcited adenine. For the adenine–$(H_2O)_5$ cluster, the energy barrier for the photoreactions at the three basic sites was constructed by linear interpolation in internal coordinates from the locally excited state to the charge-transfer state. For two of the three sites, a specific reaction path to a low-lying $S_1/S_0$ conical intersection was found to be barrierless or nearly barrierless. For the reaction path at the third site the barrier could not be determined because of the steric effect discussed above.

For adenine–$H_2O$ complexes with a single hydrogen-bonded water molecule, the two-dimensional relaxed PES was computed for all reactive sites in the $n\pi^*$ ($\pi\pi^*$) excited states. The location and energy level of local minima and saddle point were clearly shown in the two-dimensional PES. Similar to what was found in the adenine–$(H_2O)_5$ cluster, the energy barriers of all reaction paths were observed to be lower or more or less the same as the vertical excitation energy to the bright $^1\pi\pi^*$ state, whicn means the reaction paths are likely to be barrierless.

For the second mechanism the adenine-to-water H-atom transfer reaction at the N9H or $N10H_2$ groups of adenine, minimum-energy profiles of the $^1\pi\sigma^*$ states show large driving forces and no energy barrier for the reaction. However, when an H-atom is ejected to the surrounding water, an $H_3O^\bullet$ radical forms and the energy of the electronic ground state is strongly stabilized. As a result, the $S_1/S_0$ conical intersection disapears. This means in a water environment, the photoejected electron can form a hydrated electron, which is a unique feature of this mechanism. As a matter of fact, it is well known that homolytic photodetachment of H-atoms from acidic aromatic chromophores via repulsive $^1\pi\sigma^*$ states in aqueous solution can yield hydrated electrons [84-87]. In finite-size clusters, the hydrated hydronium radical, $H_3O(H_2O)_n$, is analogue of the hydrated electron in solution [88,89]. Recently Roberts et al. reported the detection of hydrated electrons generated by irradiation of adenine in aqueous solution at 220 nm and thus confirmed the possibility of the joint photodetachment of an electron and a proton from adenine in aqueous solution [83].

These two photodeactivation mechanisms discussed above involve the intrisic reactivity of hydrogen-bonded water molecules with adenine and are specific for the ultrafast excited-state deactivation of adenine in a water environment. They account for the significantly shorted excited-state lifetime of adenine in aqueous environments.

They provide additional mechamisms which compete with the well-established intrinsic excited-state deactivation mechanisms of adenine via ring-puckering or ring-opening conical intersections and contribute to the photostability of adenine in aqueous solution.

We also have characterized the PE functions for the photodetachment of the excess H-atom from the (adenine+H) radical as well as the corresponding H-atom transfer reaction from the radical to a hydrogen-bonded water molecule. The H-atom photodetachment reaction can be stimulated by low-energy photons and the H-atom transfer reaction to water may even be approximately thermoneutral. It should be noted that the transfer of a H-atom from a water molecule to adenine represents the oxidation of water and the reduction of adenine. When an H-atom of the (adenine+H) radical (reduced adenine) is photoejected by the absorption of another photon via a repulsive πσ* state, adenine is regenerated (possibly as a different tautomer) and a water molecule is thereby homolytically decomposed into H and OH radicals. Adenine may thus have the functionality of a photocatalyst for water splitting by UV light. The UV-induced decomposition of water catalyzed by adenine and possibly other RNA/DNA bases may have been the beginning of solar energy harvesting of life. The RNA/DNA bases likely were not only photostabilizers, [28,90-92] but also the primordial catalysts for solar energy harvesting by the oxidation of water.

Pairing of adenine with other bases in the DNA double helix structure also affects the photochemical properties of adenine. For two HG types of anionic 8-oxo-G$^-$-A base pairs, which are common in oxidatively damaged DNA structures, I have explored the photochemical reaction paths for radiationless excited-state deactivation by ab initio electronic structure calculations. For comparison, the anionic 8-oxo-G$^-$-C base pair was investigated as well. For the anionic 8-oxo-G$^-$-A HG1 base pair and the anionic 8-oxo-G$^-$-C base pair, the calculated reaction paths and potential-energy profiles reveal the existence of a barrierless electron-driven inter-base proton-transfer reaction from 8-oxo-G$^-$ to adenine or cytosine, which leads to low-lying $S_1/S_0$ conical intersections. For the anionic 8-oxo-G$^-$-A HG2 base pair, an electron-driven inter-base proton-transfer reaction from 8-oxo-G$^-$ to adenine was identified which leads to a low-lying $S_1/S_0$ conical intersection. However, a substantial energy barrier was found in the $^1\pi\pi^*$ state for a linearly interpolated reaction path. It is noteworthy that all electron-driven inter-base proton-transfer reactions exhibit specific directions, which means that the H-atom transfers can occur only from 8-oxo-G$^-$ to adenine or cytosine. The potential-energy profiles of reaction paths in the opposite direction (from adenine or cytosine to 8-oxo-G$^-$) were also calculated. The minimum-energy profiles show that the charge-transfer states are not stabilized, which confirms that the electron-driven inter-base proton-transfer reactions mechanism does not apply for these paths.

These results are significant in two aspects. For adenine, the pairing with other bases provides new excited-state quenching pathways in photoexcited DNA, in addition to the well-known intrinsic excited-state deactivation mechanisms of adenine via ring-puckering or ring-opening conical intersections. Fom perspective of 8-oxo-G, on the other hand, the present results are relevant with respect to the potential role of 8-oxo-G as a photo-repair agent in DNA, probably having been a precursor of modern flavine cofactors [93-95]. The photo-excited state of neutral 8-oxo-G has a sub-picosecond lifetime in aqueous solution, while deprotonated 8-oxo-G$^-$ exhibits a much longer fluorescence lifetime of 43 ps [96]. The extreme shortening of the excited-state lifetime of 8-oxo-G relative to anionic 8-oxo-G has been explained by either conical intersections intrinsic to guanine, which are more easily accessible in the neutral than in the anionic form [97], or by an EDPT reaction along the H-bond between guanine and ribose in 8-oxo-guanosine, which is available in the neutral form, but not in the anionic form [98]. It has been speculated that the long lifetime of anionic 8-oxo-G$^-$ should be favorable for repair by electron transfer in the excited state, while the very short excited-state lifetime of neutral 8-oxo-G should be disadvantageous in this respect [96]. My results provide computational evidence for presumably very efficient excited-state deactivation via barrierless EDPT reactions leading to $S_1/S_0$ conical intersections in the 8-oxo-G$^-$-A and 8-oxo-G$^-$-G base pairs which call the concept of repair of CPD lesions via electron transfer from excited-state 8-oxo-G$^-$ in DNA oligomers into question. Kumar and Sevilla investigated the corresponding EDPT paths in the neutral 8-oxo-G-A and 8-oxo-G-C base pairs and found a path with a barrierless PE profile en route to a low-lying $S_1/S_0$ conical intersection in the 8-oxo-G-C base pair, while no such path was found for the 8-oxo-G-A base pair [47]. This finding led Kumar and Sevilla to the conclusion that the 8-oxo-G-A base pair, due to its longer excited-state life time, should allow for efficient repair of CPD lesions. However, the very short intrinsic lifetime of neutral 8-oxo-guanosine, not considered by Kumar and Sevilla, renders it unlikely that the neutral 8-oxo-G-A base pairs are efficient repair agents in DNA oligomers. Notwithstanding, we do however stress that isolated nucleobasic or nucleosidic forms of 8-oxo-$G^-$ may be efficient at repairing CPD lesions—as advocated by Matsika et al [96] and Tuna et al [98].

To summarize, I have shown the intrinsic photophysical properties and photochemical reactivities of several adenine-water clusters, two 8-oxo-$G^-$-A and one 8-oxo-$G^-$-C base pairs by ab initio electronic structure calculations. The identified electron-driven proton-transfer mechanisms in excited-state nucleobases in aqueous environments and in base pairs deserve further investigation by ab initio nonadiabatic nuclear-dynamics simulations. The potential-energy profiles presented in this thesis provide references for further investigations of the photoreactivity of DNA bases and DNA base pairs by ab initio nonadiabatic nuclear-dynamics simulations and spectroscopic studies.

# Bibliography

1. Valeur, B.; Berberan-Santos, M.N. *Molecular fluorescence: Principles and applications*. John Wiley & Sons, **2012**.
2. Jablonski, A. Efficiency of anti-Stokes fluorescence in dyes. *Nature* **1933**, *131*, 839.
3. Weinberg, D.R.; Gagliardi, C.J.; Hull, J.F.; Murphy, C.F.; Kent, C.A.; Westlake, B.C.; Paul, A.; Ess, D.H.; McCafferty, D.G.; Meyer, T.J. Proton-coupled electron transfer. *Chemical Reviews* **2012**, *112*, 4016-4093.
4. Sobolewski, A.L.; Domcke, W. Computational studies of the photophysics of hydrogen-bonded molecular systems. *The Journal of Physical Chemistry A* **2007**, *111*, 11725-11735.
5. Schultz, T.; Samoylova, E.; Radloff, W.; Hertel, I.V.; Sobolewski, A.L.; Domcke, W. Efficient deactivation of a model base pair via excited-state hydrogen transfer. *Science* **2004**, *306*, 1765-1768 .
6. Perun, S.; Sobolewski, A.L.; Domcke, W. Role of electron-driven proton-transfer processes in the excited-state deactivation of the adenine−thymine base pair. *The Journal of Physical Chemistry A* **2006**, *110*, 9031-9038.
7. Dargiewicz, M.; Biczysko, M.; Improta, R.; Barone, V. Solvent effects on electron-driven proton-transfer processes: adenine–thymine base pairs. *Physical Chemistry Chemical Physics* **2012**, *14*, 8981-8989.
8. Sobolewski, A.L.; Domcke, W. Ab initio studies on the photophysics of the guanine-cytosine base pair. *Physical Chemistry Chemical Physics* **2004**, *6*, 2763-2771.
9. Sobolewski, A.L.; Domcke, W.; Hättig, C. Tautomeric selectivity of the excited-state lifetime of guanine/cytosine base pairs: The role of electron-driven proton-transfer processes. *Proceedings of the National Academy of Sciences of the United States of America* **2005**, *102*, 17903-17906.

10. Schwalb, N.K.; Temps, F. Ultrafast electronic relaxation in guanosine is promoted by hydrogen bonding with cytidine. *Journal of the American Chemical Society* **2007**, *129*, 9272-9273.
11. Markwick, P.R.L.; Doltsinis, N.L. Ultrafast repair of irradiated DNA: Nonadiabatic ab initio simulations of the guanine-cytosine photocycle. *The Journal of Chemical Physics* **2007**, *126*, 175102.
12. Groenhof, G.; Schäfer, L.V.; Boggio-Pasqua, M.; Goette, M.; Grubmüller, H.; Robb, M.A. Ultrafast deactivation of an excited cytosine−guanine base pair in DNA. *Journal of the American Chemical Society* **2007**, *129*, 6812-6819.
13. Yamazaki, S.; Taketsugu, T. Photoreaction channels of the guanine-cytosine base pair explored by long-range corrected TDDFT calculations. *Physical Chemistry Chemical Physics* **2012**, *14*, 8866-8877.
14. Sobolewski, A.L.; Domcke, W. Photophysics of intramolecularly hydrogen-bonded aromatic systems: Ab initio exploration of the excited-state deactivation mechanisms of salicylic acid. *Physical Chemistry Chemical Physics* **2006**, *8*, 3410-3417.
15. Rode, M.F.; Sobolewski, A.L. Ab initio study on the excited state proton transfer mediated photophysics of 3-hydroxy-picolinic acid. *Chemical Physics* **2012**, *409*, 41-48.
16. Karsili, T.N.V.; Marchetti, B.; Ashfold, M.N.R.; Domcke, W. Ab initio study of potential ultrafast internal conversion routes in oxybenzone, caffeic acid, and ferulic acid: Implications for sunscreens. *The Journal of Physical Chemistry A* **2014**, *118*, 11999-12010.
17. Sobolewski, A.L.; Domcke, W. Computational model of photocatalytic water splitting. *The Journal of Physical Chemistry A* **2008**, *112*, 7311-7313.
18. Sobolewski, A.L.; Domcke, W. Ab initio study of the energetics of photoinduced electron and proton transfer processes in a bio-inspired model of photochemical water splitting. *Chemical Physics Letters* **2009**, *479*, 144-148.
19. Sobolewski, A.L.; Domcke, W. Photoinduced water splitting with oxotitanium porphyrin: A computational study. *Physical Chemistry Chemical Physics* **2012**,

*14*, 12807-12817.

20. Liu, X.; Sobolewski, A.L.; Borrelli, R.; Domcke, W. Computational investigation of the photoinduced homolytic dissociation of water in the pyridine-water complex. *Physical Chemistry Chemical Physics* **2013**, *15*, 5957-5966.
21. Liu, X.; Sobolewski, A.L.; Domcke, W. Photoinduced oxidation of water in the pyridine–water complex: Comparison of the singlet and triplet photochemistries. *The Journal of Physical Chemistry A* **2014**, *118*, 7788-7795.
22. Liu, X.; Karsili, T.N.V.; Sobolewski, A.L.; Domcke, W. Photocatalytic water splitting with the acridine chromophore: A computational study. *The Journal of Physical Chemistry B* **2015**, *119*, 10664-10672.
23. Karsili, T.N.V.; Tuna, D.; Ehrmaier, J.; Domcke, W. Photoinduced water splitting via benzoquinone and semiquinone sensitisation. *Physical Chemistry Chemical Physics* **2015**, *17*, 32183-32193.
24. Liu, X.; Karsili, T.N.V.; Sobolewski, A.L.; Domcke, W. Photocatalytic water splitting with acridine dyes: Guidelines from computational chemistry. *Chemical Physics* **2016**, *464*, 78-85 .
25. Ehrmaier, J.; Karsili, T.N.V.; Sobolewski, A.L.; Domcke, W. Mechanism of photocatalytic water splitting with graphitic carbon nitride: Photochemistry of the heptazine–water complex. *The Journal of Physical Chemistry A* **2017**, *121*, 4754-4764.
26. Daniels, M. Excited states of the nucleic acids: Bases, mononucleosides, and mononucleotides. In *Photochemistry and photobiology of nucleic acids*, Elsevier: **1976**, 23-108.
27. Callis, P.R. Electronic states and luminescence of nucleic acid systems. *Annual Review of Physical Chemistry* **1983**, *34*, 329-357.
28. Crespo-Hernández, C.E.; Cohen, B.; Hare, P.M.; Kohler, B. Ultrafast excited-state dynamics in nucleic acids. *Chemical Reviews* **2004**, *104*, 1977-2020.
29. Chaiwongwattana, S.; Sapunar, M.; Ponzi, A.; Decleva, P.; Došlić, N.

Exploration of excited state deactivation pathways of adenine monohydrates. *The Journal of Physical Chemistry A* **2015**, *119*, 10637-10644.

30. Ritze, H.-H.; Lippert, H.; Samoylova, E.; Smith, V.R.; Hertel, I.V.; Radloff, W.; Schultz, T. Relevance of πσ* states in the photoinduced processes of adenine, adenine dimer, and adenine–water complexes. *The Journal of Chemical Physics* **2005**, *122*, 224320.
31. Canuel, C.; Elhanine, M.; Mons, M.; Piuzzi, F.; Tardivel, B.; Dimicoli, I. Time-resolved photoelectron and photoion fragmentation spectroscopy study of 9-methyladenine and its hydrates: A contribution to the understanding of the ultrafast radiationless decay of excited DNA bases. *Physical Chemistry Chemical Physics* **2006**, *8*, 3978-3987.
32. Nam, S.H.; Park, H.S.; Song, J.K.; Park, S.M. Photoinduced dynamics of hydrated adenine clusters. *The Journal of Physical Chemistry A* **2007**, *111*, 3480-3484.
33. Mitrić, R.; Werner, U.; Wohlgemuth, M.; Seifert, G.; Bonačić-Koutecký, V. Nonadiabatic dynamics within time-dependent density functional tight binding method. *The Journal of Physical Chemistry A* **2009**, *113*, 12700-12705.
34. Barbatti, M. Photorelaxation induced by water–chromophore electron transfer. *Journal of the American Chemical Society* **2014**, *136*, 10246-10249.
35. Kanvah, S.; Joseph, J.; Schuster, G.B.; Barnett, R.N.; Cleveland, C.L.; Landman, U. Oxidation of DNA: Damage to nucleobases. *Accounts of chemical research* **2009**, *43*, 280-287.
36. Nguyen, K.V.; Burrows, C.J. A prebiotic role for 8-oxoguanosine as a flavin mimic in pyrimidine dimer photorepair. *Journal of the American Chemical Society* **2011**, *133*, 14586-14589.
37. Nguyen, K.V.; Burrows, C.J. Photorepair of cyclobutane pyrimidine dimers by 8-oxopurine nucleosides. *Journal of Physical Organic Chemistry* **2012**, *25*, 574-577.
38. Anusiewicz, I.; Świerszcz, I.; Skurski, P.; Simons, J. Mechanism for repair of thymine dimers by photoexcitation of proximal 8-oxo-7, 8-dihydroguanine.

*The Journal of Physical Chemistry A* **2012**, *117*, 1240-1253.

39. Lu, Z.; Beckstead, A.A.; Kohler, B.; Matsika, S. Excited state relaxation of neutral and basic 8-oxoguanine. *The Journal of Physical Chemistry B* **2015**, *119*, 8293-8301.
40. Crespo-Hernandez, C.E.; Cohen, B.; Kohler, B. Base stacking controls excited-state dynamics in A-T DNA. *Nature* **2005**, *436*, 1141-1144.
41. Vayá, I.; Gustavsson, T.; Douki, T.; Berlin, Y.; Markovitsi, D. Electronic excitation energy transfer between nucleobases of natural DNA. *Journal of the American Chemical Society* **2012**, *134*, 11366-11368.
42. Markovitsi, D. UV-induced DNA damage: The role of electronic excited states. *Photochemistry and photobiology* **2016**, *92*, 45-51.
43. Zhang, Y.; Dood, J.; Beckstead, A.A.; Li, X.-B.; Nguyen, K.V.; Burrows, C.J.; Improta, R.; Kohler, B. Photoinduced electron transfer in DNA: Charge shift dynamics between 8-oxo-guanine anion and adenine. *The Journal of Physical Chemistry B* **2015**, *119*, 7491-7502.
44. Zhang, Y.; Dood, J.; Beckstead, A.A.; Li, X.-B.; Nguyen, K.V.; Burrows, C.J.; Improta, R.; Kohler, B. Efficient UV-induced charge separation and recombination in an 8-oxoguanine-containing dinucleotide. *Proceedings of the National Academy of Sciences* **2014**, *111*, 11612-11617.
45. Bucher, D.B.; Schlueter, A.; Carell, T.; Zinth, W. Watson–Crick base pairing controls excited-state decay in natural DNA. *Angewandte Chemie International Edition* **2014**, *53*, 11366-11369.
46. Zhang, Y.; de La Harpe, K.; Beckstead, A.A.; Improta, R.; Kohler, B. UV-induced proton transfer between DNA strands. *Journal of the American Chemical Society* **2015**, *137*, 7059-7062.
47. Kumar, A.; Sevilla, M.D. Excited state proton-coupled electron transfer in 8-oxoG-C and 8-oxoG-A base pairs: A time dependent density functional theory (TD-DFT) study. *Photochemical & Photobiological Sciences* **2013**, *12*, 1328-1340.
48. Born, M.; Oppenheimer, R. Zur Quantentheorie der Molekeln. *Annalen der*

*Physik* **1927**, *389*, 457-484.

49. Goodisman, J.; Colgate, S.O. Diatomic interaction potential theory: Vol. 1, fundamentals; vol. 2, applications. *Physics Today* **1974**, *27*, 47 .
50. Teller, E. The crossing of potential surfaces. *Journal of Physical Chemistry* **1937**, *41*, 109-116.
51. Michl, J. Photochemical reactions of large molecules. I. A simple physical model of photochemical reactivity. *Mol. Photochem* **1972**, *4*, 243-257.
52. Michl, J.; Bonacic-Koutecky, V. *Electronic aspects of organic photochemistry*. Wiley, **1990**.
53. Mead, C.A.; Truhlar, D.G. On the determination of Born–Oppenheimer nuclear motion wave functions including complications due to conical intersections and identical nuclei. *The Journal of Chemical Physics* **1979**, *70*, 2284-2296.
54. Yarkony, D.R. Diabolical conical intersections. *Reviews of Modern Physics* **1996**, *68*, 985.
55. Bernardi, F.; Olivucci, M.; Robb, M.A. Potential energy surface crossings in organic photochemistry. *Chemical Society Reviews* **1996**, *25*, 321-328.
56. Yarkony, D.R. Conical intersections: The new conventional wisdom. *The Journal of Physical Chemistry A* **2001**, *105*, 6277-6293.
57. Worth, G.A.; Cederbaum, L.S. Beyond Born-Oppenheimer: Molecular dynamics through a conical intersection. *Annu. Rev. Phys. Chem.* **2004**, *55*, 127-158.
58. Domcke, W.; Yarkony, D. *Conical intersections: Electronic structure, dynamics & spectroscopy*. World Scientific, **2004**; Vol. 15.
59. Martinez, T.J. Physical chemistry: Seaming is believing. *Nature* **2010**, *467*, 412.
60. Matsika, S.; Krause, P. Nonadiabatic events and conical intersections. *Annual review of physical chemistry* **2011**, *62*, 621-643.
61. Stolow, A. Femtosecond time-resolved photoelectron spectroscopy of polyatomic molecules. *Annual review of physical chemistry* **2003**, *54*, 89-119.

62. Domcke, W.; Yarkony, D.R.; Köppel, H. *Conical intersections: Theory, computation and experiment*. World Scientific, **2011**; Vol. 17.

63. Domcke, W.; Yarkony, D.R. Role of conical intersections in molecular spectroscopy and photoinduced chemical dynamics. *Annual review of physical chemistry* **2012**, *63*, 325-352.

64. Koga, N.; Morokuma, K. Determination of the lowest energy point on the crossing seam between two potential surfaces using the energy gradient. *Chemical physics letters* **1985**, *119*, 371-374.

65. Bearpark, M.J.; Robb, M.A.; Schlegel, H.B. A direct method for the location of the lowest energy point on a potential surface crossing. *Chemical physics letters* **1994**, *223*, 269-274.

66. Zilberg, S.; Haas, Y. Molecular photochemistry: A general method for localizing conical intersections using the phase-change rule. *Chemistry–A European Journal* **1999**, *5*, 1755-1765.

67. Yarkony, D.R. Marching along ridges. Efficient location of energy-minimized conical intersections of two states using extrapolatable functions. *The Journal of Physical Chemistry A* **2004**, *108*, 3200-3205.

68. Levine, B.G.; Coe, J.D.; Martínez, T.J. Optimizing conical intersections without derivative coupling vectors: Application to multistate multireference second-order perturbation theory (MS-CASPT2). *The Journal of Physical Chemistry B* **2008**, *112*, 405-413.

69. Truhlar, D.G.; Gordon, M.S. From force fields to dynamics: Classical and quantal paths. *Science* **1990**, *249*, 491-498.

70. Møller, C.; Plesset, M.S. Note on an approximation treatment for many-electron systems. *Physical Review* **1934**, *46*, 618-622.

71. Schirmer, J. Beyond the random-phase approximation: A new approximation scheme for the polarization propagator. *Physical Review A* **1982**, *26*, 2395-2416.

72. Roos, B.O.; Andersson, K. Multiconfigurational perturbation theory with level shift—the $Cr_2$ potential revisited. *Chemical physics letters* **1995**, *245*,

215-223.

73. Bartlett, R.J. Many-body perturbation theory and coupled cluster theory for electron correlation in molecules. *Annual Review of Physical Chemistry* **1981**, *32*, 359-401.

74. Trofimov, A.B.; Schirmer, J. An efficient polarization propagator approach to valence electron excitation spectra. *Journal of Physics B: Atomic, Molecular and Optical Physics* **1995**, *28*, 2299.

75. Dreuw, A.; Wormit, M. The algebraic diagrammatic construction scheme for the polarization propagator for the calculation of excited states. *Wiley Interdisciplinary Reviews: Computational Molecular Science* **2015**, *5*, 82-95.

76. Shepard, R. The multiconfiguration self-consistent field method. *Ab Initio Methods in Quantum Chemistry–II* **1987**, 63-200.

77. Serrano-Andrés, L.; Merchán, M. Quantum chemistry of the excited state: 2005 overview. *Journal of Molecular Structure: THEOCHEM* **2005**, *729*, 99-108.

78. González, L.; Escudero, D.; Serrano-Andrés, L. Progress and challenges in the calculation of electronic excited states. *ChemPhysChem* **2012**, *13*, 28-51.

79. Cramer, C.J. *Essentials of computational chemistry: Theories and models*. John Wiley & Sons, **2013**.

80. Helgaker, T.; Jorgensen, P.; Olsen, J. *Molecular electronic-structure theory*. John Wiley & Sons, **2014**.

81. Roos, B.O.; Andersson, K.; Fülscher, M.P.; Serrano-Andrés, L.; Pierloot, K.; Merchán, M.; Molina, V. Applications of level shift corrected perturbation theory in electronic spectroscopy. *Journal of Molecular Structure: THEOCHEM* **1996**, *388*, 257-276.

82. Halgren, T.A.; Lipscomb, W.N. The synchronous-transit method for determining reaction pathways and locating molecular transition states. *Chemical Physics Letters* **1977**, *49*, 225-232.

83. Roberts, G.M.; Marroux, H.J.B.; Grubb, M.P.; Ashfold, M.N.R.; Orr-Ewing, A.J. On the participation of photoinduced N–H bond fission in aqueous

adenine at 266 and 220 nm: A combined ultrafast transient electronic and vibrational absorption spectroscopy study. *The Journal of Physical Chemistry A* **2014**, *118*, 11211-11225.

84. Sobolewski, A.L.; Domcke, W. Computational studies of aqueous-phase photochemistry and the hydrated electron in finite-size clusters. *Physical Chemistry Chemical Physics* **2007**, *9*, 3818-3829.

85. Sobolewski, A.L.; Domcke, W. Photoinduced electron and proton transfer in phenol and its clusters with water and ammonia. *The Journal of Physical Chemistry A* **2001**, *105*, 9275-9283.

86. Peon, J.; Hess, G.C.; Pecourt, J.-M.L.; Yuzawa, T.; Kohler, B. Ultrafast photoionization dynamics of indole in water. *The Journal of Physical Chemistry A* **1999**, *103*, 2460-2466.

87. Bussandri, A.; van Willigen, H. FT-EPR study of the wavelength dependence of the photochemistry of phenols. *The Journal of Physical Chemistry A* **2002**, *106*, 1524-1532.

88. Sobolewski, A.L.; Domcke, W.; Dedonder-Lardeux, C.; Jouvet, C. Excited-state hydrogen detachment and hydrogen transfer driven by repulsive $^1\pi\sigma^*$ states: A new paradigm for nonradiative decay in aromatic biomolecules. *Physical Chemistry Chemical Physics* **2002**, *4*, 1093-1100.

89. Abel, B.; Buck, U.; Sobolewski, A.L.; Domcke, W. On the nature and signatures of the solvated electron in water. *Physical Chemistry Chemical Physics* **2012**, *14*, 22-34.

90. Kleinermanns, K.; Nachtigallová, D.; de Vries, M.S. Excited state dynamics of DNA bases. *International Reviews in Physical Chemistry* **2013**, *32*, 308-342.

91. Serrano-Andres, L.; Merchan, M.; Borin, A.C. Adenine and 2-aminopurine: Paradigms of modern theoretical photochemistry. *Proceedings of the National Academy of Sciences* **2006**, *103*, 8691-8696.

92. Sobolewski, A.L.; Domcke, W. The chemical physics of the photostability of life. *Europhysics News* **2006**, *37*, 20-23.

93. Nguyen, K.V.; Burrows, C.J. A prebiotic role for 8-oxoguanosine as a flavin

mimic in pyrimidine dimer photorepair. *Journal of the American Chemical Society* **2011**, *133*, 14586-14589.

94. Nguyen, K.V.; Burrows, C.J. Photorepair of cyclobutane pyrimidine dimers by 8-oxopurine nucleosides. *Journal of Physical Organic Chemistry* **2012**, *25*, 574-577.

95. Nguyen, K.V.; Burrows, C.J. Whence flavins? Redox-active ribonucleotides link metabolism and genome repair to the RNA world. *Accounts of chemical research* **2012**, *45*, 2151-2159.

96. Zhang, Y.; Dood, J.; Beckstead, A.; Chen, J.; Li, X.-B.; Burrows, C.J.; Lu, Z.; Matsika, S.; Kohler, B. Ultrafast excited-state dynamics and vibrational cooling of 8-oxo-7,8-dihydro-2′-deoxyguanosine in $D_2O$. *The Journal of Physical Chemistry A* **2013**, *117*, 12851-12857.

97. Jayanth, N.; Ramachandran, S.; Puranik, M. Solution structure of the DNA damage lesion 8-oxoguanosine from ultraviolet resonance Raman spectroscopy. *The Journal of Physical Chemistry A* **2009**, *113*, 1459-1471.

98. Tuna, D.; Domcke, W. Excited-state deactivation in 8-oxo-deoxyguanosine: Comparison between anionic and neutral forms. *Physical Chemistry Chemical Physics* **2016**, *18*, 947-955.

# Acknowledgements

First and foremost, I would like to thank my supervisor Prof. Wolfgang Domcke, who offered me a position to do my doctorate study in the group. In the past four years, he gave me the patient, encouraging and inspiring guidance in science and provided many opportunities for me to learn everything new. His enthusiasm and earnest in science have impressed, influenced and will be influencing me in my future scientific career.

I would like to thank Dr. Tolga N. V. Karsili, who supervised me in the first two years of my doctorate period. He taught me a lot of calculation skills hand by hand and we had so many helpful discussion on my work. We had a pleasant time working together and look forward to more cooperation in the future.

I would like to express my thanks to my colleagues in the group. We had a wonderful working atmosphere and had so many fruitful scientific discussion. Special thanks are given to Johannes Ehrmair, who is not only a good work partner but also helped me a lot with my after-work life in Munich.

Also, I would like to thank my friends in Munich. They made my stay in Munich greater and more enjoyable. I will never forget those warm hugs, late-night talks, delicious food and happy hours on Alps.

Finally, I am so grateful for the support of my family: my father Xing Wu and my mother Yuemei Pan are always my strong supporters when I'm pursuing my own life. My sisters, brothers-in-law and brother help so much take care of my parents, which makes me at ease while studying abroad.

Scholarship support from the China Scholarship Council is greatly acknowledged.

# List of Publications

4. Mechanisms of the Photoreactivity of Adenine in Water. Xiuxiu Wu, Johannes Ehrmaier, Andrzej L. Sobolewski, Tolga N. V. Karsili and Wolfgang Domcke: submitted.

3. Photoinduced Hydrogen-Transfer Reactions in Pyridine-Water Clusters: Insights from Excited-State Electronic-Structure Calculations. Xiaojuan Pang, Johannes Ehrmaier, Xiuxiu Wu, Chenwei Jiang, Weiwei Xie, Andrzej L. Sobolewski, Wolfgang Domcke: *Chem. Phys*. Accepted.

2. Role of Electron-Driven Proton-Transfer Processes in the Ultrafast Deactivation of Photoexcited Anionic 8-oxoGuanine-Adenine and 8-oxoGuanine-Cytosine Base Pairs. Xiuxiu Wu, Tolga N. V. Karsili, Wolfgang Domcke: *Molecules* **2017**, 135, 22.

1. Excited-State Deactivation of Adenine by Electron-Driven Proton-Transfer Reactions in Adenine-Water Clusters: A Computational Study. Xiuxiu Wu, Tolga N.V. Karsili, Wolfgang Domcke: *ChemPhysChem* **2016**, 17, 1298-1304.

# Appendices

# Paper 1

**Mechanisms of the Photoreactivity of Adenine in Water.** Xiuxiu Wu, Johannes Ehrmaier, Andrzej L. Sobolewski, Tolga N. V. Karsili and Wolfgang Domcke: submitted.

# Mechanisms of the photoreactivity of adenine in water

Xiuxiu Wu[1], Johannes Ehrmaier[1], Andrzej L. Sobolewski[2], Tolga N.V. Karsili[3], and Wolfgang Domcke*[1]

[1] *Department of Chemistry, Technical University of Munich, D-85747 Garching, Germany*

[2] *Institute of Physics, Polish Academy of Sciences, PL-02668 Warsaw, Poland*

[3] *Department of Chemistry, University of Lousiana at Lafayette, LA 70504, USA*

## Abstract

The mechanisms of photoinduced reactions of adenine with water molecules in hydrogen-bonded adenine-water complexes were investigated with *ab initio* wave-function-based electronic-structure calculations. Two excited-state electron/proton transfer reaction mechanisms have been characterized: H-atom abstraction from water by photoexcited adenine as well as H-atom transfer from photoexcited adenine or the (adenine+H) radical to water. In the water-to-adenine H-atom transfer reaction, an electron from one of the p orbitals of the water molecule fills the hole in the n (π) orbital of the nπ* (ππ*) excited state of adenine, resulting in a charge-separated electronic state. The electronic charge separation is neutralized by the transfer of a proton from the water molecule to adenine, resulting in the (adenine+H)…OH biradical in the electronic ground state. In the adenine-to-water H-atom transfer reaction, πσ* states localized at the acidic sites of adenine provide the mechanism for the photoejection of an electron from adenine, which is followed by proton transfer to the hydrogen-bonded water molecule, resulting in the (adenine-H)…$H_3O$ biradical. The energy profiles of the photoreactions have been computed as relaxed scans with the ADC(2) electronic-structure method. These reaction mechanisms, which involve the reactivity of adenine with hydrogen-bonded water molecules, compete with the well-established intrinsic excited-state deactivation mechanisms of adenine via ring-puckering or ring-opening conical intersections. By providing additional decay channels, the electron/proton exchange reactions with water can account for the significantly shorted excited-state lifetime of adenine in aqueous environments. These findings indicate that adenine was not only a photostabilizer at the beginning of life, but also a primordial photocatalyst for water splitting.

Key words: adenine-water complex, electron-transfer, proton-transfer, water splitting

## 1. Introduction

The photochemistry of nucleobases in solution and in molecular beams has been intensively investigated in the past two decades.[1-3] The most studied representative of DNA bases is 9H-adenine. Its electronic spectroscopy and photophysics have been studied extensively with experimental[1, 2, 4-10] and computational[3, 11-25] methods. Several generic ultrafast decay mechanisms of excited states of 9H-adenine have been identified. There is consensus that the ultrafast excited-state decay of adenine occurs primarily via conical intersections which are accessible by out-of-plane puckering of the six-membered aromatic ring[12-15, 20, 21, 23]. It is still controversial whether the $S_1(n\pi^*)$ state is populated as a transient intermediate after photoexcitation of the two bright $^1\pi\pi^*$ states of 9H-adenine or whether the decay occurs from the main absorbing $^1\pi\pi^*(L_a)$ state directly to the ground state.[3] In addition, conical intersections accessible via NH-bond fission of the NH or $NH_2$ groups of adenine have been identified as possible ultrafast excited-state relaxation pathways.[11, 13, 18, 26-31] Overall, it is nowadays widely accepted that ultrafast excited-state deactivation of DNA/RNA bases via conical intersections is an essential mechanism of their protection from UV-induced damage.[1-3, 16, 17]

There exists diverse evidence that the photochemistry of adenine can be significantly altered in aqueous environments. For example, the excited-state lifetime of adenine, which has been determined to be 1.2 picoseconds in a molecular beam[4, 27, 28], becomes much shorter (about 200 fs) in aqueous solution[32]. Solvation effects in water may modify the electronic excitation energies which may affect the barriers which control the accessibility of conical intersections. In addition, hydrogen-bonding interactions with surrounding solvent molecules may lead to explicit participation of solvent molecules in the excited-state relaxation dynamics, resulting in new photorelaxation channels not available in the isolated adenine molecule. Although experimental data on the photoinduced dynamics of microhydrated adenine are limited,[33-35] theoretical explorations of the excited-state potential-energy surfaces and nonadiabatic dynamics simulations have predicted that electron-driven proton-transfer (EDPT) processes from hydrogen-bonded water molecules to the basic sites of adenine may contribute to ultrafast excited-state relaxation.[36, 37] Evidence for this channel was first found by Barbatti in excited-state dynamics simulations for the 7H-adenine-$(H_2O)_5$ cluster, using second-order algebraic diagrammatic construction (ADC(2)) method.[38] With the same method, Došlić and co-workers performed static reaction-path and nonadiabatic dynamics investigations for the 9H-adenine-$(H_2O)$ complex, in which a single water is hydrogen-bonded to the N3 atom.[36] They identified a photoinduced EDPT process from the water molecule to the N3 atom of adenine which could be responsible for the observed shortened excited-state lifetime of adenine in aqueous environments.[32, 35] In a previous study, we extended the work of Refs. 36, 38 by calculating the energy profiles of excited-state minimum-energy reaction paths for 9H-adenine-$(H_2O)_5$ clusters, considering reactions at the three basic sites (N1, N3 and N7) with the ADC(2) electronic-structure method.[37] For two of the basic sites (N1 and N7), a barrierless or nearly barrierless excited-state reaction path towards a low-lying $S_1$–$S_0$ conical intersection was found.[37]

Apart from the three basic sites, 9H-adenine possesses two acidic groups (N9H, N10$H_2$) which have been shown to be involved in the fast (nonstatistical) photodissociation of adenine in the gas phase.[11, 18, 29, 30] With femtosecond time-resolved fluorescence up-conversion measurements in aqueous solution an abrupt shortening of the excited-state lifetime of adenine at $\lambda_{exc} \approx 265$ nm was observed and interpreted as evidence for a radiationless electronic relaxation pathway involving the lowest $^1\pi\sigma^*$ state.[39] It is well known that the photodetachment of H atoms from acidic chromophores in aqueous solution via repulsive $^1\pi\sigma^*$ states can yield hydrated electrons.[40] By the detection of hydrated electrons formed upon at 220 nm excitation of 9H-adenine in aqueous solution, Roberts et al. found evidence for a photorelaxation pathway via a repulsive $^1\pi\sigma^*$ state.[41] Very recently, Szabla and co-workers explored features of the excited-state potential-energy (PE) surface of the 9H-adenine-$(H_2O)_5$ cluster with the ADC(2) method.[42] These authors showed that a $\pi\sigma^*$- mediated EDPT along $H_2O$ wires may be one of the deexcitation channels channels of adenine in a water environment.

Despite many experimental and computational studies of the excited-state deactivation mechanisms of 9H-adenine (henceforth adenine) in aqueous solution, the role of $^1\pi\pi^*$, $^1n\pi^*$ and $^1\pi\sigma^*$ excited states and their conical intersections in the ultrafast radiationless excited-state decay dynamics of adenine is not yet fully understood. In the present work, we carried out a systematic computational exploration of the excited-state EDPT reaction mechanisms in hydrogen-bonded complexes of adenine with a single water molecule with the ADC(2) electronic-structure method.

The EDPT reactivities of the three basic sites (N1, N3, N7) and the two acidic groups of adenine (N9H, N10H$_2$) are considered. For this purpose, the geometries of five adenine-H$_2$O complexes, shown in Figs. 1 and 2, were optimized in the electronic ground state. Minimum-energy excited-state reaction paths were computed as relaxed scans with the ADC(2) method and the energy profiles of electron/proton transfer reactions between adenine and water were characterized. The one-dimensional relaxed scans along the OH distance of the water molecule are complemented by two-dimensional relaxed PE surfaces, including the O-N donor-acceptor distance. This way, the barriers for the excited-state electron/proton transfer reaction from water to the three basic sites of adenine could be determined for the first time. In addition, we have studied the mechanism of the photodetachment of the excess hydrogen atom from the (adenine+H) radical for the example of the N3 site. It is shown that the photodetachment of the H-atom as well as the transfer of the H-atom to a hydrogen-bonded water molecule are nearly barrierless reactions which can be induced by low-energy photons. This comprehensive "bottom up" investigation of the photoreactivity of complexes of adenine with a single water molecule provides insight into the role of EDPT reactions in microsolvated adenine. These data may serve as guidelines for future investigations of the aqueous photochemistry of adenine with *ab initio* nonadiabatic nuclear-dynamics simulations.

## 2. Computational methods

The ground-state equilibrium geometries of the adenine molecule and of the five adenine-H$_2$O complexes were optimized using second-order Møller–Plesset perturbation theory (MP2)[43]. $C_s$ symmetry was imposed in these calculations, that is, the amino group of adenine was constrained to be planar and the water molecule was constrained to be oriented either in the plane of adenine (see Fig. 1) or perpendicular to this plane (see Fig. 2). The $C_s$ symmetry constraint is very helpful for the calculation of excited-state minimum-energy reaction paths and two-dimensional relaxed excited-state PE surfaces. Some of these calculations could not be performed without this constraint due to the near degeneracy of $^1\pi\pi^*$, $^1n\pi^*$ and $^1\pi\sigma^*$ excited-states. Vertical excitation energies and oscillator strengths were calculated with the ADC(2)[44, 45] method, which is a computationally efficient single-reference propagator method. The correlation-consistent double-ζ basis set augmented with polarization functions and diffuse functions on all atoms (aug-cc-pVDZ)[46] was used.

For the adenine-N1···H-OH, adenine-N3···H-OH and adenine-N7···H-OH complexes, the reaction paths and their energy profiles for H transfer from the hydrogen-bonded water molecule to adenine were constructed as so-called relaxed scans, using the bond length $R_{\mathrm{OH}}$ of the hydrogen-bonded OH group of water as the driving coordinate. For a fixed value of the driving coordinate $R_{\mathrm{OH}}$, the remaining nuclear coordinates of the adenine-$H_2O$ complex were relaxed in the respective electronic state with $C_s$ symmetry constraint. The vertical excitation energies of the $^1\pi\pi^*$ and $^1n\pi^*$ states of adenine were computed with the ADC(2) method along the reaction path optimized in the electronic ground state. The reaction paths for EDPT processes from water to adenine in the lowest $^1\pi\pi^*$ and $^1n\pi^*$ excited states were constructed as relaxed scans by optimizing the energy of the selected state for fixed $R_{\mathrm{OH}}$ with the ADC(2) method. The energies of the other excited states and the energy of the electronic ground state were computed at the optimized geometries with the MP2 and ADC(2) methods, respectively. In addition, the PE surfaces in the vicinity of the saddle point separating the Franck-Condon region from the H-atom-transfer region were computed as two-dimensional relaxed scans. For fixed values of the driving coordinates $R_{\mathrm{ON}}$ (the distance of the oxygen atom of water from the nitrogen atom of adenine) and $R_{\mathrm{OH}}$, all other nuclear coordinates were optimized in the respective excited state with $C_s$ symmetry constraint. The geometries of the saddle points were estimated from the two-dimensional relaxed PE surfaces and subsequently fully optimized.

For the complexes adenine-N9-H···$OH_2$ and adenine-N10-H···$OH_2$, involving hydrogen-bonding of water with acidic groups of adenine, the reaction paths and their energy profiles for H-atom transfer from adenine to the water molecule in the $^1\pi\sigma^*$ excited state were calculated as relaxed scans, using the bond length $R_{\mathrm{NH}}$ of the corresponding imino/amino group of adenine as the driving coordinate. $C_s$ symmetry is enforced, the water molecule being constrained to be perpendicular to the molecular plane of adenine. This geometry is suitable for the attachment of the mobile H-atom to the water molecule which generates a $H_3O$ radical. In these calculations, the energy of the electronic ground state was calculated at the relaxed geometries of the $^1\pi\sigma^*$ state using the MP2 method. For comparison, analogous relaxed scans were also computed for the free N9-H and N10-H bonds of isolated adenine. The PE profiles for the photodetachment of the excess H-atom from the (adenine+H) radical were analogously computed as relaxed scans optimized in the $^2\pi\sigma^*$ excited state of the radical using the unrestricted ADC(2) method. The energies of the $D_0$ ground state and of the $^2n\pi^*$ and $^2\pi\pi^*$

excited states were calculated along the relaxed scan with the unrestricted MP2 and ADC(2) methods, respectively. The MP2 and ADC(2) calculations were carried out with the TURBOMOLE program package[47] using the resolution-of-the-identity (RI) approximation.[48, 49]

# 3. Results and discussion

## 3.1 Molecular structures and vertical electronic excitation energies

As adenine has both basic sites (N1, N3, N7) and acidic sites (N9-H, N10-$H_2$), surrounding water molecules can act either as hydrogen-bond donors (e.g. adenine-N···H-O-H) or as hydrogen-bond acceptors (e.g. adenine-NH···$OH_2$), There exist therefore three adenine-$H_2O$ structures in which adenine is an H-atom acceptor and two structures, in which adenine is an H-atom donor. The former three structures are displayed in Fig. 1. The latter two structures are shown in Fig. 2. The calculated hydrogen-bond lengths are included in the figures.

The hydrogen bonds with the basic acceptor sites of adenine are notably shorter (and thus stronger) than the hydrogen bonds with the acidic donor sites, see Fig. 1. Among the three conformers with hydrogen-bond accepting sites, the conformer with $H_2O$ coordination at the N7 site exhibits the shortest (and thus strongest) hydrogen bond. In the adenine-$(H_2O)_5$ cluster of $C_1$ symmetry, the hydrogen-bond lengths are shorter by about 0.1 Å than the corresponding hydrogen-bond lengths in clusters of adenine with a single water molecule.[37] This implies that the hydrogen bonds are strengthened by cooperative effects in larger clusters, which is favorable for H-atom-transfer processes. Among the conformers with hydrogen bonding of water to the acidic sites of adenine, the hydrogen-bond length of conformer N9-H is slightly shorter than that of conformer N10-H, which indicates that the photoinduced H-atom transfer reaction may occur more readily in the N9-H conformer.

The vertical excitation energies and corresponding oscillator strengths (in parentheses) of the lowest four singlet excited states ($^1\pi\pi^*(L_a)$, $^1\pi\pi^*(L_b)$, $^1n\pi^*$ and $^1\pi\sigma^*$) of the five adenine-$H_2O$ complexes, computed at the ADC(2) level, are listed in Table 1. The corresponding vertical excitation energies of isolated adenine are also given for comparison. The molecular orbitals involved in the excitation of the lowest $^1\pi\pi^*$, $^1n\pi^*$ and $^1\pi\sigma^*$ excited states are displayed in Fig. 3 for the adenine-N3…H-OH and adenine-N9-H…$OH_2$ complexes (as representatives of the five conformers).

For both adenine-$H_2O$ conformers in Fig. 3, excitation from the 7"(π) orbital to the 9a"(π*) orbital gives rise to the lowest $^1\pi\pi^*$ state. The $^1n\pi^*$ excited state arises from the excitation from the 33a'(n) orbital to the 9a"(π*) orbital. It can be seen by inspection of Fig. 3 that part of the 33a′ orbital is localized on the O atom of the water molecule, which reveals that the hydrogen bond of the water molecule with the N3 atom of adenine has partially covalent character. For the conformer adenine-N9-H…$OH_2$, the diffuse σ* orbital (34a') localized mainly on the imino group of adenine is displayed.

In isolated adenine, the $^1n\pi^*$ state is the lowest singlet excited state. Excitation of this state involves the promotion of an electron from an in-plane nitrogen 2p orbital to a ring-centered π* orbital. The strongly absorbing bright $^1\pi\pi^*(L_a)$ state involves a π → π* orbital promotion, both of which are delocalized over the entire molecule. The $^1\pi\sigma^*$ state is the fourth excited state. It involves the promotion of an electron from the highest π orbital to the lowest diffuse σ* orbital which is antibonding with respect to the NH bonds. As is well known from many previous computational studies of adenine in aqueous environments, the excitation energy of the $^1\pi\pi^*(L_a)$ state is redshifted, while the excitation energy of the $^1n\pi^*$ state is blue-shifted relative to isolated adenine. As a result, the ordering of the excited states of adenine is $^1\pi\pi^*(L_a)$, $^1n\pi^*$ and $^1\pi\sigma^*$ in water clusters[36, 37] and in aqueous solution[50-52]. The stabilization of the energy of the $^1\pi\pi^*(L_a)$ state results from polarization effects which stabilize the π* orbital more strongly than the π orbital, leading to a decrease of the π-π* energy gap. The destabilization of the energy of the $^1n\pi^*$ state arises from a substantial stabilization of the nitrogen-centered nonbonding orbital by the hydrogen bonding with water, as a result of the partial delocalization of the n orbital onto the water molecule (see the 33a' orbital in Fig. 3). The lowering of the energy of the n orbital leads to an increase of the n-π* energy gap. Due to this destabilization of the $^1n\pi^*$ state, the $^1\pi\pi^*$ state becomes the lowest excited state of adenine in water clusters. The $^1\pi\pi^*(L_b)$ and $^1n\pi^*$ states are found to be nearly degenerate in adenine-$H_2O$ clusters at the ADC(2) level. The relative ordering depends on the specific cluster, see Table 1. The electronic state orderings and the vertical excitation energies calculated here with $C_s$ symmetry constraint are in agreement with those obtained by Došlić and co-workers[36] for two adenine-$H_2O$ complexes without symmetry constraints.

### 3.2 Photoinduced H-atom abstraction from water molecules

### (a) N3 site

Each of the three basic sites of adenine, N1, N3, N7, is capable of abstracting an H-atom from the hydrogen-bonded water molecule after photoexcitation. We select the conformer adenine-N3…H-OH (middle panel of Fig. 1) for a detailed analysis of the photophysics of these adenine-$H_2O$ complexes. The energy profiles of relaxed scans for the electron/proton-transfer process from water to adenine in the ground state and in the lowest two excited states of this conformer are displayed in Fig. 4. The energy profiles shown in Fig. 4 consist of two parts which are separated, for clarity, by the dashed vertical line. The left part ($R_{OH} < 1.3$ Å) corresponds to the Franck-Condon region of the adenine-$H_2O$ complex. In this region, the energies of the ground state (filled black circles), the locally excited $^1\pi\pi^*$ state (red open circles) and the locally excited $^1n\pi^*$ state (blue open circles) were calculated along the H-atom-transfer reaction path optimized in the $S_0$ state. In the right part of Fig. 4(a) ($R_{OH} > 1.3$ Å), the energies of the ground state (black open circles), $^1\pi\pi^*$ (filled red circles) and $^1n\pi^*$ (blue open circles) were calculated along the H-atom-transfer reaction path optimized in the $^1p_z\pi^*$ charge-transfer (CT) state. The $^1p_z\pi^*$(CT) state involves the transfer of an electron from the $p_z$ orbital of $H_2O$ to the lowest $\pi^*$ orbital of adenine. This part of the figure corresponds to the (adenine+H)…OH biradical, see the structure shown as inset in Fig. 4(a). The left part of Fig 4(b) is the same as the left part of Fig 4. (a). In the right part of Fig. 4(b) ($R_{OH} > 1.3$ Å), the energies of the ground state (black open circles), the $^1\pi\pi^*$ state (open red circles) and the $^1n\pi^*$ state (blue full circles) were calculated along the H-atom-transfer reaction path optimized in the $^1p_{x,y}\pi^*$ CT state. The $^1p_{x,y}\pi^*$(CT) state involves the transfer of an electron from the $p_{x,y}$ orbital of $H_2O$ to the lowest $\pi^*$ orbital of adenine. The discontinuities of the energy profiles at $R_{OH} = 1.3$ Å reflect the different geometries in two reaction paths.

Along the reaction path optimized in the $S_0$ state ($R_{OH} < 1.3$ Å), the PE functions of the locally excited $^1\pi\pi^*$ and $^1n\pi^*$ states are essentially parallel to the PE function of the electronic ground state, which indicates that there exists no driving force for the H transfer from water to adenine in these electronic states. Along the reaction paths optimized in either of the CT states ($R_{OH} > 1.3$ Å), on the other hand, the $^1p_z\pi^*$(CT) and $^1p_{x,y}\pi^*$(CT) states are strongly stabilized by the transfer of the proton from water to adenine, which neutralizes the electronic charge separation. In Fig. 4(a), the $^1p_z\pi^*$(CT) state is the lowest excited state, while in Fig. 4(b) the $^1p_{x,y}\pi^*$(CT) state is the lowest excited state.

The large gradients of the charge-transfer energies with respect to $R_{OH}$ indicate a strong driving force for proton transfer which results from the charge-separated character of the $^1p_z\pi^*$(CT) and $^1p_{x,y}\pi^*$(CT) states. The energy of the closed-shell ground state, in contrast, increases strongly with increasing $R_{OH}$. As a result, the energy curves of the $^1p_z\pi^*$(CT) and $^1p_{x,y}\pi^*$(CT) states cross the ground-state energy profile near $R_{OH}$ = 2.4 Å, see Fig. 4. Since both energy profiles were calculated at the same geometries, these curve crossings are true crossings (conical intersections). In Fig. 4(a), the $^1p_z\pi^*$(CT) state and the $S_0$ state have the same spatial and spin symmetry ($^1A'$). Therefore, the $^1p_z\pi^*(CT)/S_0$ curve crossing represents a so-called same-symmetry conical intersection[53]. In Fig. 4(b), on the other hand, the $^1p_{x,y}\pi^*$(CT) state has $^1A''$ symmetry and the $^1p_{x,y}\pi^*(CT)/S_0$ curve crossing represents a so-called symmetry-allowed conical intersection[53]. Depending on the topography of the adiabatic PE surfaces and the nonadiabatic coupling elements at these conical intersections, the reaction can lead to internal conversion to the initial ground state of the complex (adiabatic path, aborted H-atom-transfer reaction) or to an (adenine+H)...OH biradical (diabatic path, successful H-atom-transfer reaction).

The energy profiles for $R_{OH}$ < 1.3 Å and $R_{OH}$ > 1.3 Å in Fig. 4 correspond to minimum-energy reaction paths in different valleys of the multidimensional PE surface of the adenine-$H_2O$ complex. To understand the connection of these energy profiles, the barrier separating the two valleys has to be estimated. We therefore calculated two-dimensional PE surfaces as relaxed scans in the vicinity of the energy barrier for H-atom transfer from water to adenine at the ADC(2) level. Considering the proton-transfer coordinate $R_{OH}$ and the distance $R_{ON}$ between the O-atom of water and the N-atom of adenine as reaction coordinates, the energies of the lowest excited states of $^1A'$ symmetry ($^1\pi\pi^*$ and $^1p_z\pi^*$(CT) states) and $^1A''$ symmetry ($^1n\pi^*$ and $^1p_{x,y}\pi^*$(CT) states) were optimized for fixed $R_{OH}$ and $R_{ON}$ with respect to the remaining nuclear coordinates with $C_s$ symmetry constraint. The resulting relaxed PE surfaces for the adenine-N3...H-OH conformer are shown in Fig. 5.

Fig. 5(a) shows the relaxed PE surface of the lowest excited state of $^1A'$ symmetry ($^1\pi\pi^*$ and $^1p_z\pi^*$(CT) states). The well on the left-hand side of Fig. 5(a) represents the minimum of the lowest locally excited $^1\pi\pi^*$ state (red triangle at $R_{OH} \approx$ 1.0 Å, $R_{ON} \approx$ 2.8 Å), while the deep valley on the right-hand side (red triangle at $R_{OH} \approx$ 1.8 Å, $R_{ON} \approx$ 2.8 Å) represents the (adenine+H)...OH biradical. The wells are separated by a saddle point (red star at $R_{OH} \approx$ 1.25 Å, $R_{ON} \approx$ 2.4 Å), which represents the transition state for the H-atom transfer reaction. The energy of the saddle point is 5.30 eV above the energy minimum of the electronic ground state. It is about 0.60 eV higher than the energy minimum of the lowest $^1\pi\pi^*$ excited state (4.70 eV) and 0.30 eV higher than the vertical excitation energy of the lowest $^1\pi\pi^*$ state (5.03 eV). The barrier with respect to the $^1\pi\pi^*$ minimum is about 0.4 eV higher than the barrier determined by Došlić and coworkers[36] for the same adenine-$H_2O$ conformer without symmetry constraints. The $C_s$ symmetry constraint thus leads to an overestimation of the barrier. The barrier of about 0.2 eV estimated without symmetry constraints is of the order of the zero-point energy and is therefore insignificant. H-atom transfer from water to photoexcited adenine should readily occur by tunneling.

The two-dimensional relaxed PE surface for the lowest excited state of $^1A''$ symmetry ($^1n\pi^*$ and $^1p_{x,y}\pi^*$(CT) states) is displayed in Fig. 5(b). The saddle point on the $^1A''$ surface is 5.07 eV above the ground-state energy minimum, which is 0.54 eV higher than the energy minimum of the $^1n\pi^*$ excited state (4.53 eV), but lower than the vertical excitation energy of the bright $^1\pi\pi^*$ state (5.14 eV). Since interconversion of the locally excited $^1\pi\pi^*$ and $^1n\pi^*$ states of adenine is efficient,[3] a barrierless reaction path for H-atom abstraction is expected on the $^1A''$ surface of the adenine-N3…H-OH conformer.

### (b) N1 and N7 sites

The mechanisms of the H-atom abstraction reactions at the N1 and N7 sites of adenine are similar to those described in detail for the N3 site and are therefore discussed more briefly. Fig. 6 (a) displays the PE profiles of the ground state, the locally excited $^1\pi\pi^*$ and $^1n\pi^*$ states, and the $^1p_z\pi^*$(CT) and $^1p_{x,y}\pi^*$(CT) states along the H-atom-transfer coordinate $R_{OH}$ for the adenine-N1…H-OH conformer. The energy of the $^1p_z\pi^*$(CT) state has been optimized for $R_{OH} > 1.3$ Å. The corresponding data for the adenine-N7…H-OH conformer are shown in Fig. 6(b). Overall, the energy profiles are very similar to those discussed in detail for the adenine-N3…H-OH conformer above. The location of the conical intersection of the $^1p_z\pi^*$(CT) state with the $S_0$ state is near $R_{OH} \approx 2.6$ Å for the adenine-N1…H-OH conformer, 0.3 Å further out than for the other two conformers. This is an indication that the H-atom abstraction reaction may be somewhat less efficient for the adenine-N1…H-OH conformer than for the other two conformers.

Two-dimensional relaxed PE surfaces for H-atom transfer from water to adenine were also calculated for the adenine-N1…H-OH and adenine-N7…H-OH conformers, considering the lowest adiabatic $^1A'$ surface. These PE surfaces are shown in Fig. 7. In the adenine-N1…H-OH conformer, the saddle point is located at $R_{OH} \approx 1.2$ Å, $R_{ON} \approx 2.5$ Å and the energy is 5.40 eV, 0.6 eV above the energy minimum of the $^1\pi\pi^*$ state. In the adenine-N7…H-OH conformer (Fig. 7(b)), the estimated energy of the saddle point is 4.90 eV, which is about 0.30 eV higher than the energy minimum of the lowest $^1\pi\pi^*$ excited state (4.60 eV), but is almost the same as the vertical $^1\pi\pi^*$ excitation energy. The H-atom transfer reaction from water to adenine is thus likely to be barrierless in the adenine-N7…H-OH conformer.

### 3.3 H-atom transfer from adenine to water

#### (a) H-atom photodetachment from isolated adenine

As a reference for the investigation of H-atom transfer reactions from adenine to hydrogen-bonded water molecules, we calculated the PE profiles for H-atom detachment reaction from the imino and amino groups of isolated adenine as relaxed scans. The energies of the $S_0$ state and the lowest $^1\pi\pi^*$ and $^1n\pi^*$ excited states were calculated at geometries which were optimized in the $^1\pi\sigma^*$ state for fixed $R_{NH}$. Adenine was constrained to be planar. The $C_s$ symmetry constraint is necessary for successful geometry optimizations of the quasi-degenerate excited states of adenine.

The PE profiles for the detachment of the H-atom from the imino group of adenine are shown in Fig. 8(a). While the energies of the $^1\pi\pi^*$ and $^1n\pi^*$ states are parallel to the PE function of the electronic ground state, the PE profile of the $^1\pi\sigma^*$ state is dissociative with a tiny barrier near 1.2 Å. For $R_{NH} < 1.3$ Å, the energy of the optimized $^1\pi\sigma^*$ state is seen to be nearly degenerate with the energies of the $^1\pi\pi^*$ and $^1n\pi^*$ states calculated at the same geometries, see Fig. 8(a). This is an indication of the existence of extended seams of intersection among the PE surfaces of these states in the Franck-Condon region. The $^1\pi\sigma^*$ PE surface exhibits a crossing with the $S_0$ PE surface at an NH distance of 1.75 Å. It has been postulated that the nearly barrierless reaction path in the $^1\pi\sigma^*$ state from the Franck-Condon region to this conical intersection provides an additional channel for ultrafast excited-state deactivation of adenine[11, 13, 18, 27-31]. Perun et al.[13] computed relaxed PE profiles of adenine in the $^1\pi\sigma^*$ state along the N9-H and N10-H bonds with the CASSCF/CASPT2 method. Upon stretching of the N9-H bond to 1.78 Å, a $^1\pi\sigma^*/S_0$ energy crossing was found to occur at an energy of 4.7 eV, which is close to the results at the ADC(2) level. According to the present calculations, the energy barrier for dissociation is 0.50 eV for the N9-H group, which is lower than the CASSCF/CASPT2 result (1.0 eV) of Perun et al.[13] and the experimental estimate (0.9 eV)[54, 55]. Szabla et al.[42] calculated the PE profile of the $^1\pi\sigma^*$ state of adenine as a rigid scan along the N9-H bond distance at the ADC(2) level without symmetry constraint. They found a $^1\pi\sigma^*/S_0$ conical intersection which is located at $R_{NH} \approx 2.2$ Å with an energy of 5.50 eV. It is considerably further out and higher in energy than the intersection revealed by the relaxed scan ($R_{NH}$ = 1.75 eV) with an energy of 4.90 eV. As expected, the energy barrier of the minimum-energy path is lower than the barrier indicated by the rigid scan. Experimentally, Nix et al. obtained total kinetic energy release (TKER) spectra in the excitation wavelength range $280 > \lambda > 214$ nm.[29] They determined the onset of the N-H fission reaction on the $^1\pi\sigma^*$ PE surface at 233 nm.

The energy profile of the relaxed scan for the H-atom detachment reaction from the amino group (N10-H) in the $^1\pi\sigma^*$ state of isolated adenine is shown in Fig. 8(b). The barrier is notably higher (≈ 0.6 eV) than found for the stretching N9-H bond. The $^1\pi\sigma^*/S_0$ CI is located at $R_{NH} = 2.05$ Å, 0.3 Å further out than for the stretching of the N9-H bond. These results are in good agreement with results obtained earlier by Perun et al. with the CASSCF/CASPT2 method.[13] The energy of the maximum of the $^1\pi\sigma^*$ PE profile can be considered as a rough estimate of the threshold for the photodetachment of fast hydrogen atoms from adenine. By time-resolved mass spectroscopy, Stavros and coworkers found strong evidence for H-atom detachment from the amino group of adenine after excitation at 200 nm, while it was concluded that the role of $\pi\sigma^*$ states is minimal at 266 nm.[30] Zierhut and coworkers, using Doppler spectroscopy after excitation at 267 nm, also observed less H-atom loss from the amino group than the imino group.[55] These experimental findings support our computational result that the photoinduced H-atom detachment from the amino group involves a higher barrier than the H-atom detachment reaction from the imino group.

### (b) H-atom transfer from the N9-H and N10-H groups of adenine to water

We computed relaxed scans on the PE surface of the $^1\pi\sigma^*$ state along the N9-H bond length for the adenine-N9-H$\cdots$OH$_2$ conformer and along the N10-H bond length for the adenine-N10-H$\cdots$OH$_2$ conformer. The reaction-path PE profiles are shown in Fig. 9(a) for the adenine-N9-H$\cdots$OH$_2$ conformer and in Fig. 9(b) for the adenine-N10-H$\cdots$OH$_2$ conformer. As in isolated adenine, the $^1\pi\pi^*$ and $^1n\pi^*$ excited states are predissociated by the $^1\pi\sigma^*$ state. The PE profile of the $^1\pi\sigma^*$ state is flat and barrierless for both conformers. At large $R_{NH}$ ($R_{NH} \approx 2.0$ Å), the structures are biradicals consisting of dehydrogenated adenine and the $H_3O$ (hydronium) radical, see the insets in Fig. 9. The main difference between the energy profiles of Fig. 9 for adenine-$H_2O$ complexes and Fig. 8 for isolated adenine is the disappearance of the conical intersection of the $^1\pi\sigma^*$ state with the $S_0$ state. This arises from an increase of the energy of the $^1\pi\sigma^*$ state at large $R_{NH}$ and, more importantly, from a marked stabilization of the energy of the $S_0$ state at large $R_{NH}$, see Figs. 8, 9. The stabilization of the $S_0$ energy arises from a strong admixture of an ionic configuration (adenine$^-$-H3O$^+$) in the $S_0$ wave function at large $R_{NH}$. It is the high stability of the hydronium cation which stabilizes the ground-state energy and thereby removes the conical intersection with the biradicalic excited state. These findings are quite similar to those reported earlier for phenol-water clusters.[56]

It is well known that the homolytic photodetachment of H-atoms from acidic aromatic chromophores via repulsive $^1\pi\sigma^*$ states in aqueous solution yields hydrated electrons.[40, 56-58] In finite-size clusters, the hydrated hydronium radical, $H_3O(H_2O)_n$, is analogue of the hydrated electron in solution.[31, 59] Roberts et al. recently reported the detection of hydrated electrons generated by irradiation of adenine in aqueous solution at 220 nm and thus confirmed the possibility of the joint photodetachment of an electron and a proton from adenine in aqueous solution.[41]

### 3.4 H-atom transfer from the (adenine+H) radical to water

#### (a) H-atom photodetachment from the isolated N3 (adenine+H) radical

Fig. 10(a) shows the PE profiles along a rigid scan for the H-atom detachment reaction from the N3-H group of the (adenine+H) radical with the excess hydrogen atom at the N3 position. The reaction coordinate is the N-H distance between the N3 atom and the departing H-atom. Close to the Franck-Condon region (R(N-H) ≈ 1.0Å), the PE profiles of the locally excited states ($^2\pi\pi^*$ and $^2n\pi^*$) are approximately parallel to the energy profile of the $D_0$ state. The PE profile of the $^2\pi\sigma^*$ state, on the other hand, is repulsive and crosses the energy curve of the $D_0$ state at R(N-H) = 1.43 Å. It becomes the lowest electronic state for large NH-distances, where the σ* orbital contracts to the 1s orbital of the H-atom. The computed dissociation energy is 1.91 eV, which is more than 2 eV lower than the lowest H-atom detachment energy from adenine. While the $^2\pi\sigma^*$ state of the (adenine+H) radical is dark in absorption, it can be populated by radiationless relaxation from the higher-lying $^2\pi\pi^*$ state which absorbs near 2.0 eV (620 nm). At the $^2\pi\sigma^*/D_0$ conical intersection, the dynamics on the $^2\pi\sigma^*$ surface bifurcates, yielding either the hot $D_0$ state (aborted photodissociation) or adenine and a free H-atom in their electronic ground states as photodissociation products.

### (b) H-atom transfer from the N3 (adenine+H) radical to water

Fig. 10(b) displays the PE profiles of a relaxed scan for the H-atom transfer reaction from N3 (adenine+H) radical to a hydrogen-bonded water molecule, computed in the $^2\pi\sigma^*$ state. The reaction coordinate is the N-H distance between the transferred H-atom and the donating N-atom (N3) of the radical. Compared to the case of the free (adenine+H) radical (cf. Fig. 10(a)), the excited states are significantly lower in energy. The crossing point between the PE profiles of the $D_0$ state and the reactive $^2\pi\sigma^*$ state is shifted towards smaller NH distances (from 1.40 Å to 1.15 Å). The threshold for the H-atom transfer reaction is merely 0.56 eV, which is drastically lower than the threshold energy for H-atom transfer from one of the acidic sites of adenine to water. It is expected that additional water molecules will further stabilize the $H_3O$ radical, which might render the reaction thermoneutral or possibly even slightly exothermic in a liquid water environment.

## Conclusions

We performed a systematic and comprehensive exploration of excited-state electron/proton-transfer reactions in hydrogen-bonded complexes of 9H-adenine with a single water molecule by the investigation of the energy profiles of excited-state minimum-energy reaction paths. The PE profiles of the photoreactions have been computed as relaxed scans with the ADC(2) electronic structure method. We characterized, in particular, the relevant reaction barriers and the location of conical intersections. Two main excited-state reaction mechanisms have been identified in adenine-$H_2O$ complexes. The first is electron/proton abstraction from the hydrogen-bonded water molecule by the photoexcited chromophore whereby adenine acts as a photobase. This reaction mechanism has been characterized for the three basic sites of adenine (N1, N3, N7). The other mechanism is photoinduced electron/proton transfer from the acidic sites of adenine (N9H, N10$H_2$) via repulsive $^1\pi\sigma^*$ states to the hydrogen-bonded water molecule. This reaction in the adenine-$H_2O$ complex represents a finite-size model of the photoejection of an electron and a proton into a liquid aqueous environment.

For all reaction channels considered in this work, barrierless or nearly barrierless reaction paths for electron/proton transfer to water or electron/proton abstraction from water were found. Photoreactivity with hydrogen-bonded water molecules is thus a generic feature of the photochemistry of adenine in aqueous solution. These reaction mechanisms exist in addition to the well-established intrinsic excited-state decay mechanisms of adenine via ring-puckering or ring-opening conical intersections and can explain the substantially shortened excited-state lifetimes of adenine in water. The widely accepted concept of photostability of DNA/RNA bases provided by ultrafast excited-state deactivation through intramolecular conical intersections[1-3, 16, 17] has thus to be extended to include ultrafast excited-state decay channels which arise from photoinduced electron/proton exchange reactions with water. We also have characterized the PE functions for the photodetachment of the excess H-atom from the N3 (adenine+H) radical as well as the corresponding H-atom transfer reaction from the radical to a hydrogen-bonded water molecule. The H-atom photodetachment reaction can be stimulated by low-energy photons and the H-atom transfer reaction to water may even be approximately thermoneutral. The photochemical reaction mechanisms discussed herein illustrate the generic role of EDPT processes in excited states of nucleobases in aqueous environments and deserve further investigation by *ab initio* nonadiabatic nuclear-dynamics simulations.

It should be noted that the transfer of an H-atom from a water molecule to adenine represents the oxidation of water and the reduction of adenine. When an H-atom of the (adenine+H) radical (reduced adenine) is photoejected by the absorption of another photon via a repulsive $\pi\sigma^*$ state, adenine is regenerated (possibly as a different tautomer) and a water molecule is thereby homolytically decomposed into H and OH radicals. Adenine may thus have the functionality of a photocatalyst for water splitting by UV light. The UV-induced decomposition of water catalyzed by adenine and possibly other RNA/DNA bases may have been the beginning of solar energy harvesting of life. The RNA/DNA bases likely were not only photostabilizers[1, 2, 16, 17], but also the primordial catalysts for solar energy harvesting by the oxidation of water.

## Acknowledgments

This work was supported by the DFG cluster of excellence “Munich Centre for Advanced Photonics” (MAP). X.W. would like to thank the China Scholarship Council (CSC) for a doctoral scholarship. J. E. acknowledges partial support by the international Max Planck Research School of Advanced

Photon Science (IMPRS-APS). A. L. S. acknowledges support by the Alexander von Humboldt Research Award.

## References

1 C. E. Crespo-Hernández, B. Cohen, P. M. Hare and B. Kohler, *Chem. Rev.*, 2004, **104**, 1977-2020.

2 K. Kleinermanns, D. Nachtigallová and M. S. de Vries, *Int. Rev. Phys. Chem.*, 2013, **32**, 308-342.

3 R. Improta, F. Santoro and L. Blancafort, *Chem. Rev.*, 2016, **116**, 3540-3593.

4 H. Kang, B. Jung and S. K. Kim, *J. Chem. Phys.*, 2003, **118**, 6717-6719.

5 S. Ullrich, T. Schultz, M. Z. Zgierski and A. Stolow, *J. Am. Chem. Soc.*, 2004, **126**, 2262-2263.

6 C. Canuel, M. Mons, F. Piuzzi, B. Tardivel, I. Dimicoli and M. Elhanine, *J. Chem. Phys.*, 2005, **122**, 074316.

7 C. Z. Bisgaard, H. Satzger, S. Ullrich and A. Stolow, *ChemPhysChem*, 2009, **10**, 101-110.

8 N. L. Evans and S. Ullrich, *J. Phys. Chem. A*, 2010, **114**, 11225-11230.

9 H. Kang, J. Chang, S. H. Lee, T. K. Ahn, N. J. Kim and S. K. Kim, *J. Chem. Phys.*, 2010, **133**, 154311.

10 M. Kotur, T. C. Weinacht, C. Zhou and S. Matsika, *IEEE J. Sel. Top. Quant. Electron.*, 2012, **18**, 187-194.

11 A. Sobolewski and W. Domcke, *Eur. Phys. J. D*, 2002, **20**, 369-374.

12 S. Perun, A. L. Sobolewski and W. Domcke, *J. Am. Chem. Soc.*, 2005, **127**, 6257-6265.

13 S. Perun, A. L. Sobolewski and W. Domcke, *Chem. Phys.*, 2005, **313**, 107-112.

14 C. M. Marian, *J. Chem. Phys.*, 2005, **122**, 104314.

15 L. Blancafort, *J. Am. Chem. Soc.*, 2006, **128**, 210-219.

16 L. Serrano-Andres, M. Merchan and A. C. Borin, *Proc. Natl. Acad. Sci. U. S. A*, 2006, **103**, 8691-8696.

17 A. L. Sobolewski and W. Domcke, *Europhysics News*, 2006, **37**, 20-23.

18 W. C. Chung, Z. Lan, Y. Ohtsuki, N. Shimakura, W. Domcke and Y. Fujimura, *Phys. Chem. Chem. Phys.*, 2007, **9**, 2075-2084.

19 E. Fabiano and W. Thiel, *J. Phys. Chem. A*, 2008, **112**, 6859-6863.

20 M. Barbatti and H. Lischka, *J. Am. Chem. Soc.*, 2008, **130**, 6831-6839.

21 I. Conti, M. Garavelli and G. Orlandi, *J. Am. Chem. Soc.*, 2009, **131**, 16108-16118.

22 W. M. I. Hassan, W. C. Chung, N. Shimakura, S. Koseki, H. Kono and Y. Fujimura, *Phys. Chem. Chem. Phys.*, 2010, **12**, 5317-5328.

23 M. Barbatti, Z. Lan, R. Crespo-Otero, J. J. Szymczak, H. Lischka and W. Thiel, *J. Chem. Phys.*, 2012, **137**, 22A503.

24 D. Picconi, F. J. A. Ferrer, R. Improta, A. Lami and F. Santoro, *Faraday discuss.*, 2013, **163**, 223-242.

25 F. Plasser, R. Crespo-Otero, M. Pederzoli, J. Pittner, H. Lischka and M. Barbatti, *J. Chem. Theory Comput.*, 2014, **10**, 1395-1405.

26 S. B. Nielsen, T. Chakraborty and S. V. Hoffmann, *ChemPhysChem*, 2005, **6**, 2619-2624.

27 H. Satzger, D. Townsend, M. Z. Zgierski, S. Patchkovskii, S. Ullrich and A. Stolow, *Proc. Natl. Acad. Sci. U. S. A*, 2006, **103**, 10196-10201.

28 H. Satzger, D. Townsend and A. Stolow, *Chem. Phys. Lett.*, 2006, **430**, 144-148.

29 M. G. D. Nix, A. L. Devine, B. Cronin and M. N. R. Ashfold, *J. Chem. Phys.*, 2007, **126**, 124312.

30 K. L. Wells, D. J. Hadden, M. G. D. Nix and V. G. Stavros, *J. Phys. Chem. Lett.*, 2010, **1**, 993-996.

31 A. L. Sobolewski, W. Domcke, C. Dedonder-Lardeux and C. Jouvet, *Phys. Chem. Chem. Phys.*, 2002, **4**, 1093-1100.

32 B. Cohen, P. M. Hare and B. Kohler, *J. Am. Chem. Soc.*, 2003, **125**, 13594-13601.

33 N. J. Kim, H. Kang, G. Jeong, Y. S. Kim, K. T. Lee and S. K. Kim, *J. Phys. Chem. A*, 2000, **104**, 6552-6557.

34 H. Kang, K. T. Lee and S. K. Kim, *Chem. Phys. Lett.*, 2002, **359**, 213-219.

35 H.-H. Ritze, H. Lippert, E. Samoylova, V. R. Smith, I. V. Hertel, W. Radloff and T. Schultz, *J. Chem. Phys.*, 2005, **122**, 224320.

36 S. Chaiwongwattana, M. Sapunar, A. Ponzi, P. Decleva and N. Došlić, *J. Phys. Chem. A*, 2015, **119**, 10637-10644.

37 X. Wu, T. N. V. Karsili and W. Domcke, *ChemPhysChem*, 2016, **17**, 1298-1304.

38 M. Barbatti, *J. Am. Chem. Soc.*, 2014, **136**, 10246-10249.

39 T. Pancur, N. K. Schwalb, F. Renth and F. Temps, *Chem. Phys*., 2005, **313**, 199-212.

40 A. L. Sobolewski and W. Domcke, *Phys. Chem. Chem. Phys*., 2007, **9**, 3818-3829.

41 G. M. Roberts, H. J. B. Marroux, M. P. Grubb, M. N. R. Ashfold and A. J. Orr-Ewing, *J. Phys. Chem. A*, 2014, **118**, 11211-11225.

42 R. Szabla, R. W. Gora, M. Janicki and J. Sponer, *Faraday Discuss.*, 2016, **195**, 237-251.

43 C. Møller and M. S. Plesset, *Phys. Rev.*, 1934, **46**, 618-622.

44 J. Schirmer, *Phys. Rev. A*, 1982, **26**, 2395-2416.

45 A. B. Trofimov and J. Schirmer, *Chem. Phys.*, 1997, **214**, 153-170.

46 T. H. Dunning Jr, *J. Chem. Phys.*, 1989, **90**, 1007-1023.

47 TURBOMOLE, v. 6.3.1, 2011. A development of the University of Karlsruhe and Forschungszentrum Karlsruhe: see http://www.turbomole.com.

48 C. Hättig and F. Weigend, *J. Chem. Phys.*, 2000, **113**, 5154-5161.

49 C. Hättig, A. Hellweg and A. Köhn, *Phys. Chem. Chem. Phys*., 2006, **8**, 1159-1169.

50 B. Mennucci, A. Toniolo and J. Tomasi, *J. Phys. Chem. A*, 2001, **105**, 4749-4757.

51 S. Yamazaki and S. Kato, *J. Am. Chem. Soc.*, 2007, **129**, 2901-2909.

52 Z. Lan, Y. Lu, E. Fabiano and W. Thiel, *ChemPhysChem*, 2011, **12**, 1989-1998.

53 D. R. Yarkony in Conical Intersections: Electronic Structure, Dynamics and Spectroscopy, eds. W. Domcke, D. R. Yarkony and H. Köppel, World Scientific, Singapore, 2004, Chapter 2.

54 I. Hünig, C. Plützer, K. A. Seefeld, D. Löwenich, M. Nispel and K. Kleinermanns, *ChemPhysChem*, 2004, **5**, 1427-1431.

55 M. Zierhut, W. Roth and I. Fischer, *Phys. Chem. Chem. Phys*., 2004, **6**, 5178-5183.

56 A. L. Sobolewski and W. Domcke, *J. Phys. Chem. A*, 2001, **105**, 9275-9283.

57 J. Peon, G. C. Hess, J.-M. L. Pecourt, T. Yuzawa and B. Kohler, *J. Phys. Chem. A*, 1999, **103**, 2460-2466.

58 A. Bussandri and H. van Willigen, *J. Phys. Chem. A*, 2002, **106**, 1524-1532.

59 B. Abel, U. Buck, A. L. Sobolewski and W. Domcke, *Phys. Chem. Chem. Phys*., 2012, **14**, 22-34.

**Table 1**. Vertical excitation energies (in eV) and oscillator strengths (in parentheses) for five conformers of the adenine-$H_2O$ complex, calculated at the ADC(2)/aug-cc-pVDZ level. The data for isolated adenine are included for comparison. The conformers are shown in Figs. 1 and 2.

| Conformer | State | | | |
|---|---|---|---|---|
| | $^1\pi\pi^*(L_a)$ ($f$) | $^1\pi\pi^*(L_b)$ ($f$) | $^1n\pi^*$ ($f$) | $^1\pi\sigma^*$ ($f$) |
| Ade-N1…H-OH | 5.09 (0.1876) | 5.12 (0.1200) | 5.15 (0.0008) | 5.41 (0.0094) |
| Ade-N3…H-OH | 5.03 (0.2834) | 5.11 (0.0317) | 5.14 (0.0004) | 5.42 (0.0104) |
| Ade-N7…H-OH | 4.90 (0.2437) | 5.08 (0.0600) | 5.03 (0.0009) | 5.24 (0.0038) |
| Ade-N9-H…$OH_2$ | 5.04 (0.2791) | 5.10 (0.0353) | 5.08 (0.0007) | 5.36 (0.0100) |
| Ade-N10-H…$OH_2$ | 5.00 (0.2597) | 5.06 (0.0623) | 5.10 (0.0008) | 5.32 (0.0061) |
| isolated adenine | 5.06 (0.2287) | 5.09 (0.1876) | 5.03 (0.0008) | 5.32 (0.0086) |

Ade-N1…H-OH

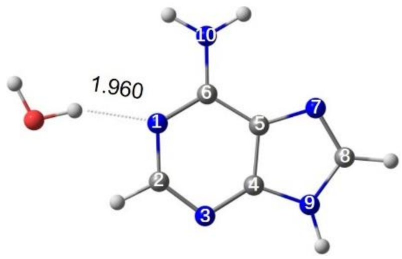
1.960
10
6
1
5
7
8
2
4
3
9

Ade-N3…H-OH

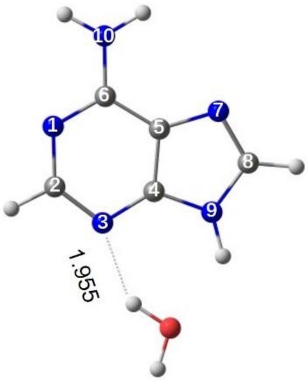
10
6
7
1
5
8
2
4
3
9
1.955

Ade-N7…H-OH

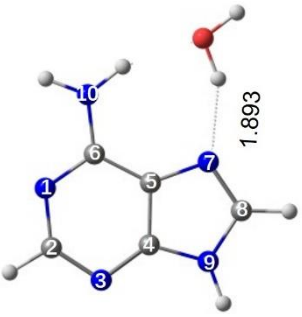
1.893
10
6
5
7
1
8
2
4
9
3

Fig. 1. Ground-state equilibrium geometries of the three H-atom accepting conformers of the hydrogen-bonded adenine-$H_2O$ complex, obtained with $C_s$ symmetry constraint at the MP2/aug-cc-pVDZ level. The hydrogen-bond lengths are given in Ångstrom.

Ade-N9-H…OH$_2$

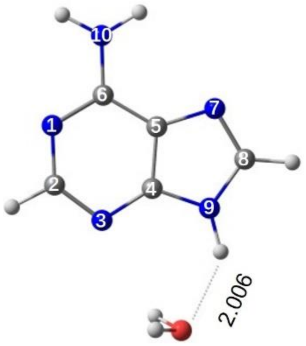
10
6
1
5
7
8
2
4
9
3
2.006

Ade-N10-H…OH$_2$

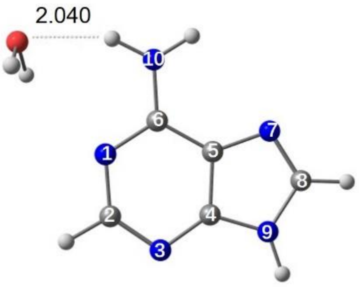
2.040
10
6
1
5
7
8
2
4
9
3

Fig. 2. Ground-state equilibrium geometries of the three H-atom donating conformers of the hydrogen-bonded adenine-H$_2$O complex, obtained with $C_s$ symmetry constraint at the MP2/aug-cc-pVDZ level. The hydrogen-bond lengths are given in Ångstrom.

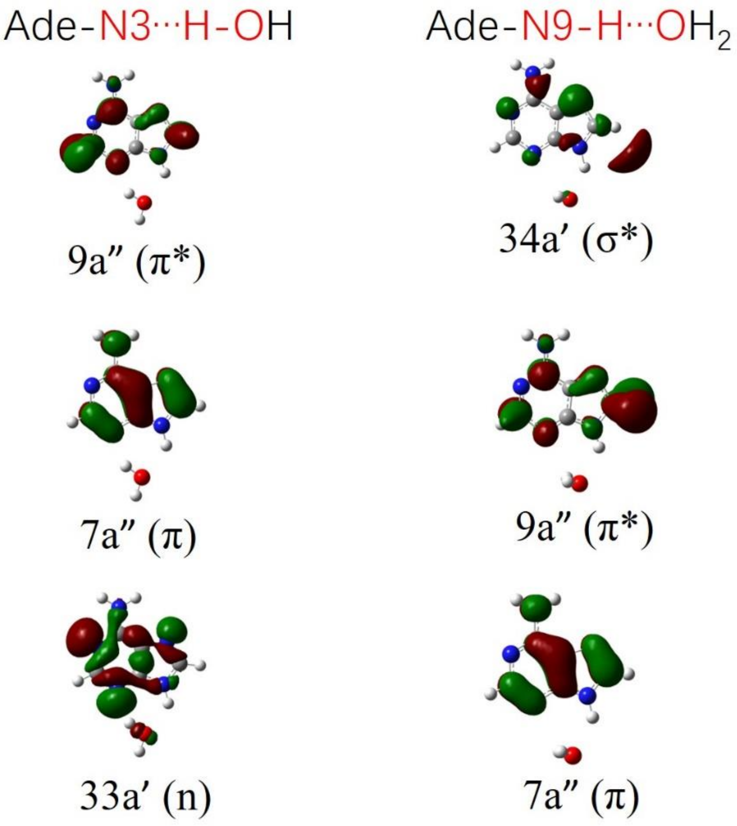
Ade-N3···H-OH
Ade-N9-H···OH2
9a″ (π*)
34a′ (σ*)
7a″ (π)
9a″ (π*)
33a′ (n)
7a″ (π)

Fig. 3. Hartree-Fock molecular orbitals involved in the lowest excited states of the adenine-$H_2O$ conformers adenine-N3…H-OH (left) and adenine-N9-H…$OH_2$ (right) at the ground-state equilibrium geometry. The outer part of the 34a'(σ*) orbital is actually more diffuse than is visible in this graphical representation.

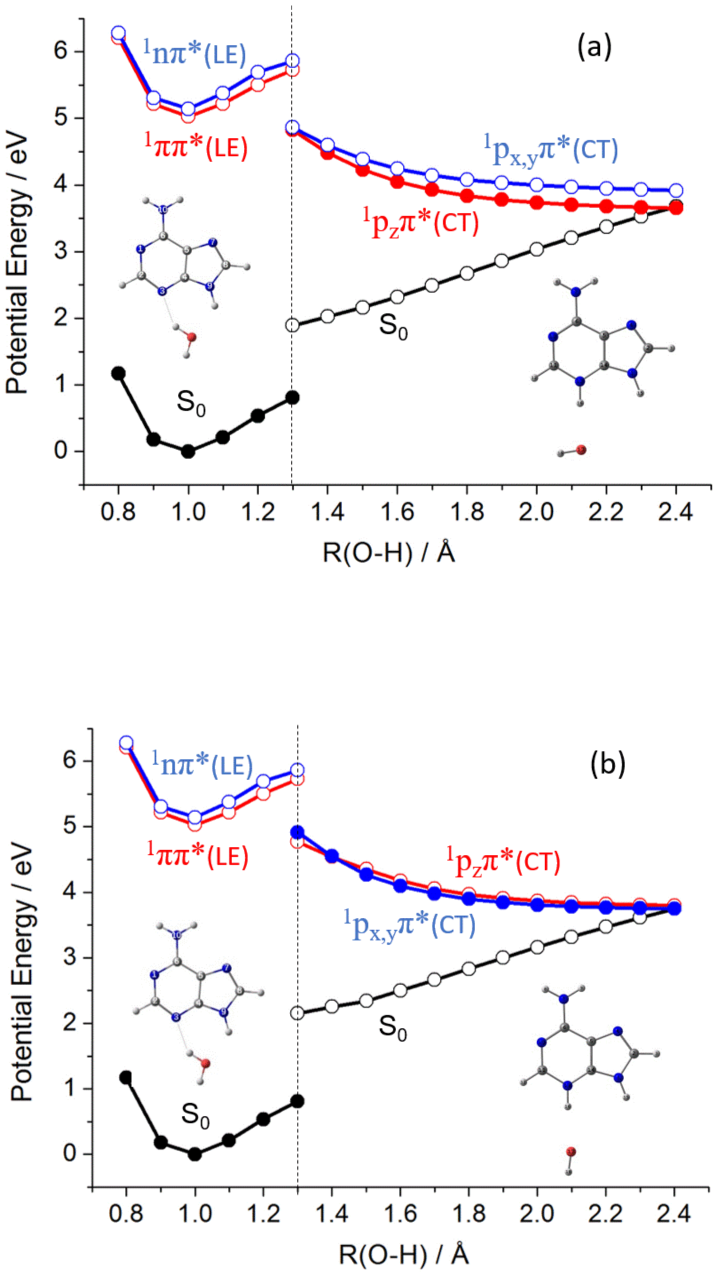

Fig. 4. Energy profiles of minimum-energy paths for hydrogen transfer from water to adenine for the electronic ground state (black), the $^1\pi\pi^*$ (red) and $^1n\pi^*$ (blue) locally excited states and the $^1p_z\pi^*$ (red) and $^1p_{x,y}\pi^*$ (blue) charge-transfer states, for the adenine-N3…H-OH conformer. (a) relaxed scan calculated by optimizing the energy of the $^1p_z\pi^*$ state; (b) relaxed scan calculated by optimizing the energy of the $^1p_{x,y}\pi^*$ state. The educt and product structures are shown as insets.

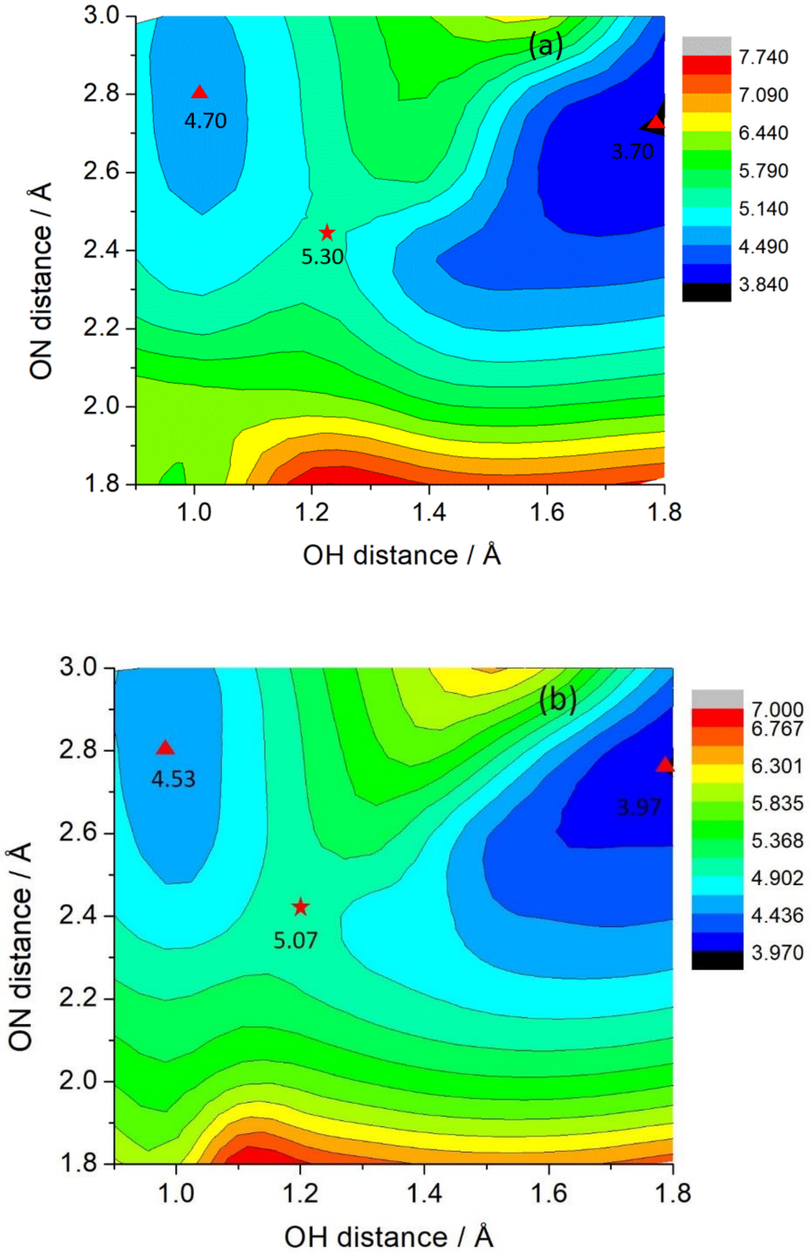

Fig. 5. Relaxed PE surface of the lowest excited state of $^1$A' symmetry ($^1\pi\pi^*$ and $^1p_z\pi^*$ states) (a) and PE surface of the lowest excited state of $^1$A" symmetry ($^1n\pi^*$ and $^1p_{x,y}\pi^*$states) (b) in the vicinity of the barrier for H-atom transfer from water to adenine for the adenine-N3…H-OH conformer, calculated with the ADC(2) method. The nuclear coordinates are the OH bond length $R_{OH}$ of the water molecule and the distance $R_{ON}$ of the oxygen atom of water from the N3-atom of adenine. The numbers give the energy of local minima (triangles) and the saddle point (star) relative to the ground-state minimum energy in electron volts.

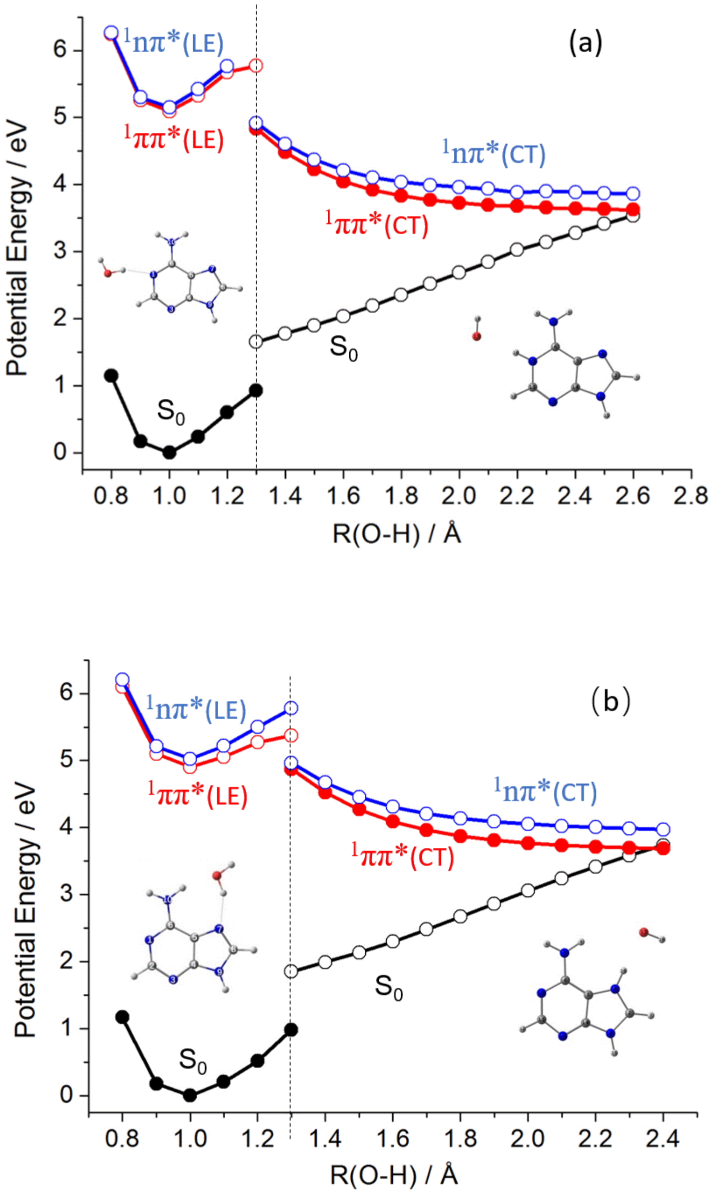

Fig. 6. Energy profiles of minimum-energy paths for hydrogen transfer from water to adenine for the electronic ground state (black), the $^1\pi\pi^*$ (red) and $^1n\pi^*$ (blue) locally excited states and the $^1p_z\pi^*$ (red) $^1p_{x,y}\pi^*$ (blue) charge-transfer states, for the adenine-N1…H-OH conformer (a) and the adenine-N7…H-OH conformer (b). The educt and product structures are shown as insets.

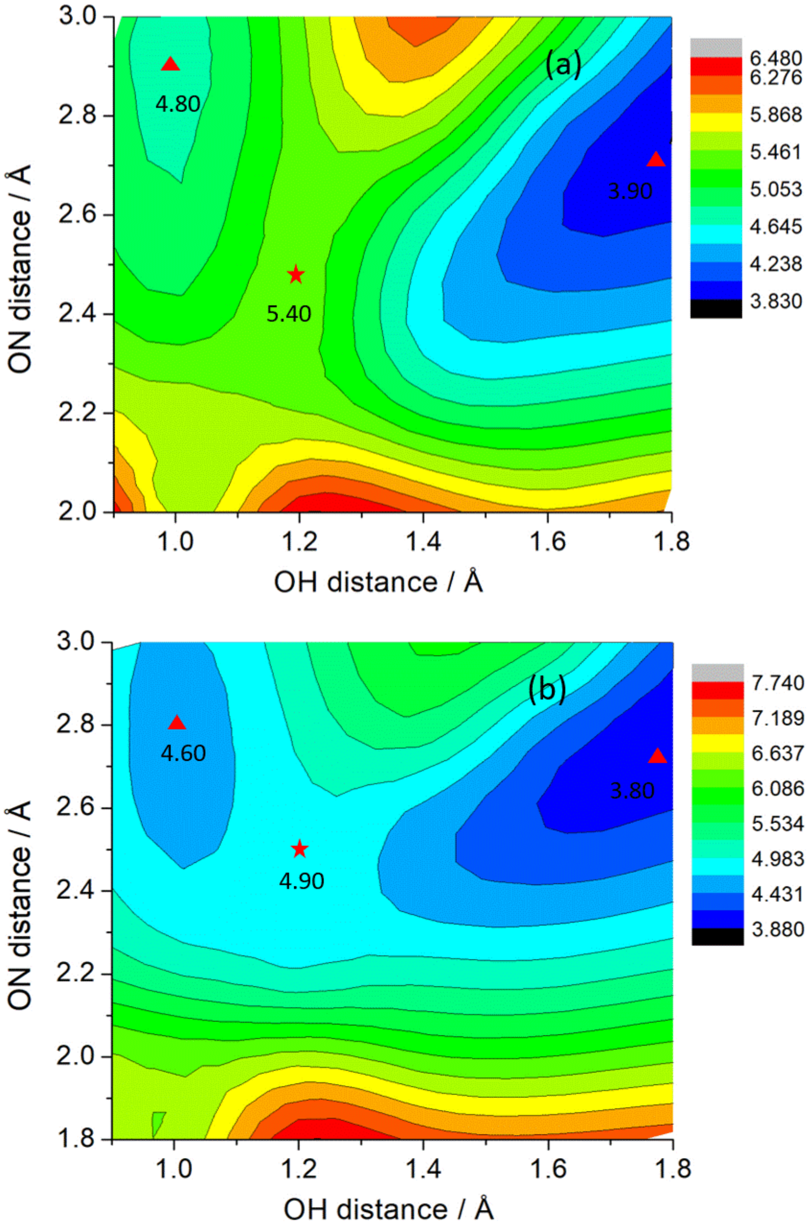

Fig. 7. Relaxed PE surface of the lowest excited state of $^1$A' symmetry ($^1\pi\pi^*$ and $^1p_z\pi^*$ states) in the vicinity of the barrier for H-atom transfer from water to adenine for the adenine-N1…H-OH conformer (a) and the adenine-N7…H-OH conformer (b), calculated with the ADC(2) method. The nuclear coordinates are the OH bond length $R_{OH}$ of the water molecule and the distance $R_{ON}$ of the oxygen atom of water from the corresponding N-atom of adenine. The numbers give the energy of local minima (triangles) and the saddle point (star) relative to the ground-state minimum energy in electron volts.

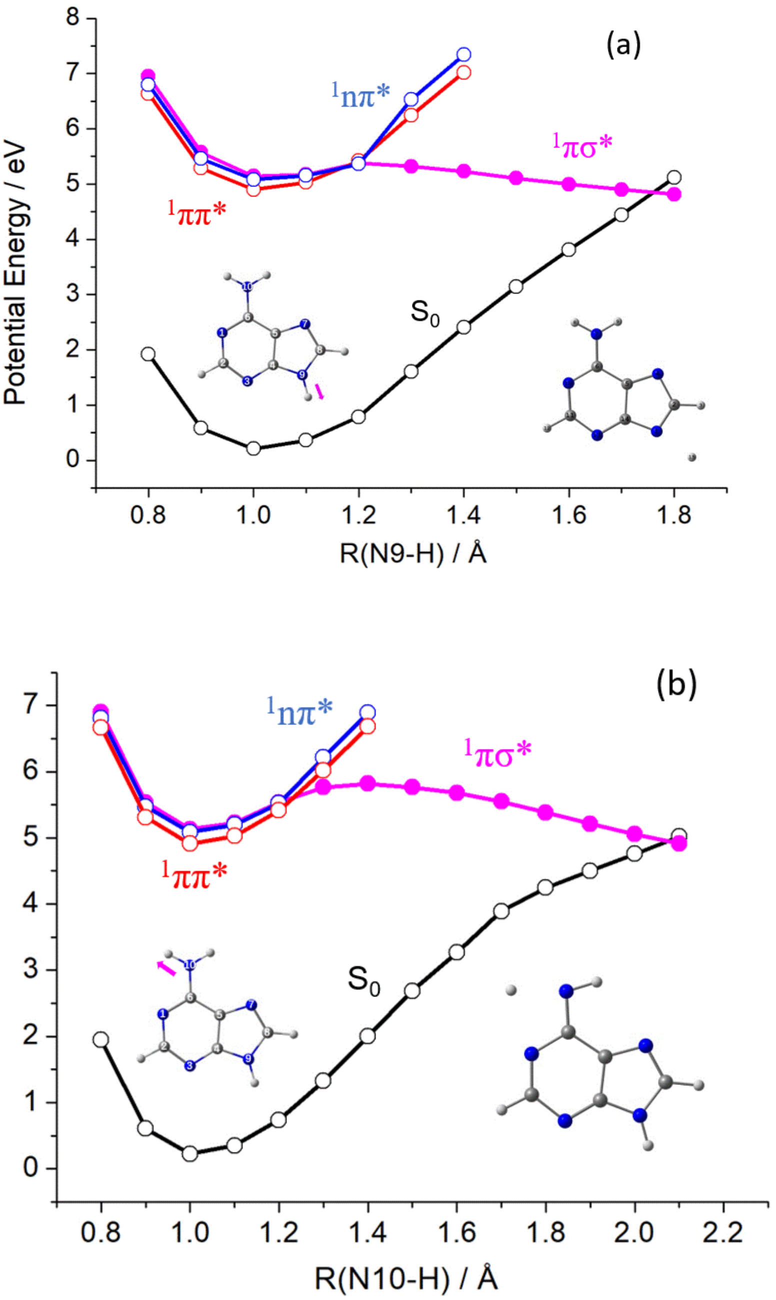

Fig. 8. PE profiles of minimum-energy reaction paths for hydrogen detachment from adenine in the electronic ground state (black) and the lowest $^1n\pi^*$ (blue), $^1\pi\pi^*$ (red) and $^1\pi\sigma^*$ (pink) excited states as a function of the N9-H stretching coordinate (a) and the N10-H stretching coordinate (b), calculated with the ADC(2) method. The relaxed scan is optimized in the $^1\pi\sigma^*$ state. The educt and product structures are shown as insets.

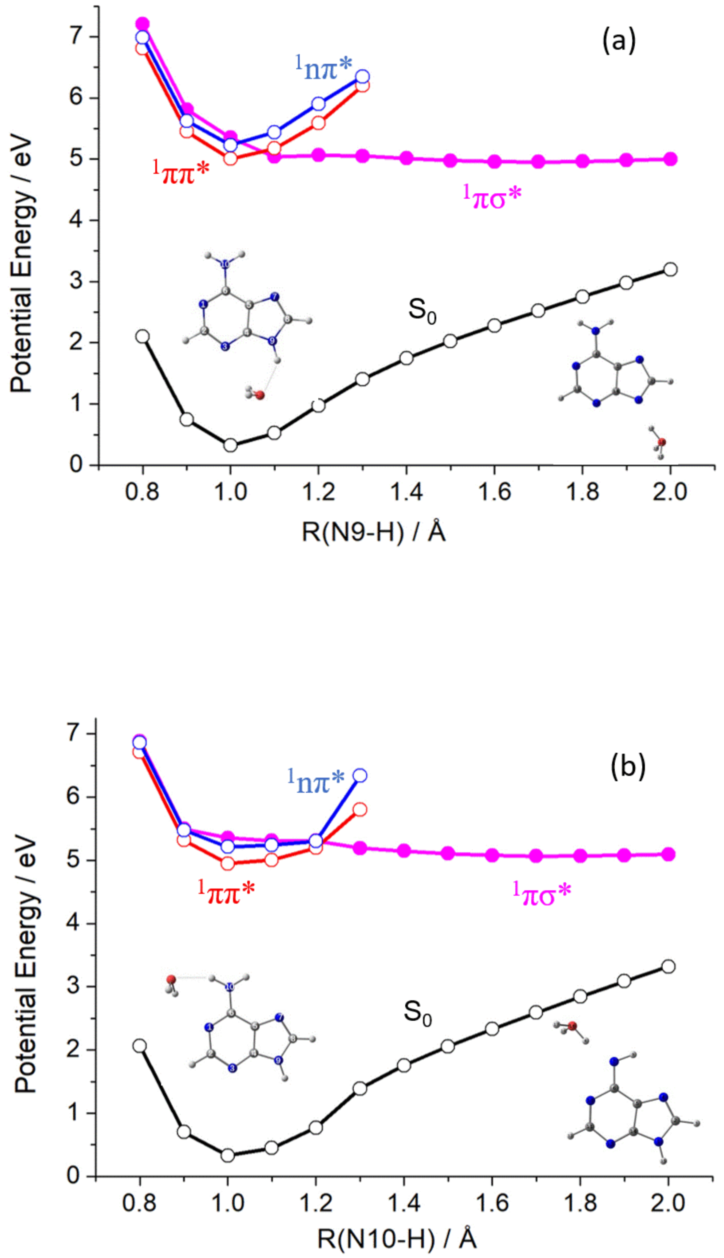

Fig. 9. PE profiles of minimum-energy reaction paths for hydrogen transfer from adenine to the hydrogen-bonded water molecule in the electronic ground state (black) and the lowest $^1n\pi^*$ (blue), $^1\pi\pi^*$ (red) and $^1\pi\sigma^*$ (pink) excited states, calculated with the ADC(2) method. The relaxed scan is optimized in the $^1\pi\sigma^*$ state. The educt and product structures are shown as insets.

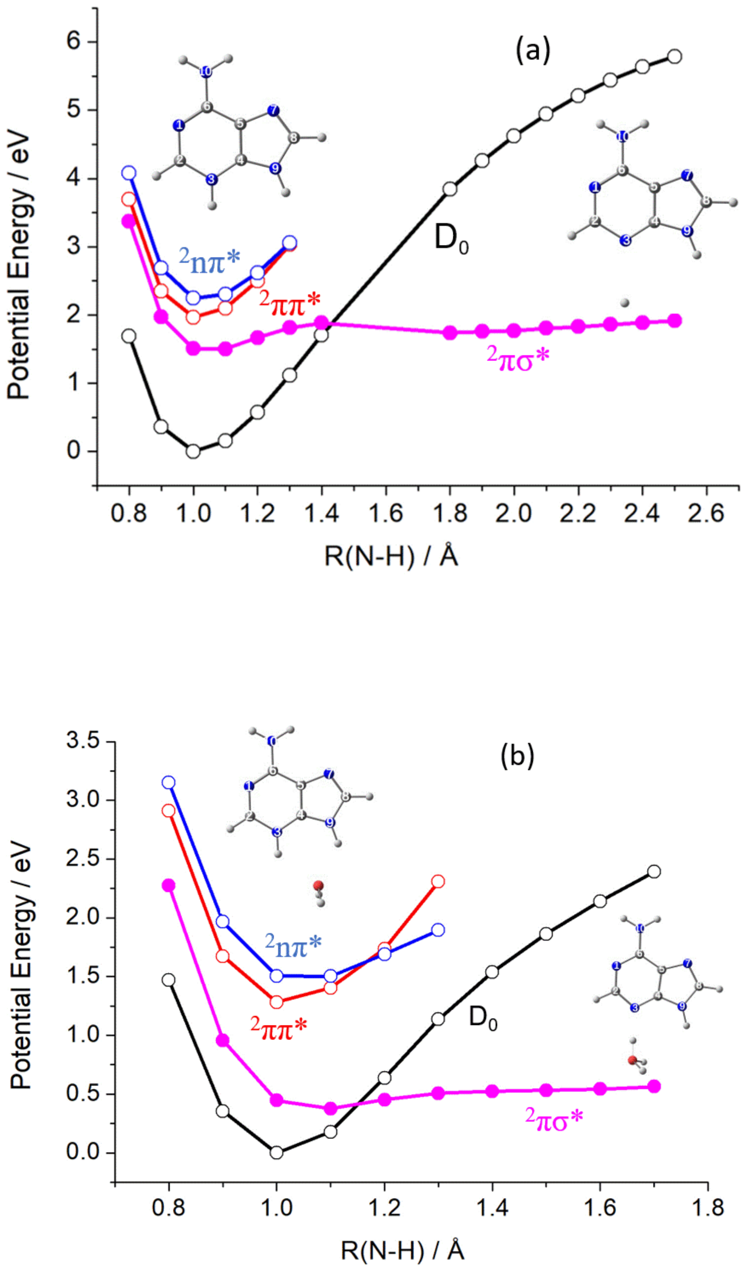

Fig. 10. (a) PE profiles for the H-atom detachment from the N3 (adenine+H) radical. The PE curve of the $D_0$ state is shown in black, the energy curves of the $^2\pi\pi^*$ and $^2n\pi^*$ states are shown in blue and red, respectively, and the reactive $^2\pi\sigma^*$ state is depicted in pink. (b) PE profiles for H-atom transfer from N3 (adenine+H) radical to a hydrogen-bonded water molecule, resulting in the formation of the $H_3O$ radical. Educt and product structures are shown as insets.

# Paper 2

**Excited-State Deactivation of Adenine by Electron-Driven Proton-Transfer Reactions in Adenine-Water Clusters: A Computational Study.** Xiuxiu Wu, Tolga N.V. Karsili, Wolfgang Domcke: *ChemPhysChem* **2016**, 17, 1298-1304. Copyright © 2016 WILEY-VCH Verlag GmbH & Co. KGaA, Weinheim.

ChemPubSoc Europe

DOI: 10.1002/cphc.201501154

CHEMPHYSCHEM
Articles

Special Issue

# Excited-State Deactivation of Adenine by Electron-Driven Proton-Transfer Reactions in Adenine–Water Clusters: A Computational Study

Xiuxiu Wu, Tolga N. V. Karsili,* and Wolfgang Domcke[a]

The reactivity of photoexcited 9*H*-adenine with hydrogen-bonded water molecules in the 9*H*-adenine–$(H_2O)_5$ cluster is investigated by using ab initio electronic structure methods, focusing on the photoreactivity of the three basic sites of 9*H*-adenine. The energy profiles of excited-state reaction paths for electron/proton transfer from water to adenine are computed. For two of the three sites, a barrierless or nearly barrierless reaction path towards a low-lying $S_1$–$S_0$ conical intersection is found. This reaction mechanism, which is specific for adenine in an aqueous environment, can explain the substantially shortened excited-state lifetime of 9*H*-adenine in water. Depending on the branching ratio of the nonadiabatic dynamics at the $S_1$–$S_0$ conical intersection, the electron/proton transfer process can enhance the photostability of 9*H*-adenine in water or can lead to the generation of adenine-H$^{\cdot}$ and OH$^{\cdot}$ free radicals. Although the branching ratio is yet unknown, these findings indicate that adenine might have served as a catalyst for energy harvesting by water splitting in the early stages of the evolution of life.

## 1. Introduction

DNA and RNA nucleobases exhibit a remarkable degree of photostability, which is believed to be essential for the protection of the genetic information of life. Although DNA and RNA nucleobases absorb strongly in the wavelength range 200–300 nm via their $^1\pi\pi^*$ excited states, their fluorescence quantum yields are very low, which has been attributed to ultrafast deactivation of the excited states to the electronic ground state.[1] A typical representative of the purine nucleobases is 9*H*-adenine, which was the tautomer of focus in this investigation.

Time-resolved spectroscopy in supersonic jets has revealed an excited-state lifetime of isolated 9*H*-adenine of 1.2 ps following excitation at 267 nm.[2–4] Extensive computational studies in the mid-2000s led to a consensus view of the photophysics of adenine that explains the ultrafast radiationless decay by nonadiabatic dynamics through several conical intersections (CIs) that occur at out-of-plane distorted geometries,[5–15] although it has remained controversial whether the $S_1(n\pi^*)$ excited state is populated as a transient intermediate or whether the decay occurs from the mainly absorbing $L_a(\pi\pi^*)$ state directly to the ground state. At shorter excitation wavelengths (<250 nm), additional relaxation pathways via dissociative $^1\pi\sigma^*$ states associated with the NH and $NH_2$ groups of adenine might become accessible.[3,4,6–7,16–18]

The excited-state lifetime of 9*H*-adenine (measured by femtosecond time-resolved transient absorption) becomes even shorter in aqueous solution (≈200 fs).[19] An abrupt shortening of the lifetime for $\lambda < 265$ nm (measured by femtosecond time-resolved fluorescence upconversion) has been interpreted as evidence for radiationless relaxation via the lowest $^1\pi\sigma^*$ state.[20] Recently, Roberts et al. searched for the spectroscopic signatures of the adeninyl [adenine−H] radical upon excitation of 9*H*-adenine in liquid water with excitation at 266 and 220 nm.[21] Adeninyl radicals are expected to be formed by the photodissociation of H atoms from the NH and/or $NH_2$ groups of adenine through repulsive $^1\pi\sigma^*$ states. Although dehydrogenated adenine radicals could not unequivocally be detected due to spectral overlap with adenine radical cations, hydrated electrons were detected upon 220 nm excitation.[21] It is known that photodetachment of H atoms from acidic chromophores via repulsive $^1\pi\sigma^*$ states in aqueous environments can yield hydrated electrons.[22] The latter can thus be considered as fingerprints of H-atom photodissociation from adenine in liquid water.

These findings indicate that the acidic groups of adenine (NH, $NH_2$) might actively participate in the excited-state relaxation dynamics of adenine in water. Theoretical solvent effects on the known conical intersections in 9*H*-adenine were investigated with polarized continuum models,[23,24] free-energy calculations,[25] and with quantum mechanics/molecular mechanics (QM/MM) simulations.[26,27] The shortening of the excited-state lifetime of adenine in polar solvents has been explained by a redshift of the $L_a$ state, a blue-shift of the $^1n\pi^*$ state and a lowering of the barriers along the reaction paths to the out-

---

[a] *X. Wu, Dr. T. N. V. Karsili, Prof. W. Domcke*
*Department of Chemistry*
*Technische Universität München*
*85747 Garching (Germany)*
*E-mail: Tolga.Karsili@tum.de*

Supporting Information for this article can be found under http://dx.doi.org/10.1002/cphc.201501154.

An invited contribution to a Special Issue on Fast Spectroscopy: Biosystems

© 2016 Wiley-VCH Verlag GmbH & Co. KGaA, Weinheim

of-plane distorted CIs.[26] Overall, the relaxation dynamics of adenine in water are similar to those demonstrated previously for isolated adenine.[23–27]

An alternative approach to investigating the effects of solvent on the photophysical properties of nucleobases is the spectroscopic study of size-selected nucleobase–water clusters in supersonic jets. In a pioneering study, S. K. Kim and co-workers found extensive and ultrafast fragmentation of adenine–water clusters upon excitation at 262 nm.[28,29] The hydrated clusters lost all of the solvent molecules within approximately 200 fs, regardless of cluster size. Kim and co-workers interpreted this observation as dissociation of the adenine–water hydrogen bonds in the $^{1}n\pi^{*}$ excited state.[28,29] Ritze et al. applied femtosecond time-resolved photoionization spectroscopy to study the photophysics of adenine–water clusters.[30] They confirmed the substantially shortened excited-state lifetime ($\approx$100 fs) of adenine–water clusters compared to isolated adenine. The ultrafast excited-state relaxation was explained by a lowering of the energy of the photoreactive $^{1}\pi\sigma^{*}$ state in microhydrated adenine.[30] Canuel et al. investigated the excited-state dynamics of microhydrated 9-methyladenine with femtosecond time-resolved photoelectron and photo-ion spectroscopy.[31] They reported a strongly accelerated excited-state decay (lifetime of $\approx$200 fs), which they explained as a lowering of the energy and direct population of the short-lived $L_a$ state in the clusters. Park and co-workers applied multiphoton ionization spectroscopy to adenine–water clusters and observed a significant amount of protonated adenine after cluster fragmentation, which is an indication of proton transfer (PT) processes operating in excited or ionized clusters.[32] Brutschy and co-workers reported the first evidence of isomer-specific photophysics in adenine–water clusters.[33] Two isomers (N9—H-, see assigned atomic numbering in Figure 1, and amino-bound hydrates, respectively) were shown to exhibit very different fragmentation patterns in the ion depletion spectra. These authors suggested that excited-state cluster dissociation dominates in the N9—H-bound hydrate, whereas intra-adenine internal conversion (IC) prevails in the amino-bound hydrate.[33]

Although the available experimental data on the photoinduced dynamics of microhydrated adenine are limited, the diversity of the observed effects and of their interpretation indicates that hydrogen bonding with water results in nontrivial modifications of the photophysics of the adenine chromophore. Systematic theoretical studies of the reaction mechanisms and the nonadiabatic dynamics are needed. Mitrić et al. explained the shortening of the $^{1}\pi\pi^{*}$ lifetime in microhydrated 9*H*-adenine within the framework of conventional mechanisms,[34] and Ritze et al. emphasized the redshift of reactive $^{1}\pi\sigma^{*}$ states in the hydrates.[30] Recently, Barbatti found evidence for an unexpected electron-transfer pathway from water to adenine in the 7*H*-adenine–$(H_2O)_5$ cluster by using excited-state dynamics simulations with the second-order algebraic diagrammatic construction [ADC(2)] method.[35] This is the first indication that not only the acidic sites of adenine (NH, $NH_2$), but also the basic sites (N) might be relevant for the excited-state relaxation dynamics of adenine in water. Using the same methods, Došlić and co-workers performed nonadiabatic dynamics simulations for two 9*H*-adenine monohydrates with the aim of explaining the measured 100 fs excited-state lifetime.[36] These simulations predicted that an electron-driven proton-transfer (EDPT)[37] process from water to the N3 nitrogen atom (see assigned atom numbering in Figure 1) could be responsible for the ultrafast excited-state deactivation. Taken together, these results provide preliminary evidence that novel reaction mechanisms, involving explicitly the electronic structure and chemical reactivity of hydrogen-bonded water molecules, need to be taken into account. These reaction mechanisms are ignored, by construction, in all simulations in which only the chromophore is described at the QM level, whereas the solvent is described by continuum polarization or MM models.

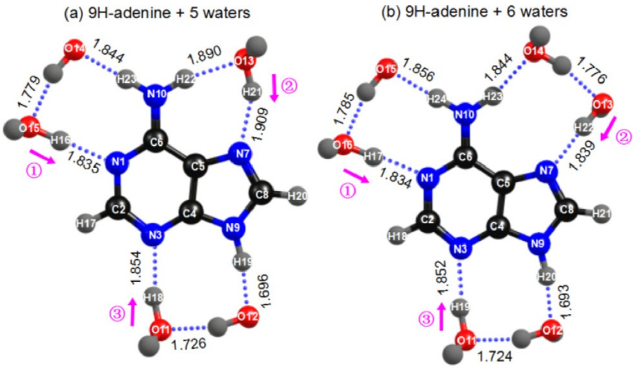

**Figure 1.** Ground-state equilibrium geometry of a) a representative 9*H*-adenine–$(H_2O)_5$ cluster and b) a representative 9*H*-adenine–$(H_2O)_6$ cluster, determined at the MP2/cc-pVDZ level. Bond lengths are expressed in Angstroms.

In this work, we have investigated in detail the excited-state EDPT reaction mechanism in the 9*H*-adenine–$(H_2O)_5$ cluster with the ADC(2) electronic structure method. We focused on the characterization of vertical excitation energies, minimum-energy excited-state reaction paths and the identification of relevant conical intersections. This study complements and extends the prior work of Barbatti[35] and Došlić and co-workers.[36]

## Computational Methods

The ground-state equilibrium geometries were optimized using second-order Møller–Plesset perturbation theory (MP2)[38] using Dunning's correlation-consistent split-valence double-$\zeta$ basis set with polarization functions (cc-pVDZ).[39] The cc-pVDZ basis set was found to provide an appropriate balance between qualitatively correct potential energy (PE) profiles and reducing the computational expense (which is clearly desirable for supramolecular systems of this size). Vertical excitation energies and oscillator strengths were calculated using the ADC(2) method.[40] In both methods, the resolution of the identity (RI) approximation for the electron repulsion integrals was used.[41] The reaction path for H-atom transfer from one of the hydrogen-bonded water molecules to adenine in the electronic ground state was calculated at the MP2 level using the bond length $R_{O-H}$ of the hydrogen-bonded OH group of water as the driving coordinate. The energies of the $^{1}\pi\pi^{*}$ excited states along the relaxed ground-state path were computed using the ADC(2) method. Relaxed scans along $R_{O-H}$ were also computed for

© 2016 Wiley-VCH Verlag GmbH & Co. KGaA, Weinheim

the lowest excited state of charge-transfer (CT) character (vide infra) using the ADC(2) method. This involves scanning of the appropriate $R_{O-H}$ driving coordinate, while allowing the rest of the nuclear framework to relax. In these calculations, the energies of the electronic ground state and the $^1\pi\pi^*$ states were computed at the relaxed geometries of the CT state using the MP2 and ADC(2) methods, respectively. If calculations of relaxed scans were not possible due to a failure of excited-state geometry optimization, an approximate reaction path was constructed by linear interpolation in internal coordinates (LIIC). All calculations were carried out with Turbomole.[42]

For benchmarking purposes, vertical excitation energies were also computed using complete active space with second-order perturbation theory (CASPT2). These calculations were based on a state-averaged complete active space self-consistent field (SA4-CASSCF) reference wavefunction using an active space of 10 electrons distributed in eight orbitals (10,8). The active orbitals comprised three $\pi$, three $\pi^*$ and two occupied nonbonding orbitals (i.e. two N-centered $2p_y$ lone pairs). An imaginary level shift of 0.5 $E_H$ was used in order to aid convergence and avoid the effects of intruder states.

## 2. Results

### 2.1. Ground-State Equilibrium Structures

The MP2/cc-pVDZ-optimized ground-state geometries of 9*H*-adenine, hydrated by five [adenine–$(H_2O)_5$] and six [adenine–$(H_2O)_6$] water molecules, respectively, are shown in Figure 1 a and Figure 1 b. The associated Cartesian coordinates of optimized clusters with five and six water molecules are included in the Supporting Information. These represent the lowest energy structures and were inspired in part by previous work by Barbatti.[35] Adenine retains a planar geometry, with the exception of the wagging angle of the amino group, just as in the isolated structure (i.e., the local geometry around N10).[9] The wagging angle of the amino group in 9*H*-adenine–$(H_2O)_5$ is reduced (cf. isolated 9*H*-adenine).

As 9*H*-adenine has both basic N-atom acceptor sites (N1, N3, N7) as well as acidic N–H donor sites (N9–H19, N10–H22, N10–H23), the surrounding water molecules act as either as hydrogen-bond acceptors (e.g., $H_2O\cdots$HN-adenine) or as hydrogen-bond donors (e.g. H–O–H···N-adenine). The resulting network consists of a mixture of $H_2O\cdots$HN-adenine, H–O–H···N-adenine and H–O–H···$OH_2$ (i.e., water–water) hydrogen bonds (Figure 1). The hydrogen-bonded H atoms remain within the molecular plane defined by the fused rings of the adenine molecule. This can be understood by considering that the location of the ring-centered nitrogen $2p_y$ acceptor lone pair is within the molecular frame of adenine. In contrast, the free (non-hydrogen bonded) OH groups of the water molecules are oriented out-of-plane with respect to the adenine chromophore such that the 2p lone-pair orbitals of water accommodate further hydrogen bonding.

The calculated hydrogen-bond lengths are also shown in Figure 1 and are consistent with previous theoretical findings.[35] In the ground electronic configuration, all N acceptor sites have similar basicities; this is reflected in the almost equivalent H–O–H···N-adenine hydrogen-bond lengths. In contrast, the proton of the N1–H group is more acidic than those of the $NH_2$ group and, as such, the former exhibits a shorter $H_2O\cdots$HN-adenine hydrogen-bond length.

As the geometric parameters of adenine–$(H_2O)_5$ and adenine–$(H_2O)_6$ clusters are similar, the forthcoming description of the photophysics of microhydrated 9*H*-adenine is focused exclusively on the former, which reduced the computational expense. In view of the minor difference in the H-bond lengths between the cluster containing six water molecules and that with five, we would not expect qualitatively different photophysics after the addition of a sixth $H_2O$ molecule to the adenine–$(H_2O)_5$ cluster. We are confident that our choice of five water molecules is sufficient, as all the important hydrogen-bond donor and acceptor interactions of the acidic and basic sites of the adenine chromophore are included. Each acidic and basic site has the possibility of partaking in excited-state proton transfer. The chosen locations of the proximal water molecules also provide stability through a water wire-type network.

### 2.2. Vertical Excitation Energies

Table 1 lists the calculated vertical excitation energies and corresponding oscillator strengths of the lowest three singlet excited states of the adenine–$(H_2O)_5$ cluster. For comparison, the analogous vertical excitation energies of isolated 9*H*-adenine are also given. In addition to this table, the reader is referred to Figure 2, which depicts the orbitals and orbital promotions associated with the formation of the lowest three excited electronic states of isolated adenine and adenine–$(H_2O)_5$.

**Table 1.** Vertical excitation energies and oscillator strengths of the three lowest excited states of 9*H*-adenine–$(H_2O)_5$ and isolated 9*H*-adenine calculated at the ADC(2)/cc-pVDZ level of theory. The numbers in parentheses correspond to the analogous vertical excitation energies computed at the CASPT2(10,8)/cc-pVDZ level of theory.

| 9*H*-Adenine–$(H_2O)_5$ State | *E* [eV] | *f* | 9*H*-Adenine State | *E* [eV] | *f* |
|---|---|---|---|---|---|
| $S_1$ $^1\pi\pi^*$ | 5.03 (4.90) | 0.2048 | $S_1$ $^1n\pi^*$ | 5.13 | 0.0051 |
| $S_2$ $^1\pi\pi^*$ | 5.26 (5.12) | 0.1698 | $S_2$ $^1\pi\pi^*$ | 5.27 | 0.0152 |
| $S_3$ $^1n\pi^*$ | 5.67 (5.99) | 0.0001 | $S_3$ $^1\pi\pi^*$ | 5.40 | 0.2856 |

As is well known, the lowest three singlet excited states of adenine—$S_1$, $S_2$ and $S_3$—are of $^1n\pi^*$, $^1\pi\pi^*(L_b)$ and $^1\pi\pi^*(L_a)$ character, respectively. As shown in Figure 2, the $S_1$ state involves promotion of an electron from an in-plane nitrogen $2p_y$ orbital to a ring-centered $\pi^*$ orbital. The second and third excited singlet states involve $\pi^*\leftarrow\pi$ orbital promotions, both of which are delocalized over the entire adenine structure.

In the adenine–$(H_2O)_5$ cluster, the orbital promotions are the same as for isolated adenine, highlighting that vertical excitation of the complex involves orbital transitions only within the chromophore, with no contributions from the orbitals of the water molecules. As is well known from many previous computational studies of aromatic chromophores in aqueous environments, $^1\pi\pi^*$ transitions are generally redshifted, whereas $^1n\pi^*$

© 2016 Wiley-VCH Verlag GmbH & Co. KGaA, Weinheim

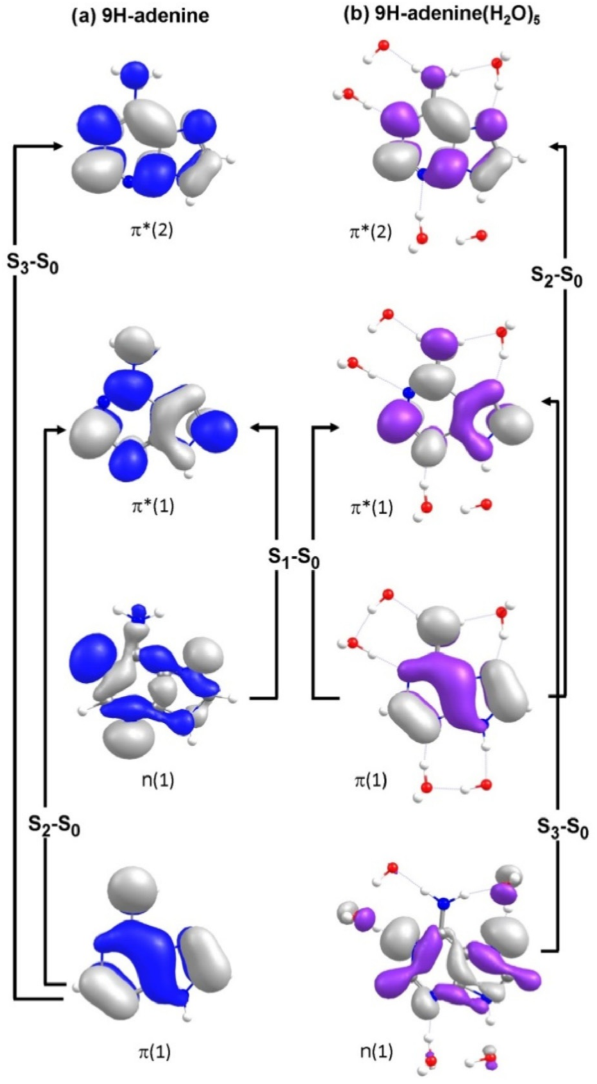

**Figure 2.** Orbitals and orbital promotions involved in forming the lowest four excited singlet states of a) 9*H*-adenine and b) the corresponding locally excited singlet states of 9*H*-adenine–$(H_2O)_5$.

transitions are generally blue-shifted relative to the gas phase. Correspondingly, the lowest three vertically excited states of adenine–$(H_2O)_5$ are $^1\pi\pi^*$ ($S_1$), $^1\pi\pi^*$ ($S_2$) and $^1n\pi^*$ ($S_3$) in nature. This has also been found in other photochemical studies of adenine in aqueous solution.[23,25,27] The stabilization of the $\pi\pi^*$ states arises due to polarization effects that stabilize $\pi^*$ orbitals more strongly than $\pi$ orbitals, leading to a net decrease in the $\pi^*$–$\pi$ energy gap. In contrast, the destabilization of the $n\pi^*$ state can be understood by recognizing that a substantial stabilization of the nitrogen-centered $2p_y$ orbital results from hydrogen bonding to water. The lowering of the energy of the $2p_y$ orbital leads to an increase in the n–$\pi^*$ energy gap. For comparative purposes, we also computed the vertical excitation energies of 9*H*-adenine–$(H_2O)_5$ at the CASPT2(10,8)/cc-pVDZ level of theory. The electronic state orderings and the vertical excitation energies so derived are in good agreement with those from ADC(2). These derived vertical excitation energies are broadly in agreement with those obtained by Došlić and co-workers for 9*H*-adenine–$H_2O$.[36] In both cases, the $n\pi^*$ state is destabilized upon complexation with $H_2O$ and the $^1\pi\pi^*$ state is the $S_1$ state.

The calculated vertical excitation energies associated with clusters of 9*H*-adenine–$(H_2O)_6$ are very similar to those of 9*H*-adenine–$(H_2O)_5$ (see Table S1 in the Supporting Information), further supporting the thesis that the latter cluster is appropriate for describing the photodynamics of hydrated adenine.

### 2.3. Electron-Driven Proton-Transfer Reaction Path

As discussed in the Introduction, the effect of hydration on the photophysics of adenine has been investigated previously using computational methods; these studies considered the reaction mechanisms of internal conversion through out-of-plane distorted CIs[23–27,31,34] and of H-atom transfer from adenine to water via a repulsive $^1\pi\sigma^*$ state.[30] Herein, we focus on the oxidative photochemistry of 9*H*-adenine in water, that is, the photoinduced abstraction of H-atoms from the aqueous environment.

In order to study how proximal water molecules contribute to the photophysical properties of the adenine chromophore, we scanned PE profiles along the possible solvent (water) → solute (adenine) electron transfer and PT paths. As noted above, adenine contains three basic nitrogen acceptor sites (N1, N3 and N7), which are expected to become more basic in the excited state, rendering adenine a photobase. Each of these sites is capable, in principle, of accepting a proton from water. In order to study the energetics associated with a particular excited-state electron transfer/PT reaction, we computed the PE profiles of adenine–$(H_2O)_5$ along the $R_{O15-H16}$, $R_{O13-H21}$ and $R_{O11-H18}$ bond stretching coordinates, which are depicted in Figures 3 a, 5 a and 6 a. These PT coordinates are henceforth referred to as PT1, PT2 and PT3, respectively. In all these figures, the filled black circles represent the $S_0$ energy profile calculated along the reaction path optimized in the $S_0$ state for the specific $R_{O-H}$ driving coordinate (see Computational Methods). The energy of the locally excited (LE) $^1\pi\pi$ state of adenine, calculated at the $S_0$-relaxed geometries, is designated by the profile plotted with red open circles. The filled red circles represent the energy of the lowest water-to-adenine CT state along the PT relaxed scan optimized for this state.

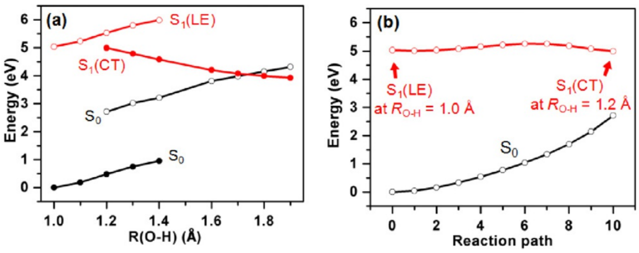

**Figure 3.** a) PE profiles of the ground state ($S_0$) and the lowest singlet excited states [$^1\pi\pi^*$(LE),$^1n\pi^*$(CT)], of the adenine–$(H_2O)_5$ complex along the $R_{O15-H16}$ PT coordinate. b) Energy profile of the linearly interpolated reaction path leading from the energy minimum of the $^1\pi\pi^*$(LE) state at $R_{O15-H16} = 1.0$ Å to the $^1n\pi^*$(CT) state at $R_{O15-H16} = 1.2$ Å.

© 2016 Wiley-VCH Verlag GmbH & Co. KGaA, Weinheim

The curve plotted with open black circles gives the energy of the $S_0$ state calculated along the minimum-energy reaction path determined in the CT state. The CT state is designated as $^1n\pi^*$(CT), but it should be noted that "n" refers here to one of the in-plane 2p orbitals of an H-bonded water molecule rather than the lone-pair orbital on the relevant N atom of adenine.

Focusing first on the PE profiles associated with the PT1 path (Figure 3a), the $S_0$ and $^1\pi\pi^*$(LE) energies calculated along the reaction path relaxed in the $S_0$ state rise steadily upon $R_{\text{O15-H16}}$ bond extension, thus showing that PT is unfavorable in these electronic states. If the energy of the $^1\pi\pi^*$(LE) state is optimized for fixed $R_{\text{O-H}}=1.2$ Å, the electronic character of this state changes from LE character (Figure 4a) to charge-transfer (CT) character (Figure 4b), the formation of which involves promotion of an electron from an in-plane O 2p orbital localized on water to the $\pi^*$ orbital localized on adenine, which corresponds to an electronic charge separation. The path connecting the $^1\pi\pi^*$(LE) state at $R_{\text{O-H}}=1.0$ Å to the $^1n\pi^*$(CT) state at its optimized geometry for $R_{\text{O-H}}=1.2$ Å was constructed as a linearly interpolated reaction path. The corresponding energy profile is shown in Figure 3b. This energy profile exhibits an apparent barrier of approximately 0.2 eV, which however, represents an upper limit to the activation barrier as the path is not a minimum-energy path. The true minimum-energy path connecting the $^1\pi\pi^*$(LE) and $^1n\pi^*$(CT) states is most likely barrierless. The relaxed $^1n\pi^*$(CT) profile (Figure 3b, red curve) shows a net decrease in energy as a function of $R_{\text{O-H}}$ stretching; this represents a driving force towards PT that results from the charge-separated character of the $^1n\pi^*$(CT) state, which is characteristic of EDPT.[37] The $S_0$ energy computed at the $^1n\pi^*$(CT)-relaxed geometries (Figure 3a, black open circles) increases as a function of the $R_{\text{O-H}}$ stretch coordinate. As a result, the energies of the $^1n\pi^*$(CT) state and the $S_0$ state cross at $R_{\text{O-H}}\approx 1.5$ Å. This $S_1/S_0$ crossing, which is allowed by symmetry in the planar system, becomes a CI if out-of-plane vibrational coordinates are taken into account. Depending on the nonadiabatic coupling at this CI, the reaction can lead to IC to the $S_0$ state of the complex (adiabatic path) or to a hydrated adenine-H$^{\cdot}$–OH$^{\cdot}$ biradical, as is discussed in more detail below.

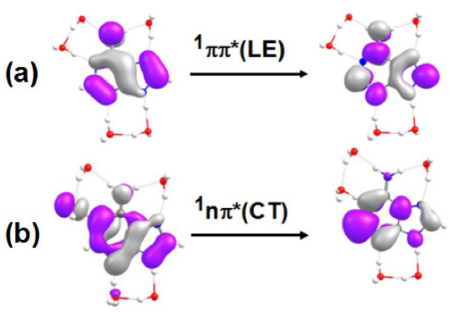

**Figure 4.** The molecular orbitals and orbital promotions involved in forming the a) $^1\pi\pi^*$(LE) and b) $^1n\pi^*$(CT) states, calculated at $R_{\text{O15-H16}}=1.0$ Å and $R_{\text{O-H}}=1.2$ Å, respectively.

The mechanistic details of the PT2 reaction path are similar to those described for the PT1 path. Figure 5a shows the PE profiles for the relevant electronic states along the $R_{\text{O13-H21}}$ driving coordinate. The relaxed $^1n\pi^*$(CT) state exhibits a distinct driving force of PT and its energy crosses the $S_0$ energy along this path, giving rise to a CI, representing another route by which ultrafast IC to the ground state or biradical formation could occur. The linearly interpolated reaction path connecting the $^1\pi\pi^*$(LE) and $^1n\pi^*$(CT) states is shown in Figure 5b. This path shows a somewhat larger apparent barrier of approximately 0.9 eV compared with that along PT1. We emphasize again that this barrier represents an upper limit to the true value.

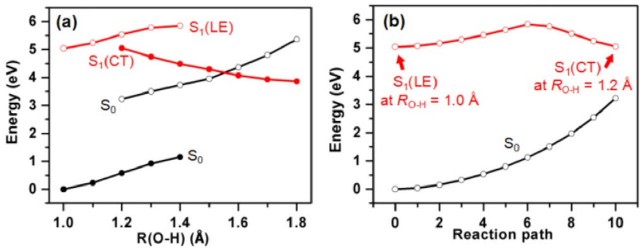

**Figure 5.** a) PE profiles of the ground state and the lowest singlet excited states of the adenine–$(H_2O)_5$ complex along the $R_{\text{O13-H21}}$ PT coordinate. b) Energy profile of the linearly interpolated reaction path leading from the minimum of the $^1\pi\pi^*$(LE) state at $R_{\text{O13-H21}}=1.0$ Å to the $^1n\pi^*$(CT) state at $R_{\text{O13-H21}}=1.2$ Å.

The final possible pathway by which intermolecular PT could occur in the adenine–$(H_2O)_5$ complex is the path PT3. Figure 6a shows the PE profiles of the $S_0$, $^1\pi\pi^*$(LE) and $^1n\pi^*$(CT) states along the $R_{\text{O11-H18}}$ driving coordinate. The LIIC path (Figure 6b) connecting the $^1\pi\pi^*$(LE) and $^1n\pi^*$(CT) states exhibits an apparent barrier of approximately 0.4 eV. As in PT1, the energy profile is likely to be barrierless along the minimum-energy path from the $^1\pi\pi^*$(LE) state to the $^1n\pi^*$(CT) state. However, the $^1\pi\pi^*$(LE) and $^1n\pi^*$(CT) energies do not cross along PT3 (Figure 6a), in contrast to the energies along PT1 and PT2. This finding is contrary to the recent work by Došlić and co-workers who reported an $S_1/S_0$ crossing along the $R_{\text{O11-H18}}$ coordinate in the adenine monohydrate. The difference between the pentahydrate and the monohydrate can be understood by recogniz-

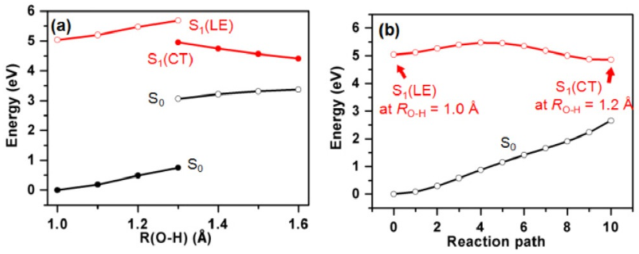

**Figure 6.** a) PE profiles of the ground state and the lowest singlet excited states of the adenine–$(H_2O)_5$ complex along the $R_{\text{O11-H18}}$ PT coordinate. b) Energy profile of the linearly interpolated reaction path leading from the energy minimum of the $^1\pi\pi^*$(LE) state to the $^1n\pi^*$(CT) state at $R_{\text{O-H}}=1.0$ Å.

© 2016 Wiley-VCH Verlag GmbH & Co. KGaA, Weinheim

ing that in the latter, a single water molecule was complexed between N9–H19 and N3, whereas in the present case we consider a dihydrate at this site. A plausible explanation for the difference between the monohydrated and dihydrated site could be that in the former the flexibility of the proximal water molecule allows for a more effective geometric relaxation that lowers the energy of the charge-separated state. Conversely, for the dihydrated site, steric effects could limit the torsional degrees of freedom of the water molecules, thus inhibiting nuclear rearrangements in order to neutralize the excess charge-separation.

## 3. Discussion and Conclusions

We investigated the photochemical reaction mechanisms associated with the three basic sites of 9*H*-adenine in the adenine–$(H_2O)_5$ cluster. For two sites, it was shown that a barrierless or nearly barrierless reaction path exists from the minimum of the light-absorbing locally excited $^1\pi\pi^*$ state via a CT state to a low-lying ($\approx$4.0 eV) CI with the electronic ground state. This CI represents an additional channel for the ultrafast excited-state deactivation of adenine, which is specific for an aqueous environment. In addition to solvent-induced modifications of the energies of the CIs, which are responsible for the intrinsic radiationless decay dynamics of 9*H*-adenine, this mechanism might contribute to the pronounced shortening of the excited-state lifetime of 9*H*-adenine in aqueous solution.

Insight into the mechanisms that govern the ultrafast excited-state deactivation of the nucleobase adenine in the gas phase, in solution as well as in the natural DNA environment is of fundamental importance for the understanding of the photoreactivity of DNA. Whereas computer-aided simulations of the photophysics of nucleobases in solution and in DNA oligomers are only possible with drastic approximations, such as QM/MM models, the photochemistry of microhydrated nucleobases can be investigated with comparatively rigorous electronic structure and dynamics methods. Microsolvated 9*H*-adenine is an important model system in this context.

Like other DNA and RNA bases, adenine has acidic sites (NH, $NH_2$) as well as basic sites (N), which serve as H-atom donors and acceptors, respectively, for hydrogen bonding with the first solvent shell. The acidic sites behave much like the OH, NH and $NH_2$ groups of phenol, indole and aniline, respectively. The photochemistry of the latter is now well understood both for isolated systems as well as for chromophore–solvent clusters. The photochemistry of the acidic sites is dominated by $^1\pi\sigma^*$ states, which drive H-atom photodetachment in the isolated species[43–50] and hydrogen transfer to the solvent in solvated species.[51–53] For 9*H*-adenine, the H-atom photodetachment reaction has been investigated with Rydberg-tagging spectroscopy[17] as well as with velocity-map ion imaging spectroscopy.[54] For 9*H*-adenine in aqueous solution, the generation of hydrated electrons has been observed upon excitation with 220 nm light.[21] This excitation energy (5.64 eV) is significantly lower than the ionization potential of 9*H*-adenine in water (7.5 eV).[55] The ejection of the electron into the solvent is nevertheless possible via a coupled electron–proton transfer process which is driven by repulsive $^1\pi\sigma^*$ states which are associated with the acidic groups of adenine. Thus, there exists convincing experimental evidence, which is supported by electronic structure calculations,[30] that UV-excited adenine behaves as a reducing (electron donating) species in aqueous environments.

By contrast, much less seems to be known about the photochemistry of the basic sites of adenine and the other nucleobases. Recent computational studies indicate that pyridine, the simplest six-membered heterocycle, can oxidize water upon UV excitation in the hydrogen-bonded pyridine–water complex.[56–58] Similar to the H-atom ejection reaction, the underlying mechanism is an EDPT process:[37] electron transfer from the 2p orbital of water to the $\pi^*$ orbital of pyridine is followed by the transfer of a proton from water to the chromophore, which results in a hydrogen-bonded neutral biradical. The results of the present work confirm recent preliminary results of Barbatti, who found evidence for electron transfer from water to 7*H*-adenine in a 7*H*-adenine–$(H_2O)_5$ cluster,[35] as well as recent results of Došlić and co-workers, who found evidence for an EDPT reaction of the 9*H*-adenine monohydrate.[36] So far, there exists no unequivocal experimental evidence that EDPT from water to adenine (or to any other DNA/RNA base) contributes to the shortening of the excited-state lifetime of these chromophores in aqueous environments. The observation of substantial amounts of adenine-$H^+$ fragments in the multiphoton ionization of adenine–$H_2O$ clusters by Park and co-workers[32] might be a signature of PT from water to adenine, although it cannot be excluded that the PT occurs in cationic species after multiple photon absorption.

The theoretical studies performed so far on the photochemistry of isolated and (micro)solvated nucleobases have focused on the explanation of the ultrafast exited-state deactivation by IC to the electronic ground state, which, after cooling on a picosecond timescale, restores the original chromophore. In this paradigm, it is assumed that the conical intersections provide funnels to the electronic ground state. In Figures 3a and 5a, this mechanism corresponds to the adiabatic (rather than diabatic) path at the CI of the CT state with the $S_0$ state. If, on the other hand, the CI is crossed diabatically, that is, if the nuclear dynamics follows the CT state rather than switching to the $S_0$ state at the CI, a neutral radical pair is formed, as the transfer of the proton neutralizes the electronic charge separation. The simulations performed in Refs. [35] and [35] are inconclusive in this respect, as the trajectories were terminated if a near-degeneracy of the CT state and the $S_0$ state were encountered. The excess energy of the reaction is sufficient to dissociate the radical pair, which yields the hypervalent adenine-$H^{\cdot}$ radical and the $OH^{\cdot}$ radical. These results show that thermodynamically at least, photoexcited adenine is able to oxidize water. If the adenine-$H^{\cdot}$ radical absorbs a second photon and ejects an H-atom via one of its acidic groups, a metastable tautomer of adenine is formed in its electronic ground state. This tautomer can relax to the lowest energy tautomer under ambient conditions, which closes the catalytic cycle. In this scenario, a water molecule is split into $H^{\cdot}$ and $OH^{\cdot}$ radicals by the sequential absorption of two UV photons. Adenine could thus be a potent

© 2016 Wiley-VCH Verlag GmbH & Co. KGaA, Weinheim

photocatalyst for water splitting by UV light. As hard UV photons were plentiful during the age of the origin of life, adenine and possibly other nucleobases might have served as the initial photosynthetic energy harvesting systems at the very beginning.

## Acknowledgements

*X.W. thanks the Chinese government for the award of a China Science Council doctoral scholarship. T.N.V.K. would like to thank the Technical University of Munich for the award of a postdoctoral fellowship and Engineering and Physical Science Research Council (Programme Grant EP/L005913) for financial support. W.D. acknowledges support by the Deutsche Forschungsgemeinschaft (DFG) excellence cluster "Munich Centre for Advanced Photonics" (MAP).*

**Keywords:** ab initio calculations · adenine · electron transfer · photochemistry · proton transfer

[1] C. E. Crespo-Hernández, B. Cohen, P. M. Hare, B. Kohler, *Chem. Rev.* **2004**, *104*, 1977 – 2020.
[2] H. Kang, B. Jung, S. K. Kim, *J. Chem. Phys.* **2003**, *118*, 11336 – 11336.
[3] H. Satzger, D. Townsend, A. Stolow, *Chem. Phys. Lett.* **2006**, *430*, 144 – 148.
[4] H. Satzger, D. Townsend, M. Z. Zgierski, S. Patchkovskii, S. Ullrich, A. Stolow, *Proc. Natl. Acad. Sci. USA* **2006**, *103*, 10196 – 10201.
[5] C. M. Marian, *J. Chem. Phys.* **2005**, *122*, 104314.
[6] S. Perun, A. L. Sobolewski, W. Domcke, *Chem. Phys.* **2005**, *313*, 107 – 112.
[7] S. B. Nielsen, T. Chakraborty, S. V. Hoffmann, *ChemPhysChem* **2005**, *6*, 2619 – 2624.
[8] H. Chen, S. Li, *J. Phys. Chem. A* **2005**, *109*, 8443 – 8446.
[9] S. Perun, A. L. Sobolewski, W. Domcke, *J. Am. Chem. Soc.* **2005**, *127*, 6257 – 6265.
[10] L. Serrano-Andrés, M. Merchán, A. C. Borin, *Chem. Eur. J.* **2006**, *12*, 6559 – 6571.
[11] L. Blancafort, *J. Am. Chem. Soc.* **2006**, *128*, 210 – 219.
[12] M. Barbatti, H. Lischka, *J. Am. Chem. Soc.* **2008**, *130*, 6831 – 6839.
[13] I. Conti, M. Garavelli, G. Orlandi, *J. Am. Chem. Soc.* **2009**, *131*, 16108 – 16118.
[14] M. Barbatti, Z. Lan, R. Crespo-Otero, J. J. Szymczak, H. Lischka, W. Thiel, *J. Chem. Phys.* **2012**, *137*, 22 – A503.
[15] W. M. I. Hassan, W. C. Chung, N. Shimakura, S. Koseki, H. Kono, Y. Fujimura, *Phys. Chem. Chem. Phys.* **2010**, *12*, 5317 – 5328.
[16] W. C. Chung, Z. Lan, Y. Ohtsuki, N. Shimakura, W. Domcke, Y. Fujimura, *Phys. Chem. Chem. Phys.* **2007**, *9*, 2075 – 2084.
[17] M. G. D. Nix, A. L. Devine, B. Cronin, M. N. R. Ashfold, *J. Chem. Phys.* **2007**, *126*, 124312.
[18] K. L. Wells, D. J. Hadden, M. G. D. Nix, V. G. Stavros, *J. Phys. Chem. Lett.* **2010**, *1*, 993 – 996.
[19] B. Cohen, P. M. Hare, B. Kohler, *J. Am. Chem. Soc.* **2003**, *125*, 13594 – 13601.
[20] T. Pancur, N. K. Schwalb, F. Renth, F. Temps, *Chem. Phys.* **2005**, *313*, 199 – 212.
[21] G. M. Roberts, H. J. B. Marroux, M. P. Grubb, M. N. R. Ashfold, A. J. Orr-Ewing, *J. Phys. Chem. A* **2014**, *118*, 11211 – 11225.
[22] A. L. Sobolewski, W. Domcke, *Phys. Chem. Chem. Phys.* **2007**, *9*, 3818 – 3829.
[23] B. Mennucci, A. Toniolo, J. Tomasi, *J. Phys. Chem. A* **2001**, *105*, 4749 – 4757.
[24] T. Gustavsson, N. Sarkar, I. Vayá, M. C. Jiménez, D. Markovitsi, R. Improta, *Photochem. Photobiol. Sci.* **2013**, *12*, 1375 – 1386.
[25] S. Yamazaki, S. Kato, *J. Am. Chem. Soc.* **2007**, *129*, 2901 – 2909.
[26] V. Ludwig, Z. M. da Costa, M. S. do Amaral, A. C. Borin, S. Canuto, L. Serrano-Andrés, *Chem. Phys. Lett.* **2010**, *492*, 164 – 169.
[27] Z. Lan, Y. Lu, E. Fabiano, W. Thiel, *ChemPhysChem* **2011**, *12*, 1989 – 1998.
[28] N. J. Kim, H. Kang, G. Jeong, Y. S. Kim, K. T. Lee, S. K. Kim, *J. Phys. Chem. A* **2000**, *104*, 6552 – 6557.
[29] H. Kang, K. T. Lee, S. K. Kim, *Chem. Phys. Lett.* **2002**, *359*, 213 – 219.
[30] H.-H. Ritze, H. Lippert, E. Samoylova, V. R. Smith, I. V. Hertel, W. Radloff, T. Schultz, *J. Chem. Phys.* **2005**, *122*, 224320.
[31] C. Canuel, M. Elhanine, M. Mons, F. Piuzzi, B. Tardivel, I. Dimicoli, *Phys. Chem. Chem. Phys.* **2006**, *8*, 3978 – 3987.
[32] S. H. Nam, H. S. Park, J. K. Song, S. M. Park, *J. Phys. Chem. A* **2007**, *111*, 3480 – 3484.
[33] Y. Nosenko, M. Kunitski, C. Riehn, P. H. P. Harbach, A. Dreuw, B. Brutschy, *Phys. Chem. Chem. Phys.* **2010**, *12*, 863 – 870.
[34] R. Mitrić, U. Werner, M. Wohlgemuth, G. Seifert, V. Bonačić-Koutecký, *J. Phys. Chem. A* **2009**, *113*, 12700 – 12705.
[35] M. Barbatti, *J. Am. Chem. Soc.* **2014**, *136*, 10246 – 10249.
[36] S. Chaiwongwattana, M. Sapunar, A. Ponzi, P. Decleva, N. Došlić, *J. Phys. Chem. A* **2015**, *119*, 10637 – 10644.
[37] A. L. Sobolewski, W. Domcke, *J. Phys. Chem. A* **2007**, *111*, 11725 – 11735.
[38] C. Møller, M. S. Plesset, *Phys. Rev.* **1934**, *46*, 618 – 622.
[39] T. H. Dunning, Jr., *J. Chem. Phys.* **1989**, *90*, 1007 – 1023.
[40] J. Schirmer, *Phys. Rev. A* **1982**, *26*, 2395 – 2416.
[41] C. Hättig, F. Weigend, *J. Chem. Phys.* **2000**, *113*, 5154 – 5161.
[42] TURBOMOLE V.6.4 2012, a development of the University of Karlsruhe and Forschungszentrum Karlsruhe GmbH, 1989 – 2007, TURBOMOLE GmbH, since 2007; www.turbomole.com.
[43] C.-M. Tseng, Y. T. Lee, C.-K. Ni, *J. Chem. Phys.* **2004**, *121*, 2459 – 2461.
[44] M. G. D. Nix, A. L. Devine, B. Cronin, R. N. Dixon, M. N. R. Ashfold, *J. Chem. Phys.* **2006**, *125*, 133318.
[45] M. N. R. Ashfold, G. A. King, D. Murdock, M. G. D. Nix, T. A. A. Oliver, A. G. Sage, *Phys. Chem. Chem. Phys.* **2010**, *12*, 1218 – 1238.
[46] A. Iqbal, L.-J. Pegg, V. G. Stavros, *J. Phys. Chem. A* **2008**, *112*, 9531 – 9534.
[47] M.-F. Lin, C.-M. Tseng, Y. T. Lee, C.-K. Ni, *J. Chem. Phys.* **2005**, *123*, 124303.
[48] A. Iqbal, V. G. Stavros, *J. Phys. Chem. A* **2010**, *114*, 68 – 72.
[49] R. Montero, Á. P. Conde, V. Ovejas, R. Martínez, F. Castaño, A. Longarte, *The J. Chem. Phys.* **2011**, *135*, 054308.
[50] G. M. Roberts, C. A. Williams, J. D. Young, S. Ullrich, M. J. Paterson, V. G. Stavros, *J. Am. Chem. Soc.* **2012**, *134*, 12578 – 12589.
[51] G. Pino, G. Gregoire, C. Dedonder-Lardeux, C. Jouvet, S. Martrenchard, D. Solgadi, *Phys. Chem. Chem. Phys.* **2000**, *2*, 893 – 900.
[52] H. Lippert, V. Stert, L. Hesse, C. P. Schulz, I. V. Hertel, W. Radloff, *J. Phys. Chem. A* **2003**, *107*, 8239 – 8250.
[53] G. A. Pino, A. N. Oldani, E. Marceca, M. Fujii, S. I. Ishiuchi, M. Miyazaki, M. Broquier, C. Dedonder, C. Jouvet, *J. Chem. Phys.* **2010**, *133*, 124313.
[54] K. L. Wells, G. M. Roberts, V. G. Stavros, *Chem. Phys. Lett.* **2007**, *446*, 20 – 24.
[55] F. Buchner, H.-H. Ritze, J. Lahl, A. Lübcke, *Phys. Chem. Chem. Phys.* **2013**, *15*, 11402 – 11408.
[56] J. R. Reimers, Z.-L. Cai, *Phys. Chem. Chem. Phys.* **2012**, *14*, 8791 – 8802.
[57] X. Liu, A. L. Sobolewski, R. Borrelli, W. Domcke, *Phys. Chem. Chem. Phys.* **2013**, *15*, 5957 – 5966.
[58] X. Liu, A. L. Sobolewski, W. Domcke, *J. Phys. Chem. A* **2014**, *118*, 7788 – 7795.

---

Manuscript received: December 13, 2015
Accepted Article published: February 2, 2016
Final Article published: February 23, 2016

© 2016 Wiley-VCH Verlag GmbH & Co. KGaA, Weinheim

# Paper 3

**Role of Electron-Driven Proton-Transfer Processes in the Ultrafast Deactivation of Photoexcited Anionic 8-oxoGuanine-Adenine and 8-oxoGuanine-Cytosine Base Pairs.** Xiuxiu Wu, Tolga N. V. Karsili, Wolfgang Domcke: *Molecules* **2017**, 135, 22.

molecules

MDPI

*Article*

# Role of Electron-Driven Proton-Transfer Processes in the Ultrafast Deactivation of Photoexcited Anionic 8-oxoGuanine-Adenine and 8-oxoGuanine-Cytosine Base Pairs

**Xiuxiu Wu [1], Tolga N. V. Karsili [2,*] and Wolfgang Domcke [1]**

[1] Department of Chemistry, Technische Universitat Munchen, Lichtenbergstr. 4, Garching D-85747, Germany; wuxiuxiu1988@gmail.com (X.W.); domcke@ch.tum.de (W.D.)

[2] Department of Chemistry, Temple University, 130 Beury Hall, 1901 N. 13th St., Philadelphia, PA 19122, USA

* Correspondence: tolga.karsili@temple.edu; Tel.: +1-215-204-2102

Academic Editor: Carlos E. Crespo-Hernández
Received: 17 November 2016; Accepted: 10 January 2017; Published: 14 January 2017

**Abstract:** It has been reported that 8-oxo-7,8-dihydro-guanosine (8-oxo-G), which is the main product of oxidative damage of DNA, can repair cyclobutane pyrimidine dimer (CPD) lesions when incorporated into DNA or RNA strands in proximity to such lesions. It has therefore been suggested that the 8-oxo-G nucleoside may have been a primordial precursor of present-day flavins in DNA or RNA repair. Because the electron transfer leading to the splitting of a thymine-thymine pair in a CPD lesion occurs in the photoexcited state, a reasonably long excited-state lifetime of 8-oxo-G is required. The neutral (protonated) form of 8-oxo-G exhibits a very short (sub-picosecond) intrinsic excited-state lifetime which is unfavorable for repair. It has therefore been argued that the anionic (deprotonated) form of 8-oxo-G, which exhibits a much longer excited-state lifetime, is more likely to be a suitable cofactor for DNA repair. Herein, we have investigated the exited-state quenching mechanisms in the hydrogen-bonded complexes of deprotonated 8-oxo-G$^-$ with adenine (A) and cytosine (C) using ab initio wave-function-based electronic-structure calculations. The calculated reaction paths and potential-energy profiles reveal the existence of barrierless electron-driven inter-base proton-transfer reactions which lead to low-lying $S_1/S_0$ conical intersections. The latter can promote ultrafast excited-state deactivation of the anionic base pairs. While the isolated deprotonated 8-oxo-G$^-$ nucleoside may have been an efficient primordial repair cofactor, the excited states of the 8-oxo-G$^-$-A and 8-oxo-G$^-$-C base pairs are likely too short-lived to be efficient electron-transfer repair agents.

**Keywords:** oxidative photochemistry; conical intersections; excited state proton-transfer

## 1. Introduction

The photoinduced dynamics of biological chromophores have been extensively studied in the past two decades. Within this class of organic chromophore systems, the most notable include DNA and RNA nucleobases [1–15], nucleosides [1,16–26], and base pairs [27–36]. Despite strongly absorbing in the near-UV, DNA and RNA nucleobases exhibit a remarkable degree of photostability, although the generation of photoinduced lesions in DNA strands is not fully suppressed [37–39]. It is generally believed that the mechanism of the observed photostability of the building blocks of DNA is ultrafast internal conversion of excited state populations to the electronic ground state with the excess energy being dissipated to the surrounding environment as heat. For the isolated nucleobases, there is consensus that internal conversion is mediated by low-lying conical intersections (CIs) which involve excited singlet states of $\pi\pi^*$ and/or $n\pi^*$ character as well as the $S_0$ state and become accessible by out-of-plane deformations of six-membered aromatic rings. These CIs dominate the nonradiative decay of the lowest excited states of cytosine (C) [5,7], uracil (U) [8,12], adenine (A) [9–11,13,14], guanine (G) [40–43], and thymine (T) [15,44,45]. At somewhat elevated excitation energies, CIs arising from so-called $\pi\sigma^*$ states associated with acidic groups are also known to play a role in the photodynamics of the nucleobases. Apart from direct UV excitation, lesions in DNA are also formed by radical-induced oxidation of DNA—leading to oxidized bases such as 8-oxo-guanine (8-oxo-G). Additional paths for UV-induced DNA damage are the formation of radical species either via dissociation or ionization [46,47].

8-oxo-G is one of the most common lesions found in oxidatively damaged DNA [48–50]. The oxidation of G to 8-oxo-G substantially reduces the redox potential and enables it to form base pairs with adenine. This may lead to the replacement of G-C pairs by A-T pairs during replication, which is a mutagenic feature common in many forms of cancer [51,52]. Despite these adverse effects, the lower redox potential of 8-oxo-dG (cf. G) makes it a viable candidate for protecting DNA by scavenging highly oxidizing species such as OH radicals [53]. It has also been demonstrated that 8-oxo-G is capable of repairing lesions of cyclobutane pyrimidine dimers (CPD) [54,55]. In the proposed mechanism, the photoexcited state of 8-oxo-G transfers an electron to the CPD, initiating thereby bond cleavage between the pyrimidine bases. This finding suggests that 8-oxo-G may have played an analogous role to modern flavins in prebiotic redox processes [54], rendering its excited state dynamics of particular interest.

Recently, Kohler, Matsika, and coworkers investigated the ultrafast excited-state dynamics of neutral and anionic 8-oxo-deoxyguanosine (8-oxo-dG) in $D_2O$ solution with femtosecond transient absorption spectroscopy and ab initio calculations [26]. 8-oxo-dG exists in its anionic (deprotonated) form at pH > 7 [56]. The neutral form was found to deactivate to the electronic ground state in <1 ps, whereas the anionic form exhibits a significantly longer excited-state lifetime of ~43 ps [26]. Correspondingly, the latter shows a significant quantum yield for fluorescence [26]. More recent fluorescence up-conversion and theoretical studies led to the conclusion that neutral 8-oxo-G exhibits an ultrafast radiationless decay via two CIs which are accessible by certain out-of-plane deformations of guanine, whilst the longer lifetime of anionic 8-oxo-$G^-$ was attributed to the existence of sizable barriers along the reaction paths connecting the Franck-Condon region to the $S_1/S_0$ CIs [57]. This mechanism was also explored by Changenet-Barret et al. for the neutral form [58]. An alternative interpretation is provided by recent studies by Tuna et al. who performed ab initio calculations of excited-state reaction paths for electron/proton transfer between sugar and base for the neutral and anionic forms of the 8-oxo-dG nucleoside, highlighting a barrierless and therefore efficient electron/proton-transfer radiationless deactivation mechanism in the neutral form, while a barrier was found to exist along this reaction path in the anionic form [23]. This finding provides an alternative explanation for the substantially longer excited-state lifetime of the deprotonated form of the 8-oxo-dG nucleoside compared to the neutral form.

In double-stranded DNA, nucleobases are organized in horizontally oriented hydrogen-bonded base pairs and vertically oriented stacks stabilized by $\pi$-$\pi$ interactions. Both architectural motifs may modify the dynamics of the intrinsic decay paths of the individual nucleobases by providing additional decay channels by which the excited-state populations can evolve. Such modifications have been studied, for example, by Crespo-Hernandez and co-workers who have shown that base stacking of A-T DNA oligomers leads to the formation of intra-strand excimer states with lifetimes of 50–150 ps [59] with additional decay features that are somewhat longer lived [60,61]. Kohler and co-workers recently studied the excited-state dynamics of a $\pi$-stacked dinucleotide containing the 8-oxo-$G^-$ anion at the 5′-end and neutral A at the 3′-end, using time-resolved transient UV-pump IR-probe spectroscopy. They found that UV excitation of the dinucleotide leads to prompt electron transfer from 8-oxo-$G^-$ to the $\pi$-stacked A, generating a neutral 8-oxo-G radical and an A radical anion [62,63]. For stacked base pairs, the inter-base hydrogen bonds provide additioinal paths along which coupled electron/proton transfer reactions can occur [64,65].

Sobolewski and Domcke and de Vries and coworkers proposed a photoprotective role of excited-state proton transfer in the G-C Watson-Crick (WC) base pair [27,34,35,66]. In these theoretical and experimental studies, the authors suggested that ultrafast excited-state deactivation occurs by inter-base electron-driven proton transfer (EDPT) from G to C. The ab initio electronic-structure calculations identified a low-lying $^1\pi\pi^*$ charge-transfer (CT) state (arising via an electron promotion from a G-centered $\pi$ orbital to a C-centered $\pi^*$ orbital). The CT state drives the transfer of a proton from guanine to cytosine. While the CT state is stabilized by the proton transfer, the ground state is destabilized, which results in a barrierless reaction path leading to a low-energy CI of the $S_1$ state with the $S_0$ state. These findings are supported by pump-probe experiments in solution [21] as well as by recent transient UV pump and IR probe experiments in the gas phase [22]. The inter-base EDPT reaction was shown to be the main path by which internal conversion to the ground state proceeds in the G-C WC base pair in the gas phase and in the bulk DNA environment [27,29–32,34–36,66]. For the A-T WC base pair, EDPT has also been identified as an efficient deactivation path after photoexcitation by ab initio calculations [28,30,33], although an experimental verification of the predicted ultrashort lifetime of the A-T WC base pair is still lacking.

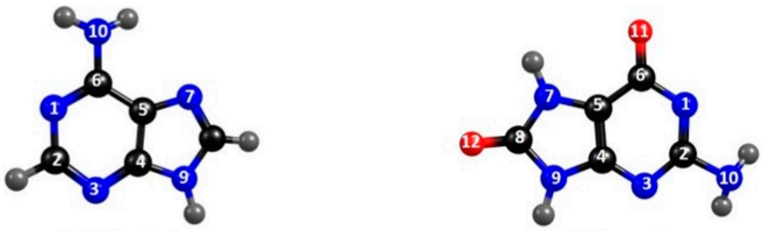

(a) 9H-adenine (b) 8-oxo-G$^-$

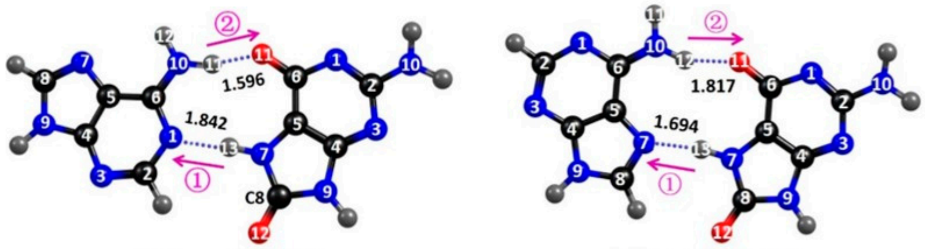

(c) 8-oxo-G$^-$-A: HG1 (d) 8-oxo-G$^-$-A: HG2

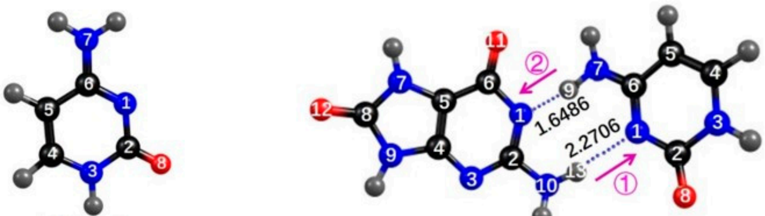

(e) Cytosine (f) 8-oxo-G$^-$-C

**Figure 1.** Ground-state equilibrium geometry of (**a**) isolated 9*H*-adenine; (**b**) isolated 8-oxo-G$^-$; (**c**) HG1 form of 8-oxo-G$^-$A; (**d**) HG2 form of 8-oxo-G$^-$A; (**e**) isolated cytosine; and (**f**) 8-oxo-G$^-$-C.

8-oxo-G$^-$ can pair with A via Hoogsteen (HG) base pairing in two low-energy conformations [67]: HG1 and HG2 (see Figure 1). 8-oxo-G$^-$ can also form a stable pair with cytosine in a structure involving two hydrogen bonds, see Figure 1f. EDPT processes in the neutral 8-oxo-G-A and 8-oxo-G-C base pairs were investigated by Kumar and Sevilla with time-dependent density functional (TD-DFT) calculations [67]. In the present work, we focus on EDPT reactions in the anionic 8-oxo-G$^-$-A and 8-oxo-G$^-$-C base pairs. Since anionic 8-oxo-G$^-$ has been shown to have a substantially longer excited-state lifetime than neutral 8-oxo-G, the former appears better suited for light-driven DNA repair reactions than the short-lived neutral 8-oxo-G. It is therefore of interest to explore how base-pairing with A or C affects the excited-state lifetime of anionic 8-oxo-G$^-$. As well as base pairing with cytosine (i.e., the complementary base to G), 8-oxoG$^-$ is also well-known to form mismatched base pairing with A via a Hoogsteen configuration [68–70]. This propensity for forming Hoogsteen base pairs with adenine is due to the enhanced redox potential of 8-oxoG$^-$ compared with that of natural guanine.

Using ab initio wave-function based electronic-structure calculations, we identify the EDPT reaction paths leading to CIs through which the excited-state population can internally convert to $S_0$. Our findings provide evidence for barrierless EDPT reaction paths and therefore likely highly efficient excited-state deactivation of the 8-oxo-G$^-$-A and 8-oxo-G$^-$-C base pairs. The efficient excited-state deactivation of the base pairs enhances their photostability, but inevitably also lowers their repair efficiency.

## 2. Results

### 2.1. Ground State Geometries

Figure 1 presents the MP2/cc-pVDZ-optimized ground-state structures of 9*H*-adenine (**a**); 8-oxo-G$^-$ (**b**); HG1 (**c**) and HG2 (**d**) 8-oxo-G$^-$-A conformers; cytosine (**e**); and the 8-oxo-G$^-$-C base pair (**f**). In both 8-oxo-G$^-$-A HG base pairs, all atoms are in a common plane with the exception of the wagging angle of the amino group of 8-oxo-G$^-$. Adenine retains a planar geometry since the amino group of adenine is involved in the inter-base hydrogen bonding, while in the structure of isolated adenine there is some pyramidization of the amino group.

In the HG1 and HG2 8-oxo-G$^-$-A base pairs, 8-oxo-G$^-$ and A act both as hydrogen-bond donors and as hydrogen-bond acceptors. There are two hydrogen bonds in the HG1 base pair: N10−H11(A)•••O11(8-oxo-G$^-$) and N7−H13(8-oxo-G$^-$)•••N1(A). The HG2 base pair also has also two hydrogen bonds, N10−H12(A)•••O11(8-oxo-G$^-$) and N7−H13(8-oxo-G$^-$)•••N7(A). The calculated hydrogen-bond lengths are included in Figure 1. In the HG1 base pair, the length of N10−H11•••O11(1.596 Å) is shorter than that of N7−H13•••N1(1.842 Å). In contrast, in the HG2 base pair, N10−H12•••O11(1.817 Å) is longer than N7−H13•••N7(1.694 Å). The optimized ground-state energy of the HG2 base pair is found to be lower than that of the HG1 base pair by 0.05 eV, which indicates a Boltzmann population of 13:87 for HG1:HG2. For the 8-oxo-G$^-$-C base pair, three low-energy H-bonded configurations have been optimized. Among these, the structure shown in Figure 1f is the lowest-energy conformer.

### 2.2. Vertical Excitation Energies

Table 1 lists the calculated vertical excitation energies and corresponding oscillator strengths (in parentheses) of the lowest four singlet excited states of the 8-oxoG$^-$ containing base pairs presently studied. For comparison, the analogous vertical excitation energies of isolated cytosine, 9*H*-adenine and 8-oxo-G$^-$ are presented in Table 2. In addition to Table 1, the reader is directed to Figure 2, which depicts the orbitals and orbital promotions associated with the formation of the lowest four excited electronic states of isolated 9*H*-adenine, cytosine, 8-oxo-G$^-$, as well as the 8-oxo-G$^-$-A and 8-oxo-G$^-$-C base pairs.

**Table 1.** Vertical excitation energies ($\Delta E$) and oscillator strengths ($f$) of the lowest four excited states of the two 8-oxo-G$^-$-A HG base pairs and the 8-oxo-G$^-$-C base pair, calculated at the ADC(2)/cc-pVDZ level of theory. Here O$^-$ stands for 8-oxo-G$^-$.

| State | $\Delta E$/eV ($f$) | State | $\Delta E$/eV ($f$) | State | $\Delta E$/eV ($f$) |
|---|---|---|---|---|---|
| 8-oxo-G$^-$-A HG1 | | 8-oxo-G$^-$-A HG2 | | 8-oxo-G$^-$-C | |
| $S_1$ $^1\pi\pi^*$(O$^-$→A) | 4.44 (0.0139) | $S_1$ $^1\pi\pi^*$(O$^-$→A) | 4.39 (0.0091) | $S_1$ $^1\pi\pi^*$(O$^-$→C) | 4.48 (0.0023) |
| $S_2$ $^1\pi\pi^*$(O$^-$→O$^-$) | 4.85 (0.2321) | $S_2$ $^1\pi\pi^*$(O$^-$→O$^-$) | 4.89 (0.1025) | $S_2$ $^1\pi\pi^*$(C→C) | 4.76 (0.0176) |
| $S_3$ $^1\pi\pi^*$(A→A) | 4.91 (0.1050) | $S_3$ $^1\pi\pi^*$(A→A) | 4.95 (0.0922) | $S_3$ $^1\pi\pi^*$(O$^-$→O$^-$) | 4.88 (0.0695) |
| $S_4$ $^1\pi\pi^*$(O$^-$→A) | 5.09 (0.0109) | $S_4$ $^1\pi\pi^*$(O$^-$→A) | 5.18 (0.0281) | $S_4$ $^1\pi\pi^*$(O$^-$→C) | 4.94 (0.0782) |

**Table 2.** Vertical excitation energies ($\Delta E$) and oscillator strengths ($f$) of the lowest four excited states of isolated 9*H*-adenine, anionic 8-oxo-guanine, and cytosine, calculated at the ADC(2)/cc-pVDZ level of theory.

| **State** | **$\Delta E$/eV ($f$)** | **State** | **$\Delta E$/eV ($f$)** | **State** | **$\Delta E$/eV ($f$)** |
|---|---|---|---|---|---|
| **9*H*-adenine** | | **8-oxo-G$^-$** | | **Cytosine** | |
| $S_1$ $^1n\pi^*$ | 5.13 (0.0051) | $S_1$ $^1\pi\pi^*$ | 4.92 (0.0629) | $S_1$ $^1\pi\pi^*$ | 4.65 (0.0545) |
| $S_2$ $^1\pi\pi^*$ | 5.27 (0.0152) | $S_2$ $^1n\pi^*$ | 5.16 (0.0000) | $S_2$ $^1n\pi^*$ | 4.81 (0.0019) |
| $S_3$ $^1\pi\pi^*$ | 5.40 (0.2856) | $S_3$ $^1\pi\pi^*$ | 5.47 (0.2964) | $S_3$ $^1n\pi^*$ | 5.29 (0.0016) |
| $S_4$ $^1n\pi^*$ | 5.82 (0.0018) | $S_4$ $^1n\pi^*$ | 5.54 (0.0003) | $S_4$ $^1\pi\pi^*$ | 5.76 (0.1261) |

As is well known, the lowest four excited states of 9*H*-adenine are of $^1n\pi^*$, $^1\pi\pi^*(L_b)$, $^1\pi\pi^*(L_a)$, and $^1n\pi^*$ character. The $S_1$ and $S_4$ states involve promotion of an electron from an in-plane nitrogen $2p_y$ orbital to a ring-centered $\pi^*$ orbital, while the $S_2$ and $S_3$ states involve $\pi^*\leftarrow\pi$ orbital promotions which are delocalized over the aromatic rings. For 8-oxo-G$^-$, the lowest four excited states are $^1\pi\pi^*(S_1)$, $^1n\pi^*(S_2)$, $^1\pi\pi^*(S_3)$, and $^1n\pi^*(S_4)$ in nature. As shown in Figure 2, the $S_2$ and $S_4$ states involve the promotion of an electron from the nitrogen $2p_y$ orbital to a ring-centered anti-bonding $\pi^*$ orbital. The $S_1$ and $S_3$ states involve excitation from a ring-centered $\pi$ orbital to the lowest $\pi^*$ orbital.

In the two 8-oxo-G$^-$-A HG base pairs, the orbital promotions are almost the same and the lowest four excited states are of $^1\pi\pi^*$ character. The $S_1$ state involves electron promotion from the ring-centered $\pi$ HOMO localized on 8-oxo-G$^-$ to the ring-centered $\pi^*$ LUMO localized on adenine, leading to a charge-separated state of CT character. The $S_2$ state involves a $\pi^*\leftarrow\pi$ promotion, whereby both orbitals are localized on 8-oxo-G$^-$. The $S_3$ state involves a $\pi^*\leftarrow\pi$ promotion localized on adenine. The $S_2$ and $S_3$ states are therefore locally-excited (LE) states on 8-oxo-G$^-$ and A, respectively. The vertical excitation energies of the $S_2$ and $S_3$ states are comparable to that of isolated 8-oxo-G$^-$ and adenine, respectively. As can be seen in Table 1, the vertical excitation energy of the $S_2$ ($^1\pi\pi^*$) state of the HG1/HG2 base pair (4.85 eV/4.89 eV) is nearly equal to that of the analogous LE state (i.e., the first $^1\pi\pi^*$ state) of isolated 8-oxo-G$^-$ (4.92 eV), suggesting that pairing of 8-oxo-G$^-$ with adenine has little effect on the lowest LE $^1\pi\pi^*$ state energy. In contrast, the vertical excitation energies of all electronic states show a significant red-shift upon complexation relative to that of isolated adenine. Similar to the $S_1$ state, the $S_4$ state also is of CT character, involving the transition from a $\pi$ orbital of 8-oxo-G$^-$ to an $\pi^*$ orbital of adenine, with a much higher excitation energy. The vertical excitation energies of the two HG base pairs are very similar and lower than those of isolated adenine and 8-oxo-G$^-$. Compared with the TD-DFT results for neutral 8-oxo-G-A HG base pair [67], the lowest $^1\pi\pi^*$ transition localized on 8-oxo-G$^-$ is blue-shifted, while the lowest $^1\pi\pi^*$ transition localized on adenine is red-shifted.

Figure 2f depicts the orbital promotions associated with the 8-oxoG$^-$-C base pair. As shown, the electronic excitation to $S_1$ involves a $\pi$ to $\pi^*$ electron promotion in which the former is localized on the 8-oxoG$^-$ moiety, whereas the latter is localized on the C moiety. As with the 8-oxo-G$^-$-A base pairs, electronic excitation to $S_1$ involves a significant charge separation and is thus of CT character. In contrast, electronic excitation to the $S_2$, $S_3$, and $S_4$ states involves electron promotions between $\pi$/n to $\pi^*$ orbitals that are localized on the same nucleobase within the base pair. The observed orbital ordering is very similar to that of the WC-type G-C base pair which also has an $S_1$ state of CT character, whilst the higher-lying states are of LE character [34,35].

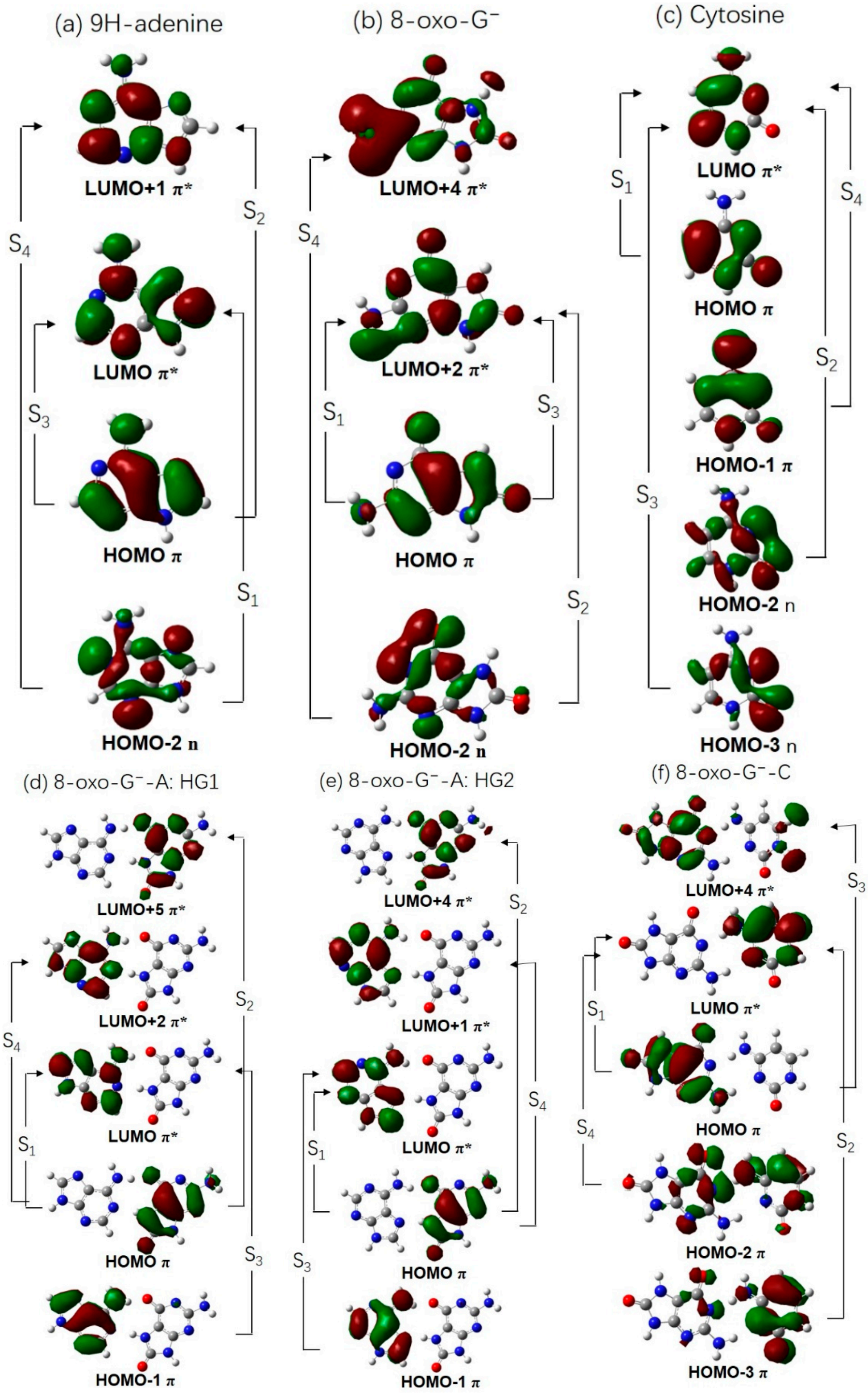
(a) 9H-adenine
LUMO+1 π*
LUMO π*
HOMO π
HOMO-2 n
S4
S3
S2
S1
(b) 8-oxo-G⁻
LUMO+4 π*
LUMO+2 π*
HOMO π
HOMO-2 n
S4
S1
S3
S2
(c) Cytosine
LUMO π*
HOMO π
HOMO-1 π
HOMO-2 n
HOMO-3 n
S1
S4
S2
S3
(d) 8-oxo-G⁻-A: HG1
LUMO+5 π*
LUMO+2 π*
LUMO π*
HOMO π
HOMO-1 π
S4
S1
S2
S3
(e) 8-oxo-G⁻-A: HG2
LUMO+4 π*
LUMO+1 π*
LUMO π*
HOMO π
HOMO-1 π
S2
S4
S1
S3
(f) 8-oxo-G⁻-C
LUMO+4 π*
LUMO π*
HOMO π
HOMO-2 π
HOMO-3 π
S3
S1
S4
S2

**Figure 2.** Orbitals and orbital promotions involved in forming the lowest four excited states of 9*H*-adenine (**a**), 8-oxo-G$^-$ (**b**), cytosine (**c**), and the three base pairs (**d**–**f**).

### 2.3. Electron-Driven Proton-Transfer Decay Paths

#### 2.3.1. 8-oxoG$^-$-A

In order to study the intrinsic photophysical properties of the two HG base pairs, we explored the details of the potential-energy (PE) profiles along possible inter-base electron and proton transfer paths. The HG1 and HG2 base pairs have two potential reaction paths for proton transfer, one involving the transfer of a proton from adenine to 8-oxo-G⁻ along the N10−H11•••O11 or N10−H12•••O11 hydrogen bonds, the other involving the transfer of a proton from 8-oxo-G⁻ to adenine along the N7−H13•••N1 or N7−H13•••N7 hydrogen bonds (as indicated by the arrows in Figure 1c,d). In order to study the energetics associated with a particular excited-state electron/proton transfer reaction, we computed the PE profiles along the $R_{\mathrm{N10-H11}}$, $R_{\mathrm{N7-H13}}$ bond-stretching coordinates for the HG1 base pair and along the $R_{\mathrm{N10-H12}}$, $R_{\mathrm{N7-H13}}$ bond-stretching coordinates for the HG2 base pair. The results are depicted in Figures 3 and 4, respectively. In these figures, the filled black circles represent the $S_0$ energy profile calculated along the reaction path optimized in the $S_0$ state for the specific $R_{\mathrm{N-H}}$ driving coordinate. The energy of the unrelaxed $^1\pi\pi^*$ CT state (henceforth $^1\pi\pi^*$(uCT)) of the base pairs, calculated at the $S_0$-relaxed geometries, is designated by the profile plotted with the open red circles. The filled red circles represent the energy of the lowest inter-base CT state along the proton-transfer relaxed scan optimized for this state. The curve plotted with open black circles gives the energy of the $S_0$ state calculated along the minimum-energy reaction path determined in the CT state.

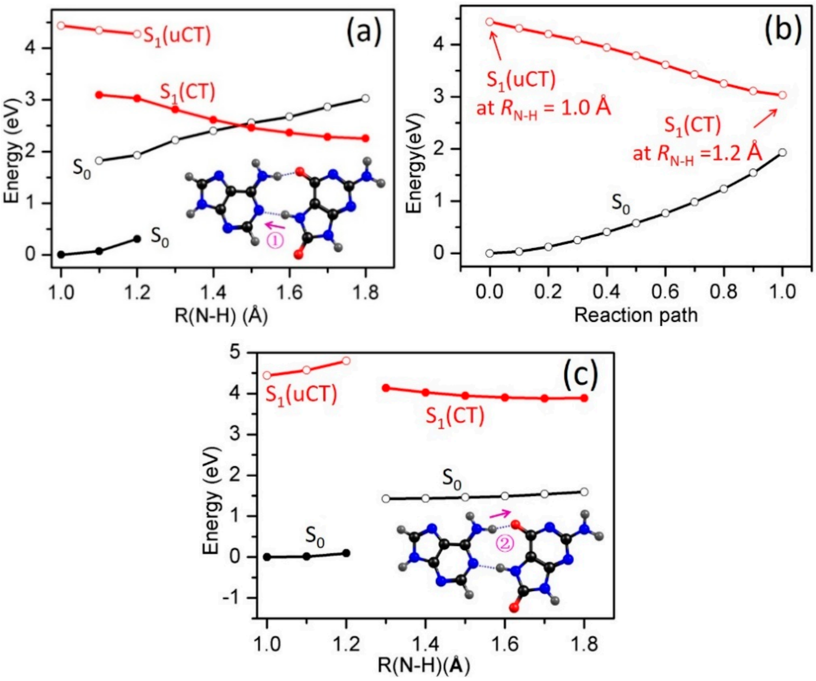

**Figure 3.** PE profiles of the ground state and the lowest singlet excited states of the HG1 8-oxo-G⁻-A base pair along $R_{\mathrm{N7-H13}}$ (**a**) and $R_{\mathrm{N10-H11}}$ (**c**) proton-transfer coordinates; (**b**) shows the energy profiles of the LIIC path connecting $S_1$(uCT) with $S_1$(CT) in (**a**).

Figure 3a shows the PE profiles associated with proton transfer along N7−H13•••N1 (Path 1, see inset in Figure 3a) in the HG1 base pair. The $S_0$ energies calculated along the reaction path relaxed in the $S_0$ state rise steadily upon $R_{\mathrm{N7-H13}}$ bond extension, showing that proton transfer is unfavorable in this electronic state. When the energy of the $^1\pi\pi^*$(uCT) state is optimized for fixed $R_{\mathrm{N7-H13}}$ = 1.2 Å, the electronic character of this state changes from LE character to CT character, which implies the transfer of an electron localized on 8-oxo-G⁻ to the $\pi^*$ orbital localized on 9*H*-adenine, resulting in an electronic charge separation. The path connecting the $^1\pi\pi^*$(uCT) state at $R_{\mathrm{N7-H13}}$ = 1.0 Å to the $^1\pi\pi^*$(CT) state at its optimized geometry for $R_{\mathrm{N7-H13}}$ = 1.2 Å was constructed as a linearly interpolated reaction path. The corresponding energy profile is shown in Figure 3b. This energy profile exhibits no barrier, which ensures that the minimum-energy path connecting the $^1\pi\pi^*$(uCT) and $^1\pi\pi^*$(CT) states is barrierless. The relaxed $^1\pi\pi^*$(CT) profile (Figure 3a, full red circles) shows a strong decrease of the energy as a function of $R_{\mathrm{N7-H13}}$ stretching; this represents the driving force towards proton transfer that results from the charge-separated character of the $^1\pi\pi^*$(CT) state, which is characteristic of EDPT [71]. The $S_0$

energy computed at the ${}^1\pi\pi^*$(CT)-relaxed geometries (Figure 3a, black open circles) increases as a function of the $R_{\mathrm{N7-H13}}$ stretching coordinate. As a result, the energies of the ${}^1\pi\pi^*$(CT) state and the $S_0$ state cross at $R_{\mathrm{N7-H13}} \approx 1.45$ Å. This $S_1/S_0$ crossing becomes a CI when the appropriate coupling modes are taken into account. Depending on the topography of the PE surfaces and the nonadiabatic coupling at the CI, the reaction can lead to internal conversion to the $S_0$ state of the complex (adiabatic path) or to a biradical.

The other possible pathway by which inter-base proton transfer can occur in the HG1 base pair is along the N10−H11•••O11 hydrogen bond (Path 2, see inset in Figure 3c). Figure 3c shows the PE profiles of the $S_0$, ${}^1\pi\pi^*$(uCT) and ${}^1\pi\pi^*$(CT) states along the $R_{\mathrm{N10-H11}}$ driving coordinate. The LIIC path connecting the ${}^1\pi\pi^*$(uCT) and ${}^1\pi\pi^*$(CT) states (not shown) exhibits no barrier. As for Path 1, the energy profile along the minimum-energy path from the ${}^1\pi\pi^*$(uCT) state to the ${}^1\pi\pi^*$(CT) state is barrierless. However, the ${}^1\pi\pi^*$(uCT) and ${}^1\pi\pi^*$(CT) energies do not cross along $R_{\mathrm{N10-H11}}$ (Figure 3c), in contrast to the energies along $R_{\mathrm{N7-H13}}$. This result can easily be rationalized. While the electron transfer occurs from 8-oxo-G$^-$ to A, the proton has to move in the opposite direction, from A to 8-oxo-G$^-$, which is not energetically favorable. The $S_1$(CT) state is therefore not stabilized by the transfer of the proton and the EDPT mechanism does not apply for Path 2 in the HG1 base pair.

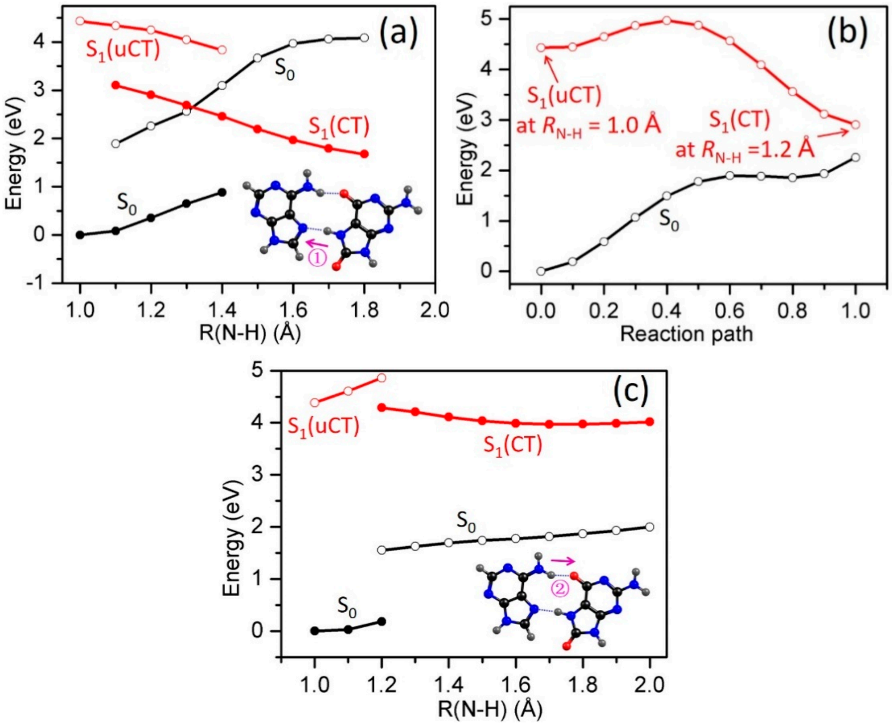

**Figure 4.** PE profiles of the ground state and the lowest singlet excited states of the HG2 8-oxo-G$^-$-A base pair along the $R_{\mathrm{N7-H13}}$ (**a**) and the $R_{\mathrm{N10-H12}}$ (**c**) proton-transfer coordinates; (**b**) shows the energy profiles of the LIIC path connecting $S_1$(uCT) with $S_1$(CT) in (**a**).

The PE profiles of the lowest excited states of ${}^1\pi\pi^*$ (uCT) and ${}^1\pi\pi^*$ (CT) character of the HG2 base pair as a function of the $R_{\mathrm{N7-H13}}$ are shown in Figure 4a. In the HG2 base pair, there likewise exists a proton-transfer path (N7−H13•••N7), which leads to a low-lying $S_1/S_0$ CI, and a proton-transfer path (N10−H12•••O11) which does not lead to a CI. The mechanistic details of the N7−H13•••N7 reaction path (Path 1, see inset in Figure 4a) are similar to those described for the Path 1 in the HG1 base pair. The relaxed ${}^1\pi\pi^*$ (CT) state exhibits a distinct driving force for proton transfer and its energy crosses the $S_0$ energy along this path at $R_{\mathrm{N7-H13}} \approx 1.30$ Å, giving rise to a CI, representing a route by which either ultrafast IC to the ground state or biradical formation can occur. The linearly interpolated reaction path connecting the ${}^1\pi\pi^*$ (uCT) and ${}^1\pi\pi^*$ (CT) states is shown in Figure 4b. The energy profile exhibits a substantial barrier of approximately 0.5 eV, which represents an upper limit to the reaction barrier along the minimum-energy path. The access of the photoexcited HG2 8-oxo-G$^-$-A base pair to the $S_1/S_0$ CI may thus be kinetically hindered.

The proton-transfer path along the $R_{N10-H11}$ driving coordinate in the HG2 base pair is similar to Path 2 in the HG1 base pair. Figure 4c shows the PE profiles of the $S_0$, $^1\pi\pi^*$(uCT) and $^1\pi\pi^*$(CT) states along the $R_{N10-H11}$ driving coordinate. While the LIIC path connecting the $^1\pi\pi^*$(uCT) and $^1\pi\pi^*$(CT) states (not shown) exhibits no barrier, the $^1\pi\pi^*$(uCT) and $^1\pi\pi^*$(CT) energies do not exhibit a crossing along $R_{N10-H11}$, as is shown in Figure 3c. As in the HG1 base pair, the Coulomb attraction after electron transfer from 8-oxo-G$^-$ to adenine renders the proton transfer from 8-oxo-G to the adenine anion (Path 1) favorable, while it renders the proton transfer from the adenine anion to 8-oxo-G$^-$ (Path 2) unfavorable.

### 2.3.2. 8-oxo-G$^-$-C

We now turn our attention to the 8-oxoG$^-$-C base pair.The PE profiles along the $R_{N\text{-}H}$ driving coordinate are depicted in Figure 5. As with 8-oxoG$^-$-A, the base pair under consideration exhibits two possible inter-molecular proton-transfer paths along hydrogen bonds as depicted in the insets in Figure 5a,c. Path 1, which involves PT from the N-H donor group of 8-oxo-G$^-$ to the N acceptor group of C, shows a barrierless profile with respect to EDPT on $S_1$ (Figure 5a). Along this coordinate, the decreasing energy of the $S_1$ state is accompanied by an increasing energy of the $S_0$ state, which leads to an $S_1/S_0$ curve crossing at $R_{O\text{-}H} \approx 1.2$ Å. At this crossing, the excited-state population can return to the $S_0$ state—providing enhanced photostability of the 8-oxoG$^-$-C base pair—or a radical pair can be formed. The energy profiles along the LIIC path connecting the $^1\pi\pi^*$(uCT) state to the $^1\pi\pi^*$(CT) state are shown in Figure 5b. This energy profile exhibits no barrier and leads in fact to an $S_1/S_0$ energy crossing. This result ensures that the minimum-energy path connecting the $^1\pi\pi^*$(uCT) and $^1\pi\pi^*$(CT) states is barrierless and that the $S_1/S_0$ crossing seam is easily accessible from the Franck-Condon region of the $S_1$(uCT) state.

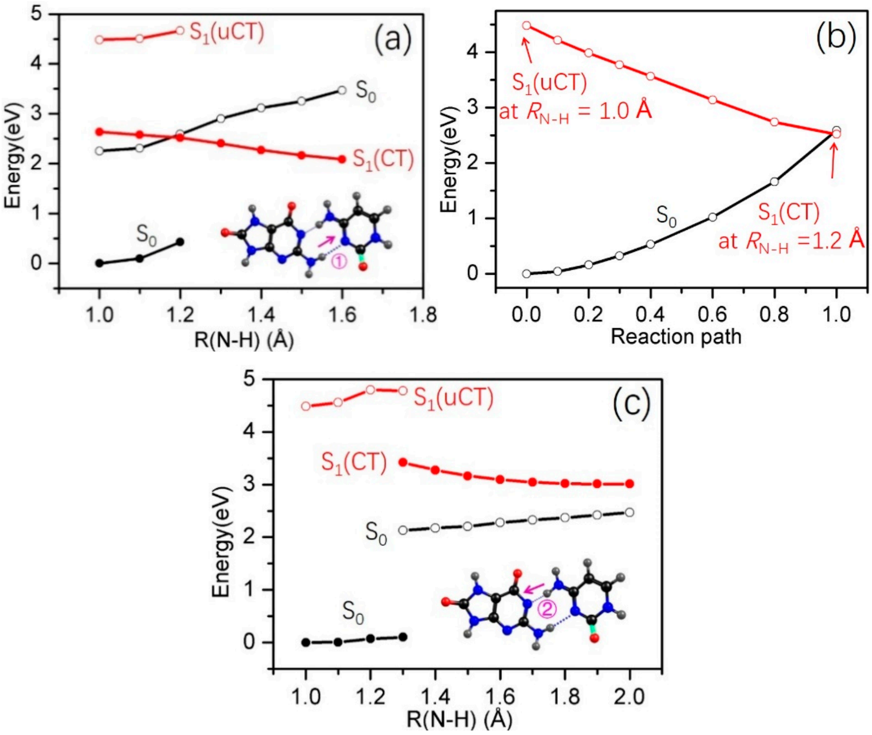

**Figure 5.** PE profiles of the ground state and the lowest excited states of the 8-oxo-G$^-$-C base pair along the $R_{N10-H13}$ (**a**) and $R_{N7-H9}$ (**c**) proton-transfer coordinates; (**b**) shows the energy profiles of the LIIC path connecting $S_1$(uCT) with $S_1$(CT) in (**a**).

An $S_1/S_0$ crossing is not observed for the second possible proton-transfer path (energy profiles depicted in Figure 5c), although the overall gradients of the $S_0$ and $S_1$ energy profiles mimick those observed in Figure 5a. The respective decrease and increase of the energies of $S_1$(CT) and $S_0$ are too weak to lead to a degeneracy of the $S_1$ and $S_0$ energies. As in the HG1 and HG2 base pairs of 8-oxo-$G^-$-A, there exists no substantial driving force for EDPT from cytosine to the 8-oxo-guanine anion.

## 3. General Discussions and Conclusions

We explored the excited-state reaction paths and PE profiles associated with coupled electron/proton transfer reactions in the two most stable hydrogen-bonded conformers of the 8-oxo-$G^-$-A base pair as well as in the lowest-energy conformer of the 8-oxo-$G^-$-C base pair. In both cases, the 8-oxo-G moiety was assumed to be in its deprotonated (anionic) form which is found in aqueous solution at pH > 7. In the 8-oxo-$G^-$-A HG1 base pair as well as in the 8-oxo-$G^-$-C base pair, the calculated PE profiles reveal the existence of a barrierless path for EDPT from 8-oxo-$G^-$ to A or C, leading to a low-lying $S_1/S_0$ conical intersection which can promote ultrafast excited-state deactivation. In the 8-oxo-$G^-$-A HG2 base pair, on the other hand, a low barrier may exist on the $S_1$ PE surface which may possibly kinetically hinder the access of this conformer to the $S_1/S_0$ CI. We did not find evidence for the existence of $S_1/S_0$ conical intersections along reaction paths for proton transfer from adenine or cytosine to the 8-oxo-$G^-$ anion in any of the three base pairs. The EDPT reactions revealed in the present work for the 8-oxo-$G^-$-A HG1 and 8-oxo-$G^-$-C base pairs are rather similar to those identified earlier in the G-C and A-T WC base pairs [33,34].

These results are of relevance for the current discussion on the potential role of 8-oxo-G as a photo-repair agent in DNA, possibly being a precursor of modern flavine cofactors [54,55,72]. It is firmly established that the photo-excited state of neutral 8-oxo-G has a sub-picosecond lifetime in aqueous solution, while deprotonated 8-oxo-$G^-$ exhibits a much longer fluorescence lifetime of 43 ps [26]. The drastic shortening of the excited-state lifetime of 8-oxo-$G^-$ relative to neutral 8-oxo-G has been explained by either CIs intrinsic to guanine, which are more easily accessible in the neutral than in the anionic form [57], or by an EDPT reaction along the H-bond between guanine and ribose in 8-oxo-guanosine, which is available in the neutral form, but not in the anionic form [23]. It has been speculated that the long lifetime of anionic 8-oxo-$G^-$ should be favorable for repair by electron transfer in the excited state, while the very short excited-state lifetime of neutral 8-oxo-G should be detrimental in this respect [26]. Herein, we have found computational evidence for presumably very efficient excited-state deactivation via barrierless EDPT reactions leading to $S_1/S_0$ conical intersections in the 8-oxo-$G^-$-A and 8-oxo-$G^-$G base pairs which call the concept of repair of CPD lesions via electron transfer from excited-state 8-oxo-$G^-$ in DNA oligomers into question. Kumar and Sevilla investigated the corresponding EDPT paths in the neutral 8-oxo-G-A and 8-oxo-G-C base pairs and found a path with a barrierless PE profile en route to a low-lying $S_1/S_0$ conical intersection in the 8-oxo-G-C base pair, while no such path was found for the 8-oxo-G-A base pair [67]. This finding led Kumar and Sevilla to the conclusion that the 8-oxo-G-A base-pair, due to its longer excited-state life time, should allow for efficient repair of CPD lesions. However, the very short intrinsic lifetime of neutral 8-oxo-guanosine, not considered by Kumar and Sevilla, renders it unlikely that the neutral 8-oxo-G-A base pairs are efficient repair agents in DNA oligomers. Notwithstanding, we do however stress that isolated nucleobasic or nucleosidic forms of 8-oxoG- may be efficient at repairing CPD lesions—as advocated by Matsika and co-workers [26] and Tuna et al. [23].

There exist additional complexities in a bulk DNA environment which are not taken into account in the present calculations. Electrostatic and dispersive interactions between stacked DNA bases may modify the topographies of the PE profiles and the locations and energies of CIs. Nonetheless, the present calculations for isolated base pairs are useful as they can serve as a starting point for forthcoming studies which include the effect of complex environments, albeit at a more approximate level of theory.

## 4. Computational Methods

The ground-state minimum-energy geometries of the 8-oxo-G$^-$-A base pairs, in the two HG conformations, and of the 8-oxo-G$^-$-C base pair were optimized at the MP2/cc-pVDZ level of theory [73,74]. At these ground-state minimum-energy geometries, the vertical excitation energies and oscillator strengths of the lowest four singlet excited states were calculated using the ADC(2) method. [75]. In the MP2 and ADC(2) calculations, the resolution of the identity (RI) approximation was employed in the evaluation of the electron repulsion integrals [76].

The reaction path for inter-base hydrogen-atom transfer from 8-oxo-G$^-$ to adenine in the electronic ground state was calculated as a relaxed scan at the MP2 level using $R_{\text{N-H}}$ of the hydrogen-bonded NH group of 8-oxo-G$^-$ as the driving coordinate. This involves scanning of the appropriate $R_{\text{N-H}}$ driving coordinate, while allowing the rest of the nuclear framework to relax. The energies of the $^1\pi\pi^*$ excited states along the relaxed ground-state path were computed using the ADC(2) method. Relaxed scans along $R_{\text{N-H}}$ were also computed for the lowest excited state of charge-transfer (CT) character using the ADC(2) method. In these calculations, the energies of the electronic ground state and the uCT $^1\pi\pi^*$ states were computed at the relaxed geometries of the CT state using the MP2 and ADC(2) methods, respectively. When calculations of relaxed scans were not possible due to failure of excited-state geometry optimization, an approximate reaction path was constructed by linear interpolation in internal coordinates (LIIC). All calculations were carried out with Turbomole [77].

**Acknowledgments:** X.W. would like to thank China Scholarship Council (CSC) for the award of doctoral scholarship. T.N.V.K. is thankful to TUM for the award of a post-doctoral fellowship.

**Author Contributions:** The results were obtained by X.W and overseen by T.N.V.K and W.D. All authors contributed equally in writing the manuscript.

**Conflicts of Interest:** The authors declare no conflict of interest.

## References

1. Pecourt, J.-M.L.; Peon, J.; Kohler, B. DNA excited-state dynamics: Ultrafast internal conversion and vibrational cooling in a series of nucleosides. *J. Am. Chem. Soc.* **2001**, *123*, 10370–10378. [CrossRef]
2. Kim, N.J.; Jeong, G.; Kim, Y.S.; Sung, J.; Keun Kim, S.; Park, Y.D. Resonant two-photon ionization and laser induced fluorescence spectroscopy of jet-cooled adenine. *J. Chem. Phys.* **2000**, *113*, 10051–10055. [CrossRef]
3. Nir, E.; Kleinermanns, K.; Grace, L.; de Vries, M.S. On the photochemistry of purine nucleobases. *J. Phys. Chem. A* **2001**, *105*, 5106–5110. [CrossRef]
4. Canuel, C.; Mons, M.; Piuzzi, F.; Tardivel, B.; Dimicoli, I.; Elhanine, M. Excited states dynamics of DNA and RNA bases: Characterization of a stepwise deactivation pathway in the gas phase. *J. Chem. Phys.* **2005**, *122*, 074316. [CrossRef] [PubMed]
5. Ismail, N.; Blancafort, L.; Olivucci, M.; Kohler, B.; Robb, M.A. Ultrafast decay of electronically excited singlet cytosine via a π,π* to no,π* state switch. *J. Am. Chem. Soc.* **2002**, *124*, 6818–6819. [CrossRef] [PubMed]
6. Sobolewski, A.; Domcke, W. On the mechanism of nonradiative decay of DNA bases: ab initio and tddft results for the excited states of 9*H*-adenine. *Eur. Phys. J. D* **2002**, *20*, 369–374. [CrossRef]
7. Merchán, M.; Serrano-Andrés, L. Ultrafast internal conversion of excited cytosine via the lowest $\pi\pi^*$ electronic singlet state. *J. Am. Chem. Soc.* **2003**, *125*, 8108–8109. [CrossRef] [PubMed]
8. Matsika, S. Radiationless decay of excited states of uracil through conical intersections. *J. Phys. Chem. A* **2004**, *108*, 7584–7590. [CrossRef]
9. Perun, S.; Sobolewski, A.L.; Domcke, W. Ab initio studies on the radiationless decay mechanisms of the lowest excited singlet states of 9*H*-adenine. *J. Am. Chem. Soc.* **2005**, *127*, 6257–6265. [CrossRef] [PubMed]
10. Perun, S.; Sobolewski, A.; Domcke, W. Photostability of 9*H*-adenine: Mechanisms of the radiationless deactivation of the lowest excited singlet states. *Chem. Phys.* **2005**, *313*, 107–112. [CrossRef]
11. Marian, C.M. A new pathway for the rapid decay of electronically excited adenine. *J. Chem. Phys.* **2005**, *122*, 104314. [CrossRef] [PubMed]
12. Zgierski, M.Z.; Patchkovskii, S.; Fujiwara, T.; Lim, E.C. On the origin of the ultrafast internal conversion of electronically excited pyrimidine bases. *J. Phys. Chem. A* **2005**, *109*, 9384–9387. [CrossRef] [PubMed]

13. Chen, H.; Li, S. Theoretical study toward understanding ultrafast internal conversion of excited 9*H*-adenine. *J. Phys. Chem. A* **2005**, *109*, 8443–8446. [CrossRef] [PubMed]
14. Blancafort, L. Excited-State potential energy surface for the photophysics of adenine. *J. Am. Chem. Soc.* **2006**, *128*, 210–219. [CrossRef] [PubMed]
15. Perun, S.; Sobolewski, A.L.; Domcke, W. Conical intersections in thymine. *J. Phys. Chem. A* **2006**, *110*, 13238–13244. [CrossRef] [PubMed]
16. Buchner, F.; Ritze, H.-H.; Lahl, J.; Lübcke, A. Time-Resolved photoelectron spectroscopy of adenine and adenosine in aqueous solution. *Phys. Chem. Chem. Phys.* **2013**, *15*, 11402–11408. [CrossRef] [PubMed]
17. Camillis, S.D.; Miles, J.; Alexander, G.; Ghafur, O.; Williams, I.D.; Townsend, D.; Greenwood, J.B. Ultrafast non-radiative decay of gas-phase nucleosides. *Phys. Chem. Chem. Phys.* **2015**, *17*, 23643–23650. [CrossRef] [PubMed]
18. Gustavsson, T.; Sarkar, N.; Vaya, I.; Jimenez, M.C.; Markovitsi, D.; Improta, R. A joint experimental/theoretical study of the ultrafast excited state deactivation of deoxyadenosine and 9-methyladenine in water and acetonitrile. *Photochem. Photobiol. Sci.* **2013**, *12*, 1375–1386. [CrossRef] [PubMed]
19. Pecourt, J.-M.L.; Peon, J.; Kohler, B. Ultrafast internal conversion of electronically excited RNA and DNA nucleosides in water. *J. Am. Chem. Soc.* **2000**, *122*, 9348–9349. [CrossRef]
20. Peon, J.; Zewail, A.H. DNA/RNA nucleotides and nucleosides: Direct measurement of excited-state lifetimes by femtosecond fluorescence up-conversion. *Chem. Phys. Lett.* **2001**, *348*, 255–262. [CrossRef]
21. Schwalb, N.K.; Temps, F. Ultrafast electronic relaxation in guanosine is promoted by hydrogen bonding with cytidine. *J. Am. Chem. Soc.* **2007**, *129*, 9272–9273. [CrossRef] [PubMed]
22. Stavros, V.G.; Verlet, J.R. Gas-Phase femtosecond particle spectroscopy: A bottom-up approach to nucleotide dynamics. *Annu. Rev. Phys. Chem.* **2016**, *67*, 211–232. [CrossRef] [PubMed]
23. Tuna, D.; Domcke, W. Excited-State deactivation in 8-oxo-deoxyguanosine: Comparison between anionic and neutral forms. *Phys. Chem. Chem. Phys.* **2016**, *18*, 947–955. [CrossRef] [PubMed]
24. Tuna, D.; Sobolewski, A.L.; Domcke, W. Mechanisms of ultrafast excited-state deactivation in adenosine. *J. Phys. Chem. A* **2013**, *118*, 122–127. [CrossRef] [PubMed]
25. Zgierski, M.Z.; Alavi, S. Quantum chemical study of biradical decay channels in cytidine nucleosides. *Chem. Phys. Lett.* **2006**, *426*, 398–404. [CrossRef]
26. Zhang, Y.; Dood, J.; Beckstead, A.; Chen, J.; Li, X.-B.; Burrows, C.J.; Lu, Z.; Matsika, S.; Kohler, B. Ultrafast excited-state dynamics and vibrational cooling of 8-oxo-7,8-dihydro-2′-deoxyguanosine in $D_2O$. *J. Phys. Chem. A* **2013**, *117*, 12851–12857. [CrossRef] [PubMed]
27. Abo-Riziq, A.; Grace, L.; Nir, E.; Kabelac, M.; Hobza, P.; de Vries, M.S. Photochemical selectivity in guanine-cytosine base-pair structures. *Proc. Natl. Acad. Sci. USA* **2005**, *102*, 20–23. [CrossRef] [PubMed]
28. Gobbo, J.P.; Saurí, V.; Roca-Sanjuán, D.; Serrano-Andrés, L.; Merchán, M.; Borin, A.C. On the deactivation mechanisms of adenine-thymine base pair. *J. Phys. Chem. B* **2012**, *116*, 4089–4097. [CrossRef] [PubMed]
29. Groenhof, G.; Schäfer, L.V.; Boggio-Pasqua, M.; Goette, M.; Grubmüller, H.; Robb, M.A. Ultrafast deactivation of an excited cytosine−guanine base pair in DNA. *J. Am. Chem. Soc.* **2007**, *129*, 6812–6819. [CrossRef] [PubMed]
30. Marchetti, B.; Karsili, T.N.V.; Ashfold, M.N.R.; Domcke, W. A ‘bottom up’, ab initio computational approach to understanding fundamental photophysical processes in nitrogen containing heterocycles, DNA bases and base pairs. *Phys. Chem. Chem. Phys.* **2016**, *18*, 20007–20027. [CrossRef] [PubMed]
31. Markwick, P.R.L.; Doltsinis, N.L. Ultrafast repair of irradiated DNA: Nonadiabatic ab initio simulations of the guanine-cytosine photocycle. *J. Chem. Phys.* **2007**, *126*, 175102. [CrossRef] [PubMed]
32. Nir, E.; Plützer, C.; Kleinermanns, K.; de Vries, M. Properties of isolated DNA bases, base pairs and nucleosides examined by laser spectroscopy. *Eur. Phys. J. D* **2002**, *20*, 317–329. [CrossRef]
33. Perun, S.; Sobolewski, A.L.; Domcke, W. Role of electron-driven proton-transfer processes in the excited-state deactivation of the adenine-thymine base pair. *J. Phys. Chem. A* **2006**, *110*, 9031–9038. [CrossRef] [PubMed]
34. Sobolewski, A.L.; Domcke, W. Ab initio studies on the photophysics of the guanine-cytosine base pair. *Phys. Chem. Chem. Phys.* **2004**, *6*, 2763–2771. [CrossRef]
35. Sobolewski, A.L.; Domcke, W.; Hättig, C. Tautomeric selectivity of the excited-state lifetime of guanine/cytosine base pairs: The role of electron-driven proton-transfer processes. *Proc. Natl. Acad. Sci. USA* **2005**, *102*, 17903–17906. [CrossRef] [PubMed]

36. Yamazaki, S.; Taketsugu, T. Photoreaction channels of the guanine-cytosine base pair explored by long-range corrected TDDFT calculations. *Phys. Chem. Chem. Phys.* **2012**, *14*, 8866–8877. [CrossRef] [PubMed]
37. Taylor, J.S. Unraveling the molecular pathway from sunlight to skin cancer. *Acc. Chem. Res.* **1994**, *27*, 76–82. [CrossRef]
38. Sinha, R.P.; Häder, D.-P. UV-Induced DNA damage and repair: A review. *Photochem. Photobiol. Sci.* **2002**, *1*, 225–236. [CrossRef] [PubMed]
39. Schreier, W.J.; Gilch, P.; Zinth, W. Early events of DNA photodamage. *Annu. Rev. Phys. Chem.* **2015**, *66*, 497–519. [CrossRef] [PubMed]
40. Chen, H.; Li, S. Ab initio study on deactivation pathways of excited 9*H*-guanine. *J. Chem. Phys.* **2006**, *124*, 154315. [CrossRef] [PubMed]
41. Marian, C.M. The guanine tautomer puzzle: Quantum chemical investigation of ground and excited states. *J. Phys. Chem. A* **2007**, *111*, 1545–1553. [CrossRef] [PubMed]
42. Serrano-Andres, L.; Merchan, M.; Borin, A.C. A three-state model for the photophysics of guanine. *J. Am. Chem. Soc.* **2008**, *130*, 2473–2484. [CrossRef] [PubMed]
43. Yamazaki, S.; Domcke, W. Ab initio studies on the photophysics of guanine tautomers: Out-of-plane deformation and NH dissociation pathways to conical intersections. *J. Phys. Chem. A* **2008**, *112*, 7090–7097. [CrossRef] [PubMed]
44. Hudock, H.R.; Levine, B.G.; Thompson, A.L.; Satzger, H.; Townsend, D.; Gador, N.; Ullrich, S.; Stolow, A.; Martínez, T.J. Ab initio molecular dynamics and time-resolved photoelectron spectroscopy of electronically excited uracil and thymine. *J. Phys. Chem. A* **2007**, *111*, 8500–8508. [CrossRef] [PubMed]
45. Zechmann, G.; Barbatti, M. Photophysics and deactivation pathways of thymine. *J. Phys. Chem. A* **2008**, *112*, 8273–8279. [CrossRef] [PubMed]
46. Gomez-Mendoza, M.; Banyasz, A.; Douki, T.; Markovitsi, D.; Ravanat, J.-L. Direct oxidative damage of naked DNA generated upon absorption of UV radiation by nucleobases. *J. Phys. Chem. Lett.* **2016**, *7*, 3945–3948. [CrossRef] [PubMed]
47. Banyasz, A.; Martinez-Fernandez, L.; Ketola, T.-M.; Muñoz-Losa, A.; Esposito, L.; Markovitsi, D.; Improta, R. Excited state pathways leading to formation of adenine dimers. *J. Phys. Chem. Lett.* **2016**, *7*, 2020–2023. [CrossRef] [PubMed]
48. Cadet, J.; Douki, T.; Ravanat, J.-L. Oxidatively generated damage to the guanine moiety of DNA: Mechanistic aspects and formation in cells. *Acc. Chem. Res.* **2008**, *41*, 1075–1083. [CrossRef] [PubMed]
49. Kanvah, S.; Joseph, J.; Schuster, G.B.; Barnett, R.N.; Cleveland, C.L.; Landman, U. Oxidation of DNA: Damage to nucleobases. *Acc. Chem. Res.* **2010**, *43*, 280–287. [CrossRef] [PubMed]
50. Markus, T.Z.; Daube, S.S.; Naaman, R.; Fleming, A.M.; Muller, J.G.; Burrows, C.J. Electronic structure of DNA-unique properties of 8-oxoguanosine. *J. Am. Chem. Soc.* **2009**, *131*, 89–95. [CrossRef] [PubMed]
51. Shibutani, S.; Takeshita, M.; Grollman, A.P. Insertion of specific bases during DNA synthesis past the oxidation-damaged base 8-oxodG. *Nature* **1991**, *349*, 431–434. [CrossRef] [PubMed]
52. Greenman, C.; Stephens, P.; Smith, R.; Dalgliesh, G.L.; Hunter, C.; Bignell, G.; Davies, H.; Teague, J.; Butler, A.; Stevens, C.; et al. Patterns of somatic mutation in human cancer genomes. *Nature* **2007**, *446*, 153–158. [CrossRef] [PubMed]
53. Steenken, S.; Jovanovic, S.V.; Bietti, M.; Bernhard, K. The trap depth (in DNA) of 8-oxo-7,8-dihydro-2′deoxyguanosine as derived from electron-transfer equilibria in aqueous solution. *J. Am. Chem. Soc.* **2000**, *122*, 2373–2374. [CrossRef]
54. Nguyen, K.V.; Burrows, C.J. A prebiotic role for 8-oxoguanosine as a flavin mimic in pyrimidine dimer photorepair. *J. Am. Chem. Soc.* **2011**, *133*, 14586–14589. [CrossRef] [PubMed]
55. Nguyen, K.V.; Burrows, C.J. Photorepair of cyclobutane pyrimidine dimers by 8-oxopurine nucleosides. *J. Phys. Org. Chem.* **2012**, *25*, 574–577. [CrossRef]
56. Jayanth, N.; Ramachandran, S.; Puranik, M. Solution structure of the DNA damage lesion 8-oxoguanosine from ultraviolet resonance Raman spectroscopy. *J. Phys. Chem. A* **2009**, *113*, 1459–1471. [CrossRef] [PubMed]
57. Lu, Z.; Beckstead, A.A.; Kohler, B.; Matsika, S. Excited state relaxation of neutral and basic 8-oxoguanine. *J. Phys. Chem. B* **2015**, *119*, 8293–8301. [CrossRef] [PubMed]
58. Changenet-Barret, P.; Gustavsson, T.; Improta, R.; Markovitsi, D. Ultrafast excited-state deactivation of 8-hydroxy-2′-deoxyguanosine studied by femtosecond fluorescence spectroscopy and quantum-chemical calculations. *J. Phys. Chem. A* **2015**, *119*, 6131–6139. [CrossRef] [PubMed]

59. Crespo-Hernandez, C.E.; Cohen, B.; Kohler, B. Base stacking controls excited-state dynamics in A-T DNA. *Nature* **2005**, *436*, 1141–1144. [CrossRef] [PubMed]
60. Vayá, I.; Gustavsson, T.; Douki, T.; Berlin, Y.; Markovitsi, D. Electronic excitation energy transfer between nucleobases of natural DNA. *J. Am. Chem. Soc.* **2012**, *134*, 11366–11368. [CrossRef] [PubMed]
61. Markovitsi, D. UV-induced DNA damage: The role of electronic excited states. *Photochem. Photobiol.* **2016**, *92*, 45–51. [CrossRef] [PubMed]
62. Zhang, Y.; Dood, J.; Beckstead, A.A.; Li, X.-B.; Nguyen, K.V.; Burrows, C.J.; Improta, R.; Kohler, B. Photoinduced electron transfer in DNA: Charge shift dynamics between 8-oxo-guanine anion and adenine. *J. Phys. Chem. B* **2015**, *119*, 7491–7502. [CrossRef] [PubMed]
63. Zhang, Y.; Dood, J.; Beckstead, A.A.; Li, X.-B.; Nguyen, K.V.; Burrows, C.J.; Improta, R.; Kohler, B. Efficient UV-induced charge separation and recombination in an 8-oxoguanine-containing dinucleotide. *Proc. Natl. Acad. Sci. USA* **2014**, *111*, 11612–11617. [CrossRef] [PubMed]
64. Bucher, D.B.; Schlueter, A.; Carell, T.; Zinth, W. Watson-Crick base pairing controls excited-state decay in natural DNA. *Angew. Chem. Int. Ed.* **2014**, *53*, 11366–11369. [CrossRef] [PubMed]
65. Zhang, Y.; de La Harpe, K.; Beckstead, A.A.; Improta, R.; Kohler, B. UV-induced proton transfer between DNA strands. *J. Am. Chem. Soc.* **2015**, *137*, 7059–7062. [CrossRef] [PubMed]
66. Schultz, T.; Samoylova, E.; Radloff, W.; Hertel, I.V.; Sobolewski, A.L.; Domcke, W. Efficient deactivation of a model base pair via excited-state hydrogen transfer. *Science* **2004**, *306*, 1765–1768. [CrossRef] [PubMed]
67. Kumar, A.; Sevilla, M.D. Excited state proton-coupled electron transfer in 8-oxoG-C and 8-oxoG-A base pairs: A time dependent density functional theory (TD-DFT) study. *Photochem. Photobiol. Sci.* **2013**, *12*, 1328–1340. [CrossRef] [PubMed]
68. Wang, Y.; Schlick, T. Distinct energetics and closing pathways for DNA polymerase β with 8-oxog template and different incoming nucleotides. *BMC Struct. Biol.* **2007**, *7*, 7. [CrossRef] [PubMed]
69. Hsu, G.W.; Ober, M.; Carell, T.; Beese, L.S. Error-Prone replication of oxidatively damaged DNA by a high-fidelity DNA polymerase. *Nature* **2004**, *431*, 217–221. [CrossRef] [PubMed]
70. Cheng, K.C.; Cahill, D.S.; Kasai, H.; Nishimura, S.; Loeb, L.A. 8-hydroxyguanine, an abundant form of oxidative DNA damage, causes G-T and A-C substitutions. *J. Biol. Chem.* **1992**, *267*, 166–172. [PubMed]
71. Sobolewski, A.L.; Domcke, W. Computational studies of the photophysics of hydrogen-bonded molecular systems. *J. Phys. Chem. A* **2007**, *111*, 11725–11735. [CrossRef] [PubMed]
72. Nguyen, K.V.; Burrows, C.J. Whence flavins? Redox-active ribonucleotides link metabolism and genome repair to the RNA world. *Acc. Chem. Res.* **2012**, *45*, 2151–2159. [CrossRef] [PubMed]
73. Møller, C.; Plesset, M.S. Note on an approximation treatment for many-electron systems. *Phys. Rev.* **1934**, *46*, 618–622. [CrossRef]
74. Dunning, T.H., Jr. Gaussian basis sets for use in correlated molecular calculations. I. The atoms boron through neon and hydrogen. *J. Chem. Phys.* **1989**, *90*, 1007–1023. [CrossRef]
75. Schirmer, J. Beyond the random-phase approximation: A new approximation scheme for the polarization propagator. *Phys. Rev. A* **1982**, *26*, 2395–2416. [CrossRef]
76. Hättig, C.; Weigend, F. CC2 excitation energy calculations on large molecules using the resolution of the identity approximation. *J. Chem. Phys.* **2000**, *113*, 5154–5161. [CrossRef]
77. Turbomole, V. 4. A Development of the University of Karlsruhe and Forschungszentrum Karlsruhe GmBH: Karlsruhe, Germany, 2012.

**Sample Availability:** Samples of the compounds are not available from the authors.

© 2017 by the authors; licensee MDPI, Basel, Switzerland. This article is an open access article distributed under the terms and conditions of the Creative Commons Attribution (CC-BY) license (http://creativecommons.org/licenses/by/4.0/).